SYNTHESIS AND CHARACTERIZATION OF Pd-MCM-TYPE MESOPOROUS NANOCOMPOSITE MATERIALS

A THESIS SUBMITTED TO
THE GRADUATE SCHOOL OF NATURAL AND APPLIED SCIENCES
OF
MIDDLE EAST TECHNICAL UNIVERSITY

BY

CANAN ŞENER

IN PARTIAL FULFILLMENT OF THE REQUIREMENTS
FOR
THE DEGREE OF MASTER OF SCIENCE
IN
CHEMICAL ENGINEERING

JANUARY 2006

Approval of the Graduate School of Natural and Applied Sciences

Prof. Dr. Canan Özgen
Director

I certify that this thesis satisfies all the requirements as a thesis for the degree of Master of Science.

Prof. Dr. Nurcan Baç
Head of Department

This is to certify that we have read this thesis and that in our opinion it is fully adequate, in scope and quality, as a thesis and for the degree of Master of Science.

Prof. Dr. Gülşen Doğu
Co-Supervisor

Prof. Dr. Timur Doğu
Supervisor

Examining Committee Members

Prof. Dr. İnci Eroğlu (METU, CHE)

Prof. Dr. Timur Doğu (METU, CHE)

Prof. Dr. Tülay Özbelge (METU, CHE)

Prof. Dr. Suna Balcı (Gazi University, CHE)

Assoc. Prof. Dr. Gürkan Karakaş (METU, CHE)

I hereby declare that all information in this document has been obtained and presented in accordance with academic rules and ethical conduct. I also declare that, as required by these rules and conduct, I have fully cited and referenced all material and results that are not original to this work.

Name, Last name : Canan Şener
Signature :

ABSTRACT

SYNTHESIS AND CHARACTERIZATION OF Pd-MCM-TYPE MESOPOROUS NANOCOMPOSITE MATERIALS

Şener, Canan
M.S., Department of Chemical Engineering
Supervisor: Prof. Dr. Timur Doğu
Co-Supervisor: Prof. Dr. Gülşen Doğu

January 2006, 117 pages

Noble metal incorporated MCM-41 based nanostructured mesoporous materials have attracted the attention of material researchers in recent years. Sorption characteristics of MCM materials can be improved by surface modification techniques. Besides surface modification, metal nanoparticles can also be produced within the pores of mesoporous materials. MCM-41 can act as host for several metal nanoparticles such as palladium.

The present study is focused on the synthesis of Pd-MCM-41 nanocomposite catalytic materials by using different direct synthesis procedures, as well as an impregnation method. Impregnated samples were used to synthesize Pd nanoparticles inside the pores of MCM-41. In the direct hydrothermal synthesis of Pd-MCM-41, incorporation of the Pd metal was achieved by adding $PdCl_2$, K_2PdCl_4 and $Pd(NH_3)_4(NO_2)_3$ solutions into the synthesis mixture. Syntheses were performed in acidic and basic routes. Hydrothermal synthesis was carried out in an autoclave at 120 ^{o}C. The solid

product was filtered, washed, dried, calcined at 550 ^{o}C in a stream of dry air and reduced in a stream of hydrogen at 200 ^{o}C. In the case of impregnation, $PdCl_2$ solution was added to a suspension of MCM-41. The product was evaporated to dryness, dried under vacuum and reduced with H_2 gas at 200 ^{o}C. Physical and chemical properties and surface morphology of Pd-MCM-41 nanomaterials were characterized by using XRD, XPS, EDS, BET, SEM, TEM and TPR techniques.

Very high Pd/Si ratios, as high as 0.45 and 0.18 were obtained in the mesoporous materials produced by the basic and acidic direct synthesis routes, respectively. The BET surface areas of these materials were found as 999 m^2/g and 694 m^2/g, respectively. These results showed that the basic direct synthesis procedure was highly successful for the incorporation of Pd into the mesoporous Si structure. In addition, EDS analysis of the Pd-MCM-41 materials prepared by the impregnation technique showed that Pd/Si ratios were 0.24 and 0.12 in the two samples having surface areas of 527 m^2/g and 883 m^2/g, respectively.

In conclusion, high surface area of the material synthesized by the basic route together with a higher Pd/Si ratio makes this material more attractive for catalytic and hydrogen storage applications.

Keywords: Mesoporous, nanocomposite material, MCM-41, Pd-MCM-41

ÖZ

Pd-MCM-TİP MEZO-GÖZENEKLİ NANOKOMPOZİT MALZEMELERİN SENTEZ VE KARAKTERİZASYONU

Şener, Canan
Yüksek Lisans, Kimya Mühendisliği Bölümü
Tez Yöneticisi: Prof. Dr. Timur Doğu
Ortak Tez Yöneticisi : Prof. Dr. Gülşen Doğu

Ocak 2006, 117 sayfa

Asal metal içeren nanoyapılı, mezo-gözenekli MCM-41 malzemeler son yıllarda araştırmacıların ilgisini çekmektedir. MCM malzemelerinin soğurma özellikleri yüzey modifikasyon teknikleriyle arttırılabilir. Yüzey modifikasyonunun yanısıra, mezo-gözenekli malzemelerin gözeneklerinin içinde metal nanoparçacıklar üretilebilmektedir. MCM-41, palladyum gibi birçok metal nanoparçacık için konakçı olarak kullanılabilir.

Bu çalışmada farklı doğrudan hidrotermal sentez teknikleri ve impregnasyon (emdirme) tekniğiyle Pd-MCM-41 nanokompozit katalitik malzemelerin sentezi üzerine yoğunlaşılmıştır. Emdirilmiş örnekler MCM-41'in gözeneklerinin içinde palladium nanoyapılar sentezlemekte kullanılmıştır. Pd-MCM-41 yapıların doğrudan hidrotermal sentez yöntemiyle sentezlenmesinde palladium metalinin yapıya yerleştirilmesi sentez çözeltisine $PdCl_2$, K_2PdCl_4 ve $Pd(NH_3)_4(NO_2)_3$ çözeltilerinin eklenmesiyle gerçekleştirilmiştir. Asidik ve bazik ortamlarda sentezler yapılmıştır. Hidrotermal sentez otoklavda 120 ^oC'de yürütülmüştür. Hidrotermal sentez basamağı sonrası elde edilen katı ürün yıkanmış, kurutulmuş, 550 ^oC'de kuru hava ile kalsine edilmiş ve 200 ^oC'de hidrojen ile indirgenmiştir. Impregnasyon yönteminde, $PdCl_2$ çözeltisi MCM-41

süspansiyonu üzerine eklenmiştir. Karışım kuruyuncaya kadar buharlaştırılmış, vakum altında kurutulmuş ve 200 ^{o}C'de H_2 gazıyla indirgenmiştir. Pd-MCM-41 nanomalzemelerin fiziksel ve kimyasal özellikleri ve yüzey morfolojileri XRD, XPS, EDS, BET, SEM, TEM ve TPR teknikleri kullanılarak karakterize edilmişlerdir.

Bazik ve asidik koşullarda gerçekleştirilen sentezlerde, 0.45 ve 0.18 gibi çok yüksek Pd/Si oranlarına ulaşılmıştır. Bu malzemelerin BET yüzey alanları sırasıyla 999 m^2/g ve 694 m^2/g olarak bulunmuştur. Bu sonuçlar bazik koşullarda gerçekleştirilen doğrudan hidrotermal sentez yöntemiyle paladyumun silisyum yapısına daha başarılı yerleştirildiğini göstermiştir. Bununla beraber, impregnasyon tekniğiyle sentezlenen Pd-MCM-41 malzemelerin EDS analizleri yüzey alanlarının 527 m^2/g ve 883 m^2/g olan malzemeler için Pd/Si oranının 0.24 ve 0.12 olduğunu göstermiştir.

Sonuç olarak, bazik ortamda sentezlenmiş yüksek yüzey alanlı malzemelerin aynı zamanda yüksek Pd/Si oranına sahip olması bu malzemeyi katalitik ve hidrojen depolama malzemesi olarak daha ilginç kılmaktadır.

Anahtar Kelimeler: Mezo-gözenek, nano-kompozit malzeme, MCM-41, Pd-MCM-41

To My Family & Berker,

ACKNOWLEDGEMENTS

With deep sense of gratitude and appreciation, I would like to express my sincere thanks to my supervisor Prof. Dr. Timur Doğu for his inspiring guidance, and help and excellent cooperation in supervising this research work.

I am also very grateful to my co-supervisor Prof Dr. Gülşen Doğu for her great help, continuous encouragement, several discussions and the facilities she allowed me to use in Gazi University.

I would like to thank to Prof. Dr. Tayfur Öztürk for his outstanding support in characterization of the materials.

I cannot pass without presenting my sincere thanks to Prof. Dr. Suna Balcı for letting me to use the physisorption facilities at Gazi University.

I would like to offer my sincere thanks to Dr. Sena Yaşyerli and Dr. Meltem Doğan for their guidance.

I would like to present my thanks to Prof. Dr. İnci Eroğlu for her academic and friendly support.

Special thanks to Cengiz Tan for EDS analyses and Necmi Avcı for X-ray analyses from Department of Materials and Metallurgical Engineering. I would like to thank Serkan Türk from Çimento Müstahsilleri Birliği also for X-ray analysis.

Technicians of our department Turgut Aksakal, Selahattin Uysal, Gülten Orakçı, Mihrican Açıkgöz were always ready to help, helpful and kind. I want to thank them for their technical and friendly supports.

I owe special thanks to Prof. Dr. Yuda Yürüm, Billur Sakintuna and Ahu Gümrah Dumanlı from Sabancı University for SEM images of my samples.

Special thanks to Prof. Dr. Süleyman Ali Tuncel from Hacettepe University for TEM analysis of my samples.

It was difficult to finish up this study without the support of my friend Sinan Ok. I would like to thank him not only for all the time and information he has shared with me but also his great friendship.

I would like to express my sincere thanks to Dr. Nezahat Boz and Dr. Gülsün Karamullaoğlu for the support and for the knowledge and experience they have shared with me. But the most important, thanks them for their friendship.

I want to thank my research colleagues in Kinetic Laboratory Dilek Varışlı and Zeynep Obalı. It is a great experience to be in such an environment.

I would like to thank my colleague Dr. Yeşim Güçbilmez - first MCM-builder of our department - for all information she gave about the synthesis and characterization.

I would like to thank Esin Eren for all her support and BET analyses.

Thanks are due to Burcu Mirkelamoğlu for the discussions on XPS and Umut Barış Ayhan (UBA-the master) for the discussions on the characterization techniques.

I would like to thank METU Central Laboratories for XPS analyses.

I would like to thank my friends Salih Obut, Serdar Erkan, Ela Eroğlu and Ayşe Bayrakçeken for all their support and nice time we had together during the studies.

It is difficult to describe in words for all the support, pushing, and encouragement my family have given to me. They deserve my special and sincerely gratitude. Special thanks to my mom for her great patience (she knows

all details of synthesis and characterization!) and dad for his motivation. I want to thank my brother - the anarchist - Furkan Şener for fascinating Pd-MCM-41 logo.

My sincerest thanks to Berker Fıçıcılar, my ex-lab-mate, my best friend, my fiancée and my all, for his existence in my life and outstanding support. Thanks for the nights that he waited me for hours in the laboratory and great and almost endless discussions we had about… Pd-MCM-41!

Finally, Governmental Planning Organization was also gratefully acknowledged for the research fund BAP-08-11-DPT.2002K120510 for financial support.

TABLE OF CONTENTS

LIST OF TABLES

LIST OF FIGURES

CHAPTER 1

INTRODUCTION

1.1. POROUS SOLIDS

Porous solids have been studied in detail by material scientists with regard to their technical applications as adsorbents, catalysts, catalyst supports, ion exchanging agents and micro reactors [1].

According to the IUPAC definition, porous materials are divided into three classes [3];

1) Microporous materials: their pore diameters are less than 20 A,

2) Mesoporous materials: they have pore diameters ranging from 20-500 A,

3) Macroporous materials: they have pore diameters larger than 500 A.

Pillared clays, anodic alumina, carbon nanotubes and related porous carbons are examples to microporous materials which have been described in the literature (Figure1.1.1). Among the family of microporous materials, the best known members are zeolites. Due to their crystallographically defined pore system, zeolites have a narrow and uniform size distribution in the microporous range [1-3, 5].

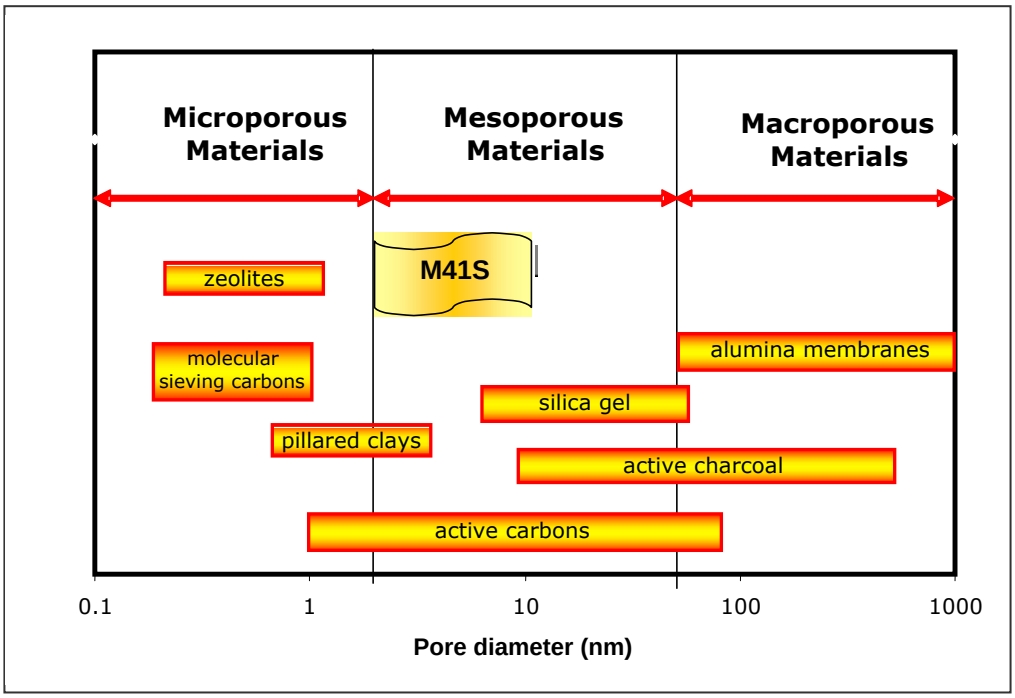

Figure 1.1.1. Porous materials as classified by their pore diameters (adapted from [2] and [56])

1.2. MICROPOROUS MATERIALS AND CATALYSTS

In most of the modern technological chemical processes, catalysts are used for the purpose of simplifying the chemical process economically. Catalysts are commonly used to interact with the reactants to increase the rate of the transformation of these reactants into products without consumption of the catalysts in the process. In the case of multiple reaction systems, catalytsts can also improve the reaction selectivity for a single desired product [6].

Zeolites are the most widely used catalysts in chemical industry. They are crystalline aluminosilicate microporous materials with uniform channels and cages and have become extremely successful as catalysts for oil refining, petrochemistry, and organic synthesis of fine and specialty chemicals (Figure 1.2.1) [1-6].

Some of the specific catalytic characteristics of the zeolites can be summarized as follows:

(1) they have very high surface area values and adsorption capacities,
(2) the dimensions of their channels are close to the kinetic diameter of many molecules of interest (0.5-1.2 nm),
(3) zeolites have controllable adsorption properties variable from hydrophobic to hydrophilic,
(4) active acid sites, can be generated in the zeolite framework and their strength and concentration can be adjusted for a particular application,
(5) their channel structure allows zeolites to exhibit different types of shape selectivity,
(6) they have high hydrothermal and thermal and stability [3, 6].

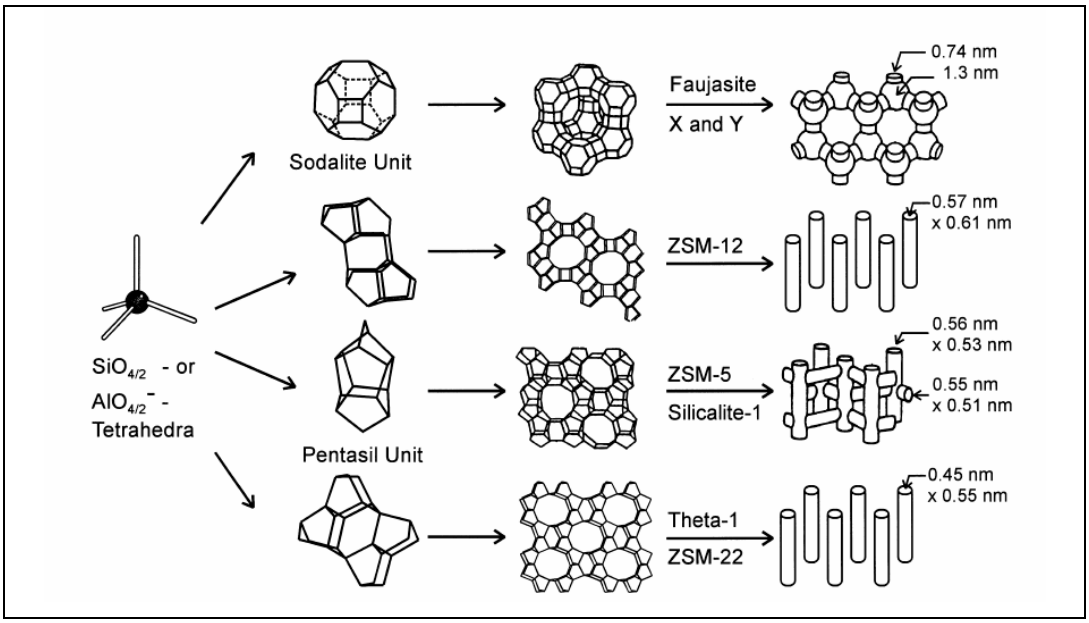

Figure 1.2.1. Structures of selected zeolites (taken from [2])

Although the zeolites have highly attractive catalytical properties, they can not be applied to reactions where the size of the reactants is greater than the dimensions of the microporous zeolites. Therefore, an ideal approach to overcome this limitation would be to maintain the porous structure of zeolites and increase their diameter to the mesoporous region. Most of the organic templates used to synthesize zeolites involves gel formation and act as void fillers in the growing porous solids. Consequently, scientists attempted to employ larger organic templates to result in larger voids in synthesized molecular sieves

(Figure 1.2.2). The presence of mesopores in these materials allows them to catalyze larger molecules. As it is reported in the literature,I amorphous silica-aluminas with a narrow pore size distribution in the mesoporous region also have similar catalytic properties to zeolites. However, these materials do not have uniform pore structure to affect selectivity for catalysis. Consequently, number of researchers attempted to synthesize mesoporous materials with a uniform pore structure [3, 6].

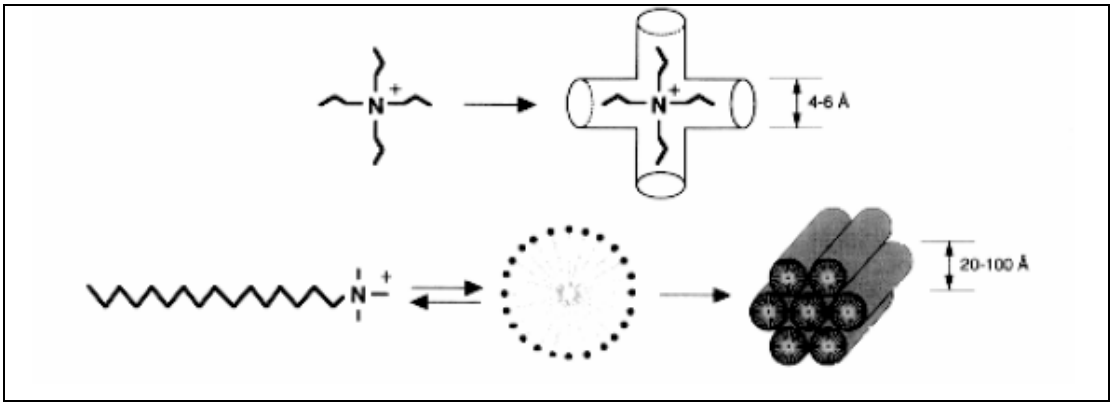

Figure 1.2.2. Amine-templating zeolites and surfactant-templating mesoporous materials [7]

1.3. A NOVEL FAMILY OF ORDERED MESOPOROUS MOLECULAR SIEVES

Discovery of a novel family of mesoporous silicate molecular sieves by liquid crystal templates is considered as one of the most exciting discoveries in the field of materials synthesis over the last two decades. This family of materials was first synthesized by Mobil scientists at the end of 1992 using relatively large surfactant molecules such as cetyltrimethylammonium chloride (CTAC) as templates [8,9]. They are generally named as M41S mesoporous materials with large uniform channels ranging from 1.5 to 10 nm. There are three main members of M41S family which are MCM-41 (short for Mobil Crystalline Matter No.41) (Figure 1.3.1.a) with a one dimensional hexagonal array of uniform mesopores, MCM-48 (Figure 1.3.1.b) with three dimensional cubic channels, and MCM-50 (Figure 1.3.1.c) with uniform lamellar phases

[1,3,4]. Among these mesoporous materials, MCM-41 and MCM-48 have very potential in catalytic applications. The mesoporous structure of the lamellar phase, MCM-50, was reported to collapse upon calcination. These mesoporous materials have long range order, and high surface area values, above 700 m^2/g These properties make them as attractive catalyst supports. Therefore, they are very promising for catalysis applications. [6]

1.4. OBJECTIVES

Being a potential energy carrier, hydrogen production has increased significantly in recent years. In order to use hydrogen on demand for fuel cell applications and other uses, it is very crucial to have an infrastructure for storage and transportation of hydrogen. Once hydrogen is generated, there are several ways to store hydrogen such as in compressed or liquid forms and in solid state form. Among these storage methods, solid state form is the most promising technology when efficiency and safety issues are considered.

Objective of this study was to synthesize high surface area, mesoporous, nanocomposite materials for hydrogen storage applications. For this purpose, Pd-MCM-41 nanomaterials were synthesized and characterized.

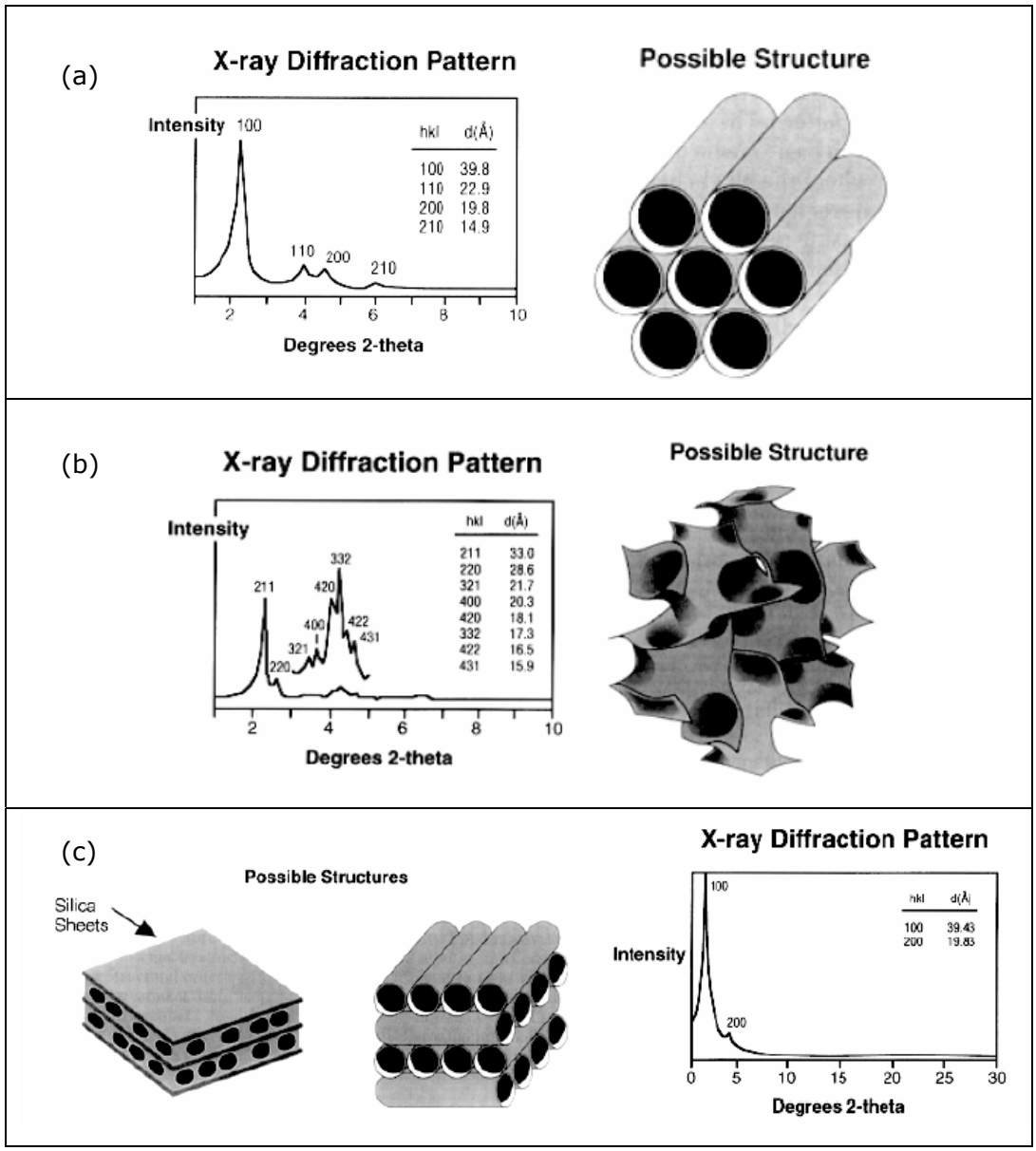

Figure 1.3.1. MCM family (a) MCM-41, (b) MCM-48, (c) MCM-50 (adapted from [7])

CHAPTER 2

LITERATURE SURVEY

2.1. HISTORY OF MESOPOROUS MATERIALS

A continuous research in developing materials with constantly larger pores finally led to the development of materials with mesopores (pores between 2-50 nm). The syntheses of these new mesoporous materials were achieved by ExxonMobil researchers in 1992 [8-13]. These materials were classified according to their different structure as belonging to the "M41S" class materials. These structures were purely siliceous materials. In order to obtain comparable structures with zeolites, the first successful attempts of aluminium incorporation into the framework of these structures were published [14].

Actual invent of ExxonMobil researchers was based on the uncomplete study of Di Renzo. Chiola achieved the synthesis of "low-bulk density silica" and Di Renzo described a recipe by reproducing the Chiola's study. Di Renzo obtained a classical hexagonally structured material (MCM-41). Unfortunately, Chiola did not present any of the characteristics of his synthesized materials [14].

2.2. MESOPOROUS STRUCTURES

The determination and classification of the structure is primarily based on the way pores are ordered within the structure. Other classification dependencies are the synthesis conditions (pH and material source) or the family of organic surfactant used to synthesize the structure. Therefore, contrary to the zeolites,

order of the atoms is not taken into consideration when classifying a mesopore material [14].

Stucky and his coworkers successfully synthesized mesoporous structures in acidic media. He identified and named the different structures as the cubic SBA-1 [16], SBA-11 [18] and SBA-16 [18], the hexagonal SBA-3 [16] and SBA-15 [15], the 3D hexagonal SBA-2 [16] and SBA-12 [18] and the rectangular SBA-8 (SBA stands for Santa Barbara Acid, the number follows the internal agreements of the Santa Barbara laboratory) [1,14].

Among the mesoporous materials, HSM, KIT-1 and the MSU series have also been identified and classified as different structures. These have the particularity of possessing mesopores, which are more randomly disposed compared to the ones previously summarized. These materials porosity are detected as wormholes by some researchers [1,14].

Inagaki [19] synthesized a mesoporous structure by folding kanemite layers and merging them together to form a hexagonal structure. Inagaki named this structure as FSM-16 (short for Folded Sheet Mechanism) [1,14].

In Table 2.1.1 the most commonly known mesoporous structures have been regrouped and classified according to their crystal system. As it could be observed from Table 2.1.1, it is clear that although a wide variety of structures exist, they can easily be classified with respect to their element of symmetry in their crystal system.

In order to have a better understanding in the structure composition of those mesoporous materials, the hexagonal and cubic unit cells will be briefly discussed.

Table 2.2.1. Mesoporous structure with their crystal system (adapted from [14])

Structure	Crystal system	Ref.
MCM-41	2D Hexagonal	8, 9, 23
FSM-16	2D Hexagonal	1, 19
SBA-3	2D Hexagonal	16
SBA-15	2D Hexagonal	15, 18
MCM-48	3D Cubic	23
SBA-1	3D Cubic	16
SBA-11	3D Cubic	18
SBA-16	3D Cubic	18
SBA-2	3D Hexagonal	16
SBA-12	3D Hexagonal	18
SBA-8	2D Rectangular	12

MCM-41

Due to interesting and promising structural properties, the MCM-41 is probably one of the most discussed and characterized structures in the literature. The MCM-41 consists of an amorphous (alumino, metalo)-silicate framework, forming hexagonal pores (Figure 2.2.1.a). MCM-41 structure is

unidirectional and arranged in a honeycomb structure. As shown in Figure 2.2.1.b, this special structure of MCM-41 can be characterized by the TEM analysis [1,3,4,6,8,9,14].

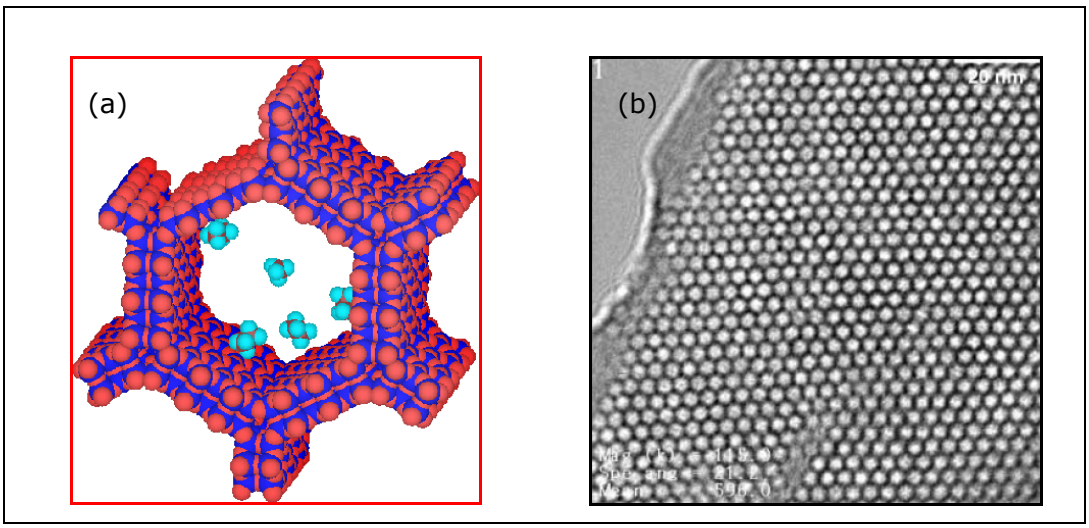

Figure 2.2.1. (a) Schematical representation of MCM-41 [21] (b) TEM image of MCM-41 [22]

Schematical representation of MCM-41 structure is shown in Figure 2.2.1.a. The hexagonal shape of the pore makes the pore surface heterogeneous. In the corners of the pore an enhanced presence of siloxane bridges has been detected [14]. These bridges help to create hydrophobic portions on the pore surface whereas the flat areas of the pore surface are hydrophilic due to the presence of hydroxyl groups – hence the sightky heterogeneous pore surfaces.

SBA-15

Similar to the MCM-41 structure, SBA-15 basically has a unidirectional hexagonal pore system. The major difference is due to the dimensions of the pores and pore walls. A typical SBA-15 structure exhibits an average pore diameter of 6 nm and amorphous pore walls of 3 nm thickness [15]. Presence of micropores within the pore walls of SBA-15 materials is a very interesting feature of this class of material [1,14,15].

MCM-48

The structure of MCM-48 was reported to be much more complex than the structure of MCM-41 or SBA-15. The unit cell of MCM-48 has a cubic symmetry. The surface of the cells was reported to divide the cube into two identical but separate compartments, creating two independent 3D pore systems. The two independent pore systems are interlocked and will run along the [111] and [100] directions, but will never cross or join each other. The pore systems are usually represented by micelle rods, which progress in spirals around each other towards the [100] direction [14,23]. Such complex symmetry gives a rather complicated XRD patterns.

Collart reported the pore diameter of the MCM-48 varied with the synthesis conditions and is situated between between 2.7 and 4.6 nm and the average pore wall thickness was about 0.9 nm [14].

2.3. SYNTHESIS OF M41S & MCM-41

Mesoporous samples are synthesized by polymerizing a silica source around an organic template in an aqueous solvent. In order to empty the pores, the organic template is removed with the aid of calcination. However, the interaction between the organic template molecules and the silicate framework is influenced by the synthesis parameters. Thus, it is crucial to understand and control those parameters to obtain the desired structure [3,14].

Mobil researchers found that the relative concentrations of the species present in the synthesis solution effect the final pore structure to be obtained [8,9]. Then, modified MCM-41 synthesis was studied by many researchers in detail to obtain the optimum conditions for the synthesis [3,14].

2.3.1. Components of MCM-41 Synthesis

The four main component of the synthesis of MCM-41 are a silica source, a structure-directing surfactant, a solvent and a catalyst (acid or base) [3].

2.3.1.1. Silica Sources

Sodium silicate (Na_4O_4Si), sodium meta-silicate (Na_2SiO_3), fumed silica, Ludox, silica gel and tetraethyl orthosilicate (TEOS) are the silica sources which are used in the synthesis of mesoporous materials. TEOS is usually used in mesoporous material synthesis under acidic conditions and the others are generally preferred for basic conditions [3, 26].

2.3.1.2. Surfactants

The term surfactant is the contracted form of "surface active agent" and refers to a class of chemical compounds known as amphiphiles (from two Greek words meaning they are not certain what they like). The molecules of surfactants contain two parts: One part is polar (dipole or charged group), and the other part is non-polar (usually a hydrocarbon or halocarbon chain) (Figure 2.3.1). The polar part is hydrophilic and the non-polar part is hydrophobic, hence the molecule self-organizes itself in water in such a way as to minimize contact between incompatible ends [26,27].

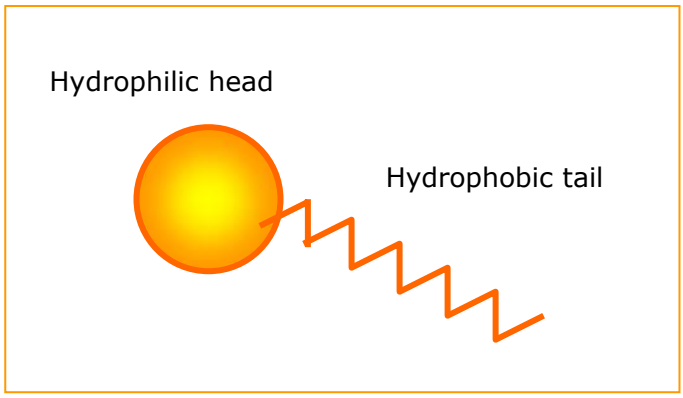

Figure 2.3.1. A typical surfactant

Ionic surfactants such as cetyltrimethylammonium chloride (CTMACl) and cetyltrimethylammonium bromide (CTMABr), are the most commonly used templating agents for the synthesis of MCM-41. In general, the use of low-molecular-weight amphiphiles with the formula $C_nH_{2n+1}(CH_3)_3N^+$ (n=8-22) or

$C_nH_{2n+1}C_5H_5N^+$ (n=12 or 16) are reported to result in the formation of MCM-41. The formation mechanism of MCM-41 is based on the electrostatic interactions between the positively charged surfactants and negatively charged silicate species in solution [26].

Varying the alkyl chain length of the surfactant molecules, the pore sizes of MCM-41 materials can be modified in the range of 2-10 nm. Table 2.2 lists some pore diameter values reported by Beck et al. [9] obtained for MCM-41 materials using different surfactants with different alkyl chain lengths. It is clearly seen that the values of the pore diameters increase as the lengths of the surfactant alkyl chains increase [3,6].

Table 2.3.1 Pore sizes of MCM-41 materials synthesized using different surfactants (adapted from [7])

Surfactant Chain Length n $C_nH_{2n+1}NMe_3$	Lattice Constant	Average Pore Size (A)
8	31	18
9	32	21
10	33	22
12	33	22
14	38	30
16	40	37

As it is reported by Taguchi et al. [1], poly(ethylene oxide) is also a versalite surfactant used for the synthesis of ordered mesoporous materials. Poly(ethylene oxide) mono ethers were tecommended to be used to form materials showing worm-like disordered or hexagonally ordered mesopores with

pore sizes being around 5 nm. One of the mostly used of groups of surfactants are the tri-block co-polymers consisting of poly(ethylene oxide)$_x$-poly-(propylene oxide)$_y$-poly(ethylene oxide)$_x$, (PEO)$_x$(PPO)$_y$-(PEO)$_x$, (trade name: Pluronics) which show the ability to form liquid-crystal structures. They are reported to be used to synthesize a variety of different ordered mesoporous materials with rather large pores in various framework compositions under strongly conditions. Here the EO (ethylene oxide) units and the cationic silicate species interact to form the mesostructured assembly [1].

2.3.1.3. Solvent

In the synthesis of MCM-41, water is used as the solvent. The amount of water used for the synthesis mixture is critical [26].

2.3.1.4. Mineralizing agents

The mineralizing agent used can be an acid or base. Mineralizing agents mineralize the silica sources into soluble species with suitable morphologies capable of associating with surfactant molecules to form various periodic mesophases. For this purpose, sodium hydroxide, tetramethylammonium huydoxide, or tetraethylammonium hydroxide can be used as basic additives and HCl, HF or HNO_3 can be used as acidic additives [3,26].

2.3.2. Formation Mechanism

The original MCM-41 synthesis was carried out in water under alkaline conditions. Organic molecules -surfactants- function as templates forming an ordered organic-inorganic composite material. Via calcination the surfactant is removed, leaving the porous silicate network. The formation of the inorganic-organic composites is based on electrostatic interactions between the positively charged surfactants and the negatively charged silicate species [9].

The first mechanism proposed in the literature for the MCM-41 synthesis was described by Beck et al. [9]. This formation mechanism was named as liquid crystal templating mechanism (LCT mechanism), which is shown in Figure 2.3.2. Beck et al. proposed that the MCM-41 structure is defined by the organization of surfactant molecules into liquid crystals which serve as templates for the formation of the MCM-41 structure. The first step in the synthesis of MCM-41 is

the formation of a micellar rod. In the second step formation of a hexagonal array of rods by the incorporation of an inorganic array of silica or silica-alumina around the rod-like structures was reported (Figure 2.3.2). Beck et al. also proposed an alternative pathway for the formation of MCM-41 as shown in Figure 3.2.3. It is a silicate anion initiated mechanism in which aggregates of cationic surfactant molecules in combination with anionic silicate species form a supermolecular structure [6].

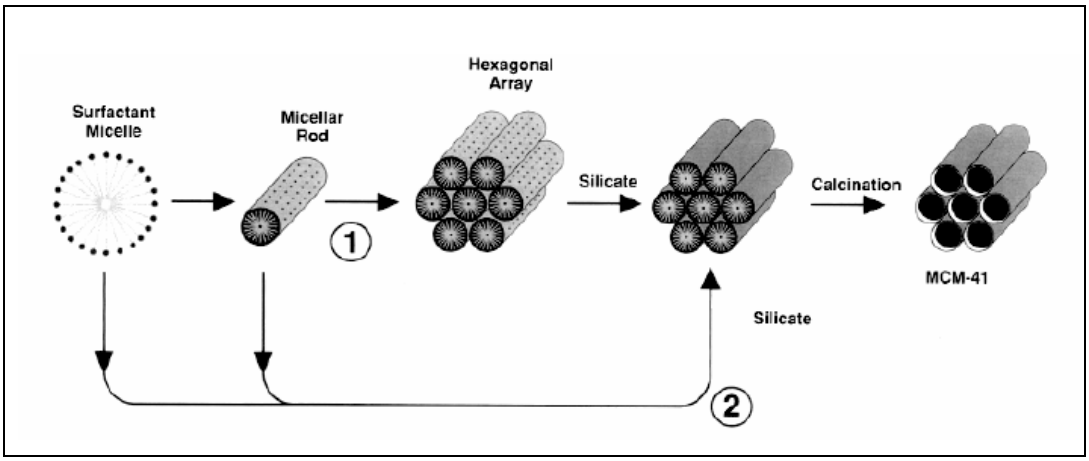

Figure 2.3.2. Liquid-crystal templating (LCT) mechanism proposed by Beck et al. [9] showing two possible pathways for the formation of MCM-41: (1) liquid-crystal-initiated and (2) silicate-initiated.

Another formation mechanism, was proposed by Stucky [28,29] and coworkers and it was called as cooperative organization of inorganic and organic molecular species into three dimensional structured arrays. In this mechanism, the formation process of MCM-41 was divided into three reaction steps (Figure 2.3.3): "(1) Prior to silica addition, the surfactant is assumed to be in a dynamic equilibrium between spherical or cylindrical micelles and single molecules. (2) Upon addition of a silica source, the predominantly multicharged silicate species ion-exchange with the OH^- or Br^- anions of surfactants to form organic-inorganic ion pairs accompanied by dissociation of the organic micelles and aggregation of the ion pairs into a new mesophase. (3) The silicatropic liquid crystal assembly process involving multidentate interaction controls the number of surfactant

molecules that can bind to a given inorganic species and determines the interface packing density and ultimately the biphase morphology" [6].

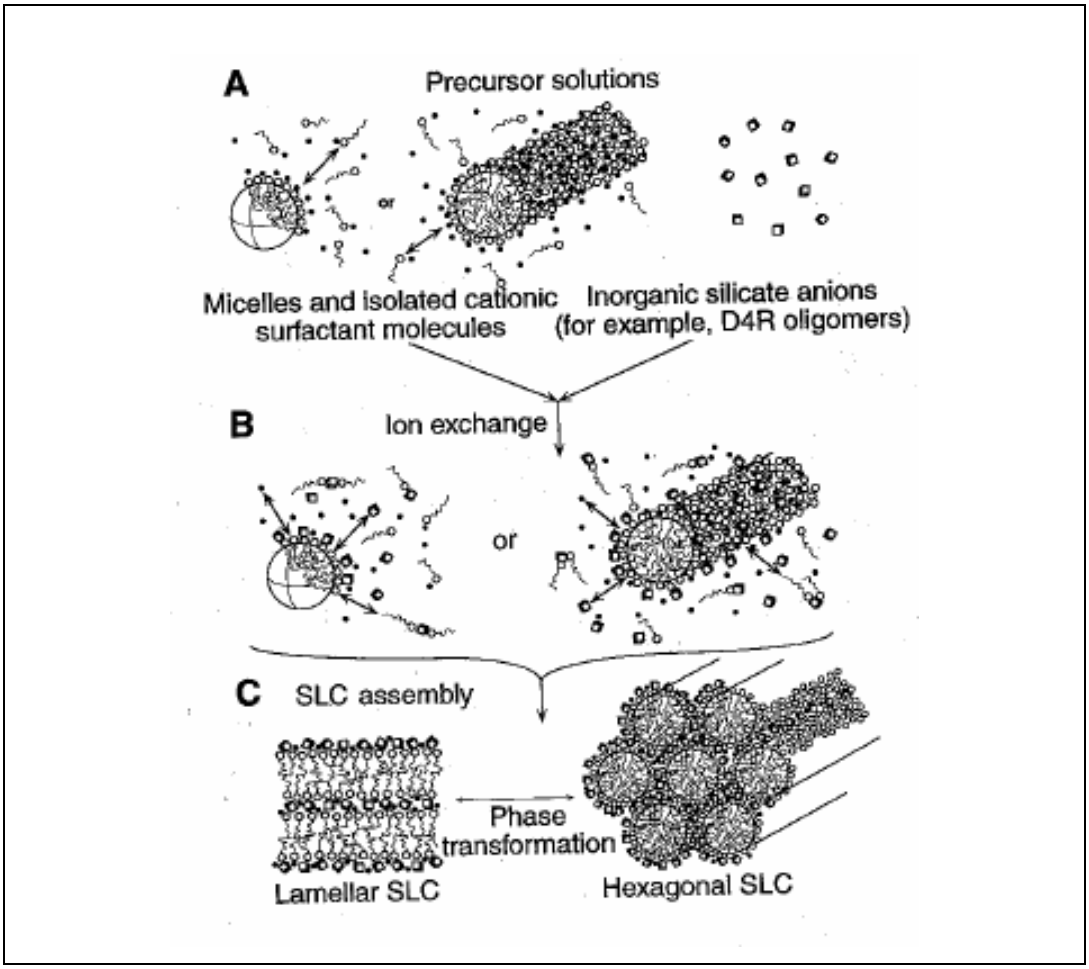

Figure 2.3.3. Cooperative formation pathway [28]

The mesopore size of these kinds of materials is primarily controlled by the length of the alkyl chain of the surfactant used. However, addition of auxiliary organic molecules such as aromatics, n-alkanes, or fatty acid can lead to an expansion of the mesopore size. Mixing of two alkyl ammnonium surfactants with different alkyl chain length can be used to fine-tune the pore size between those of the long and the short chain surfactant.

2.4. MODIFICATION OF M41S MATERIALS FOR CATALYTIC PURPOSES

MCM-41 itself is not considered as an active catalyst and sorbent for many reactions and sorption processes. Additional catalytic functions are introduced to MCM-41 by incorporation of active sites to its structure. This incorporation can be achieved by direct addition of the active sites to the structure during the synthesis, or by the modification of MCM-41 after the desired structure has been synthesized [3]. Metal or metal oxide incorporated mesoporous silicate-structured materials having high surface areas and narroe pore size distributions attracted major attention of catalysis researchers in recent years [30-34]. Certain transition metal ions are generally introduced into the framework of MCM-41 materials to produce potential catalysts with redox properties [6].

Aluminum incorporation to the MCM-41 structure was mostly studied in order to produce acidic properties. For introduction of acidic centers to the structure, alumina can be tetrahedrally introduced into the framework of MCM-41 materials [3,6].

Vanadium-containing MCM-41 materials can also be used as selective oxidation catalysts [30]. It was also found that the vanadium atoms are mostly incorporated into the silica walls and are isolated one from another [6].

Supported Pd catalysts are widely used in number of hydrogenation reactions [32,38-40] and in organic synthesis [31,41]. Catalytic combustion of VOC's [45] and catalytic decomposition of methanol to produce hydrogen [46] are some of the other recent applications of supported palladium catalysts. In a very recent comprehensive study [55], activity of Pd in the steam reforming of ethanol was also illustrated. Due to its unique property for absorbing large quantities of hydrogen, Pd also has applications in purification and storage of hydrogen. Pd incorporated high surface area porous substrates are considered as potential hydrogen storage materials [47,48]. High surface area mesoporous MCM type materials are themselves have potential applications in the confinement of hydrogen [49].

Very recently, synthesis and catalytic utilization of noble metal impregnated SiO_2 nanocomposite materials, nanoparticles and nanowires in

mesoporous silica hosts attracted the attention of number of researchers [42,46]. Such materials show attractive electrical, magnetic and catalytic properties. Fukuoka et al.[50] and Yuranov et al.[54] reported synthesis of Pd nanoparticles and nanowires with controlled size by the impregnation of palladium into the mesoporous silica templates with narrow pore size distributions, following a so called "ship-in-bottle" procedure.

2.5. CHARACTERIZATION METHODS FOR M41S MATERIALS

2.5.1 X-Ray Diffraction (XRD)

X-ray diffraction is a standard technique for describing crystal structures of solids [60]. X-ray diffraction is one of the most important techniques for characterizing the structure of ordered materials. It has been used in the study of MCM-41 materials. The two-dimensional hexagonal structure of MCM-41 can be well demonsrated by XRD. The XRD peaks do not result from crystal structure in the atomic range, but from the ordered channel walls. A well ordered two-dimensional hexagonal structure gives a sharp (100) plane diffraction peak and the diffraction peaks of higher Miller Index planes, (110), (200) and (210) [58].

2.5.2. Nitrogen Physisorption

Physisorption is a primary method for characterization of porous materials. The MCM-41 materials have uniform mesopores, ranging from 15 to 100 A, and have been characterized extensively by N_2 physisorption [58].

In nitrogen physisorption, the material is cooled to a temperature near the normal liquefaction point (77K for dinitrogen). The amount of dinitrogen is measured versus dinitrogen pressure [60]. From the resulting isotherm, pore structure information including pore sizes, surface area, and pore size distribution are obtained. For an MCM-41 isotherm, one highlight is its sharp step in the mesopore range of P/P_0=0.2 to 0.5, which represents the liquid condensation of N_2 in the uniform mesopores. The sharper the step of the isotherm the more uniform the pore size [58].

2.5.3. Transmission Electron Microscopy (TEM)

One standard method to characterize the ordered structure of materials is transmission electron microscopy (TEM). In this method, a high energy beam (100-200 keV) is used to image a thin material specimen. The high-energy electron beam transmits the sample grids and casts an image of the sample's precise structure of MCM-41, the channels, pores and the hexagonal structure. [58,60].

2.5.4. Scanning Electron Microscopy (SEM)

Scanning electron microscopy is a technique that is analogous to scanning transmission electron microscopy. The primary difference between these techniques is that scanning electron microscopy involves detection of black-scattered and secondary electrons as well as X-rays that are black-scattered from the sample, in contrast to detecting electrons transmitted through the sample. This technique can be used on thick samples, and it is effective for monitoring catalyst morphology [60].

2.5.5. X-Ray Photoelectron Spectroscopy (XPS)

Among the surface characterization methods, electron spectroscopy for chemical analysis (ESCA) is the most widely used. This method is also named as X-ray photoelectron spectroscopy (XPS). The popularity of XPS as a surface analysis technique is attributed to its high information content, its flexibility in addressing a wide variety of samples [61]. Most important is the ability of this technique to provide a quantitative analysis of the surface composition. It is of great importance because the surface and the bulk compositions may be different [60].

XPS is based on the "photoelectric effect". High energy photons hit a material with the consequent emission of electrons (photoelectrons). The basic physics of this process can be described by Einstein's law. The photoelectron kinetic energy, E_k, which is the measured quantity in the experiment, is given by:

$$E_k = h\upsilon - E_b \qquad (1)$$

where $h\nu$ is the energy of the incident radiation and E_b the binding energy of the electron in a particular level. If the incident photon is sufficiently energetic, many different levels in the sample may be ionized and thus a spectrum is produced displaying all accessible energy levels as a distribution of photoelectrons with kinetic energies governed by Eq. (1).

The surface chemical information contained in the XPS binding energies and peak shapes is also important in material studies. For example, the binding energies of core-level photoelectrons from metal atomsoften increase as the oxidation state of the atom increases. XPS can be used to monitor the surface oxidation state [60].

The complete ESCA spectrum of a material contains peaks that can be associated with the various elements (except H and He) present in the outer 10 nm of that material. The area under these peak areas and correcting them for the appropriate instrumental factors, the percentage of each element detected can be determeined [61].

CHAPTER 3

EXPERIMENTAL

3.1. SYNTHESIS OF MCM-41

MCM-41 samples were synthesized according to the procedure described by Gucbilmez et al. [30].

3.1.1. Reagents

Reagents used in the synthesis of MCM-41 are given below;

- Sodium silicate solution, $SiO_2.Na_2OH$, 27 wt% SiO_2 and 14 wt% NaOH, d 1.390, Aldrich
- Cetyltrimethylammonium bromide (CTMABr), $C_{16}H_{33}(CH_3)_3NBr$, M 364.46 g/mol, powder, 99% pure, Merck
- H_2SO_4, 4 M (prepared in the laboratory)
- Deionized water

3.1.2. Procedure

Main steps of the synthesis of MCM-41 are preparation of the synthesis solution, hydrothermal synthesis, filtering the solid product, washing, drying and calcination. Steps of synthesis of MCM-41 are displayed in Figure 3.1.1.

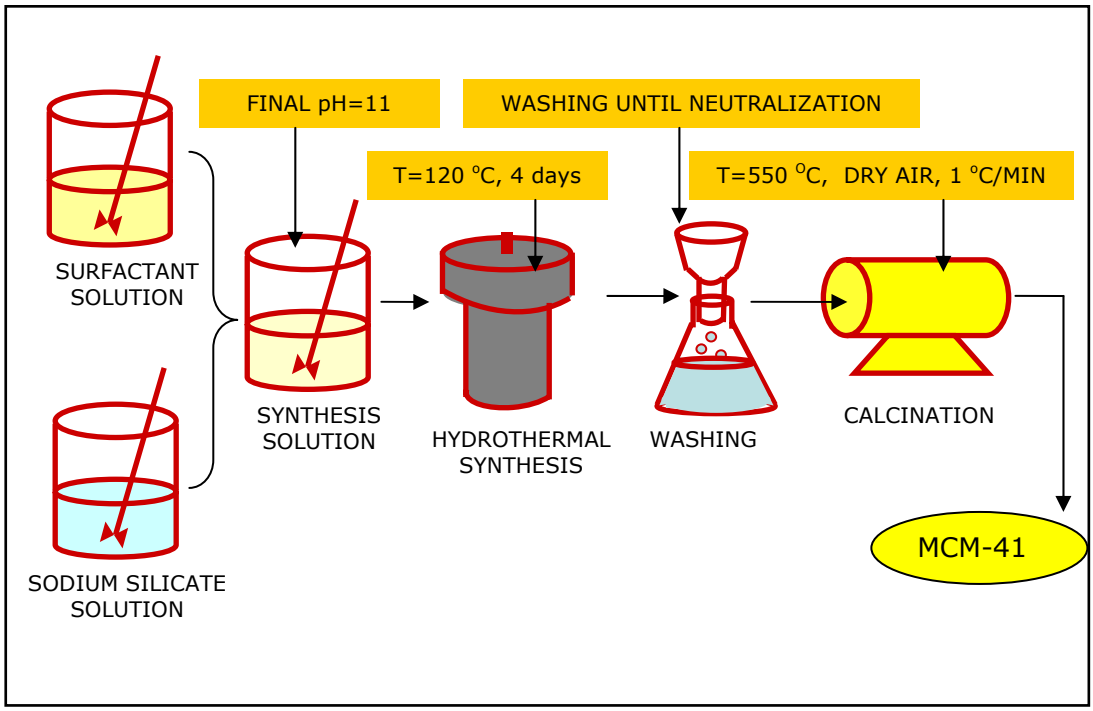

Figure 3.1.1. Main synthesis steps of MCM-41

Details of the synthesis are described below.

a. Preparation of the synthesis solution

13.2 g hexadecyltrimethylammonium bromide ($C_{16}H_{33}(CH_3)_3NBr$) (Figure 3.1.2.a) was dissolved in 87 ml deionized water (Figure 3.1.2.b). Clear solution was obtained by continuous stirring with a rate of 500 rpm. Solution temperature was kept at 30 °C. Changes in temperature may cause agglomerates. Solution temperature is important to have homogeneous solution.

When the striring was first started, color of the solution was white. After strring for 10 minutes color became lighter. Finally the clear solution was obtained. Changes in the surfactant solution were shown in Figure 3.1.3 step by step.

As shown in Figure 3.1.3.k, the pH of the surfactant solution was 6.3.

Figure 3.1.2. (a) The surfactant hexadecyltrimethylammonium bromide ($C_{16}H_{33}(CH_3)_3NBr$) (b) Starting to stir surfactant solution

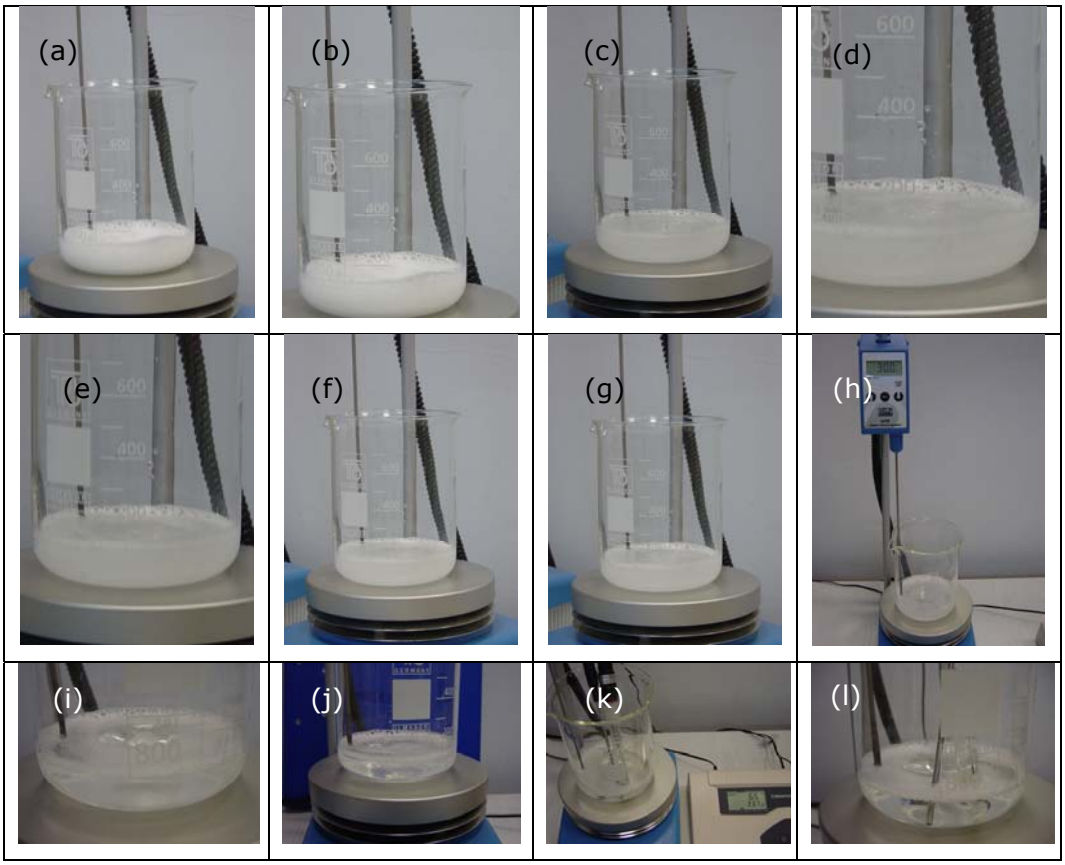

Figure 3.1.3. Preparation of clear solution from the surfactant

Sodium Silicate solution was added dropwise to the solution of hexadecyltrimetylammonium bromide (Figure 3.1.4.a).

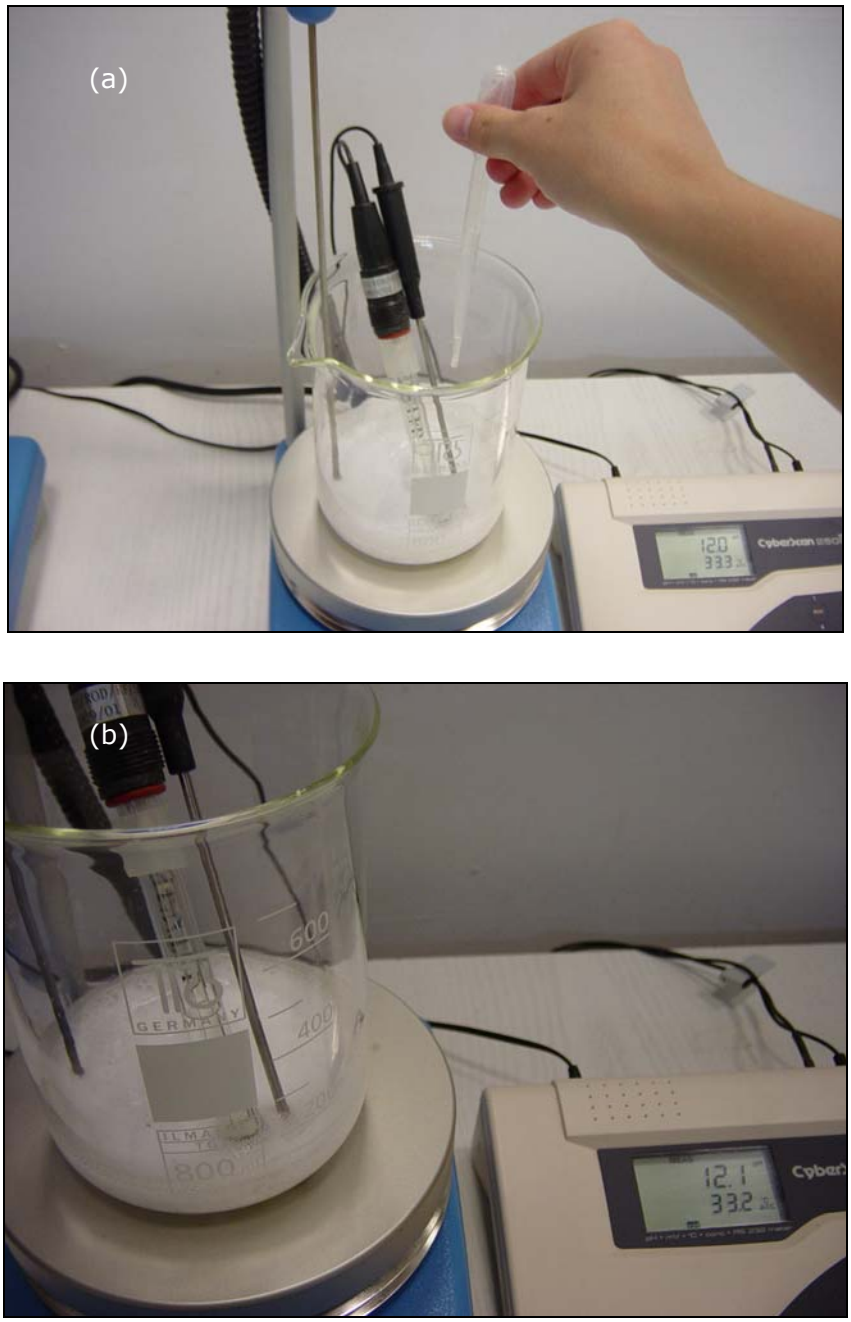

Figure 3.1.4. (a) Addition of sodium silicate solution (b) Synthesis mixture after addition of sodium silicate solution

By the addition of sodium silicate solution, pH of the synthesis mixture increased to 12.1 (Figure 3.1.4.b).

The pH of the mixture was adjusted to 11.0 by 4N H_2SO_4. Final synthesis gel was shown in Figure 3.1.5. The resulting gel was stirred for 1 h.

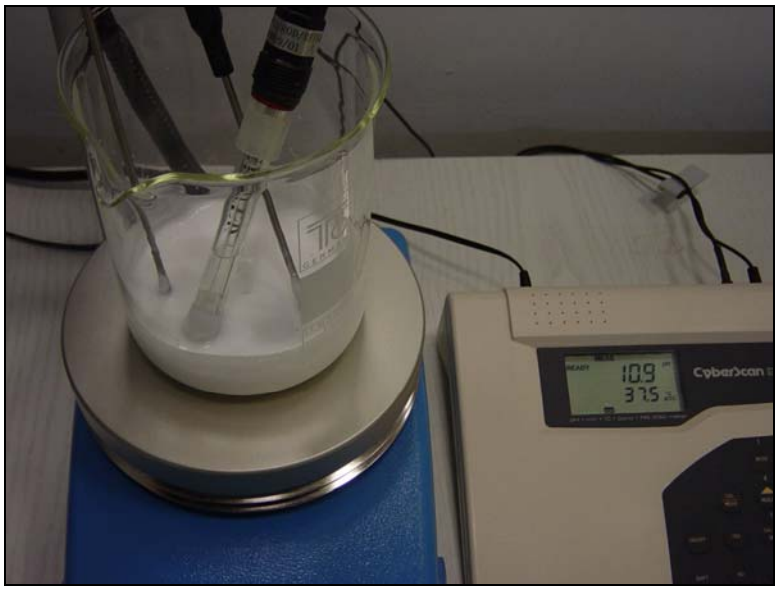

Figure 3.1.5. Final synthesis gel

b. Hydrothermal synthesis

Final synthesis gel was transferred to a teflon bottle and placed in a stainless-steel autoclave. The hydrothermal synthesis was carried out at 120 ^{o}C for 96 h (Figure 3.1.6).

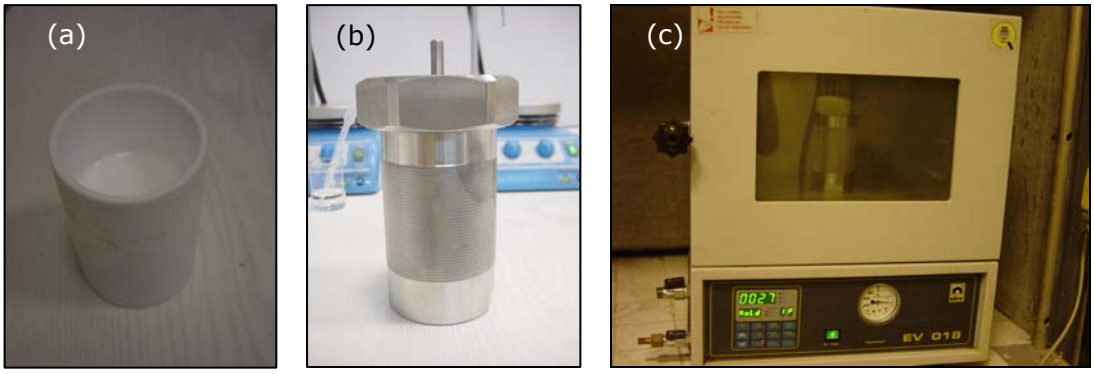

Figure 3.1.6. Hydrothermal synthesis (a) resulting gel placed in Teflon beaker, (b) autoclave (c) hydrothermal synthesis starts in etuv

c. Washing

The resultant solid was recovered by filtration, washed thoroughly with deionized water to remove Na^+ and the excess template. Washing step is shown in Figure 3.1.7. After washing, pH of the water decreases to 8.0.

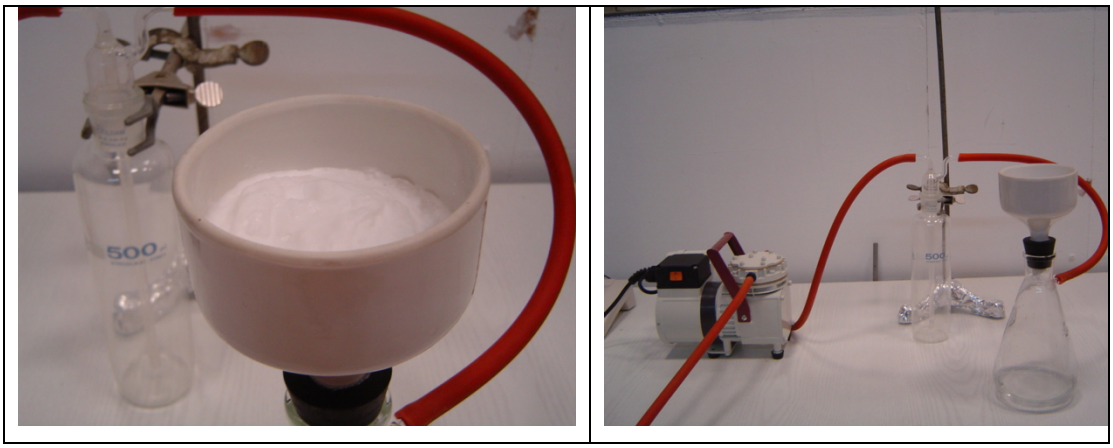

Figure 3.1.7. Washing step in the synthesis of MCM-41

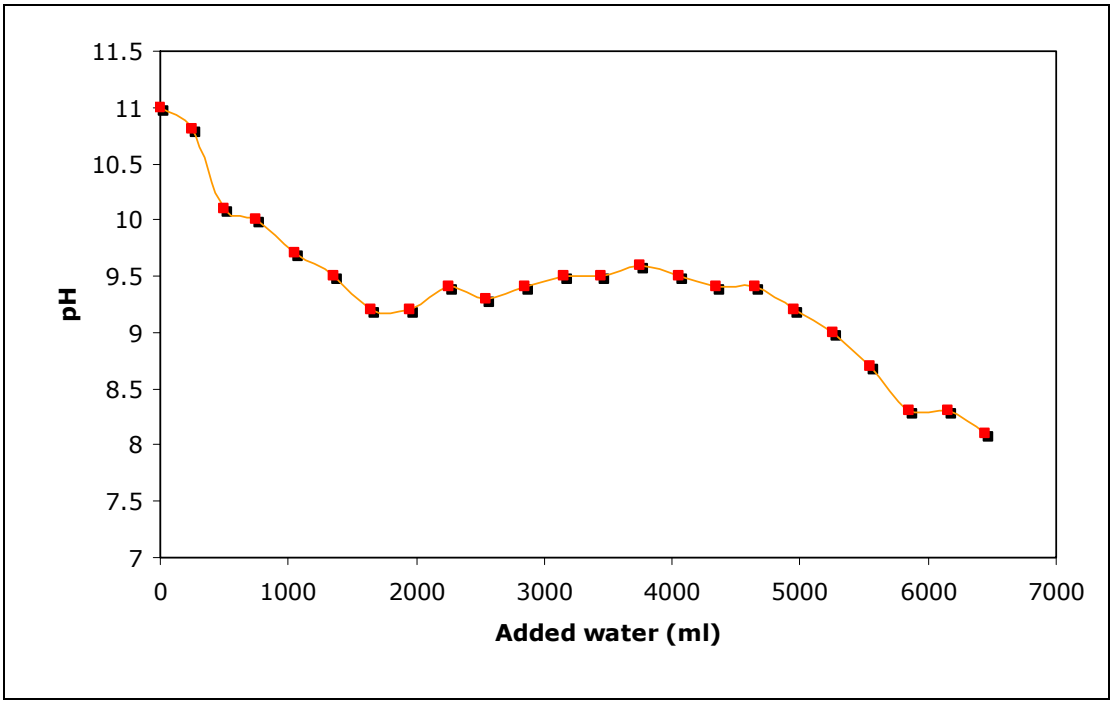

Figure 3.1.8. Decrease of pH by amount of water used for washing

Washing the material by adding water from the top was not successful. The material was too concentrated and did not allow water to expose to the pores. To overcome this situation, material was taken into a beaker, suspended in 250-500 ml of water and stirred for 15 minutes. This was repeated until the pH of the residual water remained constant. Typical pH decrease was plotted in Figure 3.1.8 by this treatment.

After washing, MCM-41 was dried at 40 ^{o}C in vacuum for 24 h.

d. Calcination

MCM-41 was finally calcined by heating from ambient temperature to 550 ^{o}C at a rate of 1 ^{o}C/min and kept at 550 ^{o}C for 6 h in a flow of dry air in a tubular furnace. A quartz tube with a membrane filter was used to place the material. The scheme of the experimental set-up for calcination is shown in Figure 3.1.9. At the end of the calcination, furnace was switched off and air was flowing while the furnace was cooling.

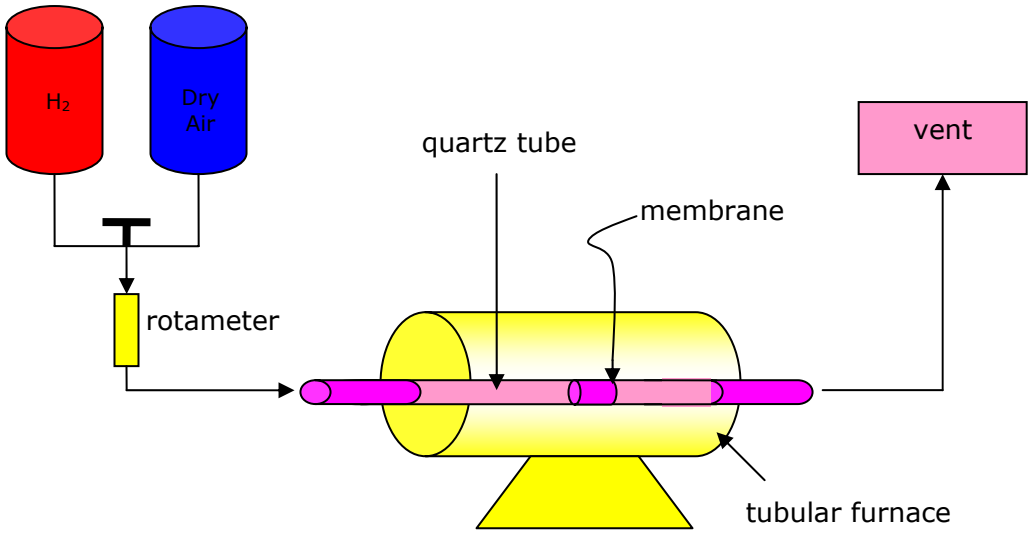

Figure 3.1.9. Experimental apparatus for calcination and reduction of the synthesized materials

3.2. SYNTHESIS OF Pd-MCM-41 BY DIRECT HYDROTHERMAL SYNTHESIS PROCEDURE

In the direct hydrothermal synthesis procedure, palladium is incorporated to MCM-41 structure during the synthesis. For this type of synthesis different palladium sources ($PdCl_2$, K_2PdCl_4, $Pd(NH_3)_4(NO_3)_2$ and different synthesis pH were studied. Also syntheses of Pd-MCM-41 nanocomposites with different Pd/Si ratio were performed.

3.2.1. Reagents

Reagents used in the synthesis of Pd-MCM-41 are given below;

- Sodium silicate solution, $SiO_2.Na_2OH$, 27 wt% SiO_2 and 14 wt% NaOH, d 1.390, Aldrich
- Cetyltrimethylammonium bromide (CTMABr), $C_{16}H_{33}(CH_3)_3NBr$, M 364.46 g/mol, powder, 99% pure, Merck
- H_2SO_4, 4 M (prepared in the laboratory)
- Deionized water
- Palladium chloride, $PdCl_2$, FW 177.3, Sigma
- Potassium tetrachloropalladate, K_2PdCl_2, Sigma
- Tetraamine palladium chloride, $Pd(NH_3)_4(NO_3)_2$, Sigma

3.2.2. Procedure

Main steps of the synthesis of MCM-41 are preparation of the synthesis solution, hydrothermal synthesis, filtering the solid product, washing, drying, calcination and reduction. Steps of synthesis of Pd-MCM-41 were displayed in Figure 3.2.1.

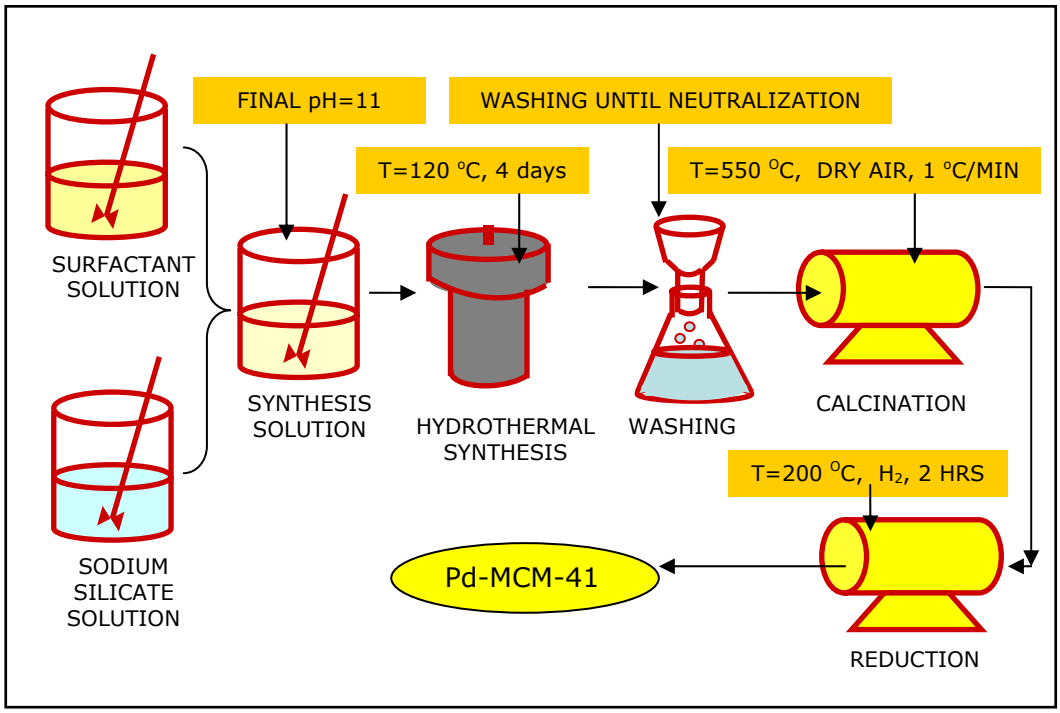

Figure 3.2.1. Steps of Pd-MCM-41 nanomaterials synthesized by direct hydrothermal synthesis procedure

a. Preparation of the synthesis solution

For direct hydrothermal synthesis, 13.2 g of cetyltrimethylammonium bromide (CTMABr) was dissolved in 87 ml of water as being in MCM-41 synthesis. Temperature of the solution was kept at 30 °C. Clear solution formed with continuous stirring at 300 rpm. 11.3 ml of sodium silicate solution was added to surfactant solution dropwise and stirried 30 minutes. pH of this solution was 11.7.

b. Preparation of the palladium solution

Palladium solution was prepared by dissolving the palladium source in water, and for some cases in water and hydrochloric acid. Palladium chloride, tetraamine palladium chloride and potassium tetrachloro palladate were used as palladium sources. The solution of Pd was added to synthesis solution dropwise (Figure 3.2.2). After the addition of Pd solution pH of the synthesis solution was adjusted to 2 or 11. Synthesis solution was stirred for 2 hours. Synthesis mixture had orange colour (Figure 3.2.3).

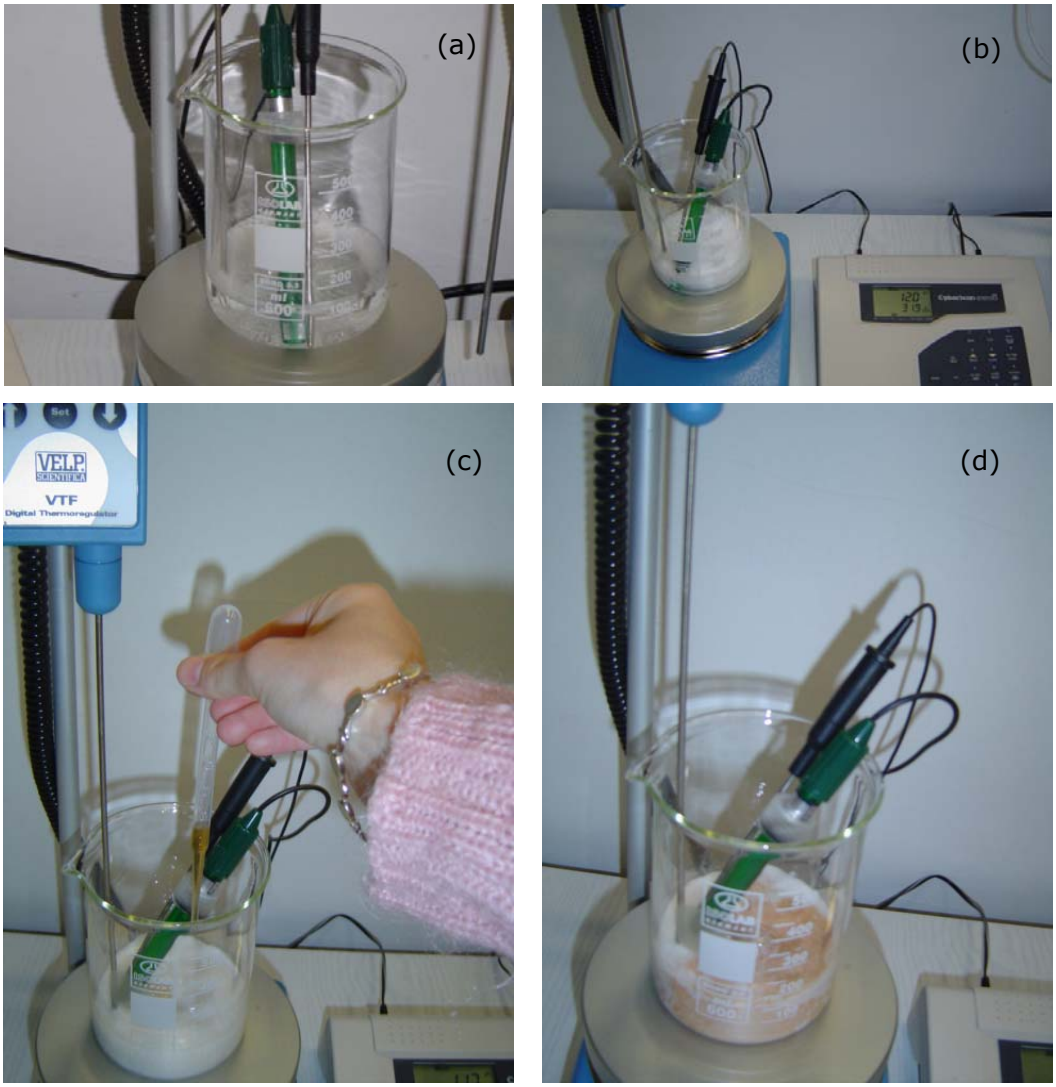

Figure 3.2.2. Direct addition of palladium solution into the synthesis solution (a) surfactant solution, (b) Synthesis gel for MCM-41, (c) Addition of palladium solution to the synthesis solution, (d) Mixing of palladium solution with synthesis solution

c. Hydrothermal synthesis

The resulting gel-solution was transferred to a Teflon bottle and placed in a stainless-steel autoclave. Then the hydrothermal synthesis was carried out at 120 ^{o}C for 96 h.

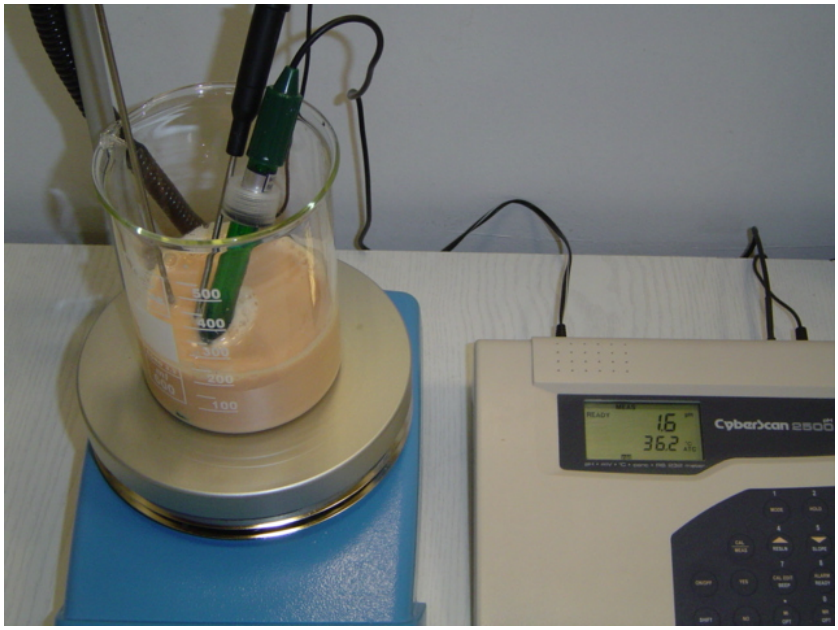

Figure 3.2.3. Final synthesis solution for Pd-MCM-41 synthesis

d. Washing

After 4 days, solid formation was observed. Color of the solid and the liquid part was orange for acidic synthesis and palladium-black for basic synthesis routes. The resultant solid was recovered by filtration. pH of the solution was 2.2 for acidic route and 11.2 for basic route.

e. Calcination

One of the Pd-MCM-41 samples [Pd-MCM-41(1)] was analyzed by TGA to find the temperature range at which calcination should be carried out. Results shown in Figure 3.2.4 indicated removal of water from the solid below 100 ^{o}C. The two peaks obtained at 284.10 ^{o}C and 364.49 ^{o}C correspond to the removal of organic template from the structure. At about 400 ^{o}C weight change due to calcination is found to be completed.

As in the syntesis of pure MCM-41, after the hydrothermal synthesis, the solid product was filtered, washed, dried and calcined at 550 ^{o}C.

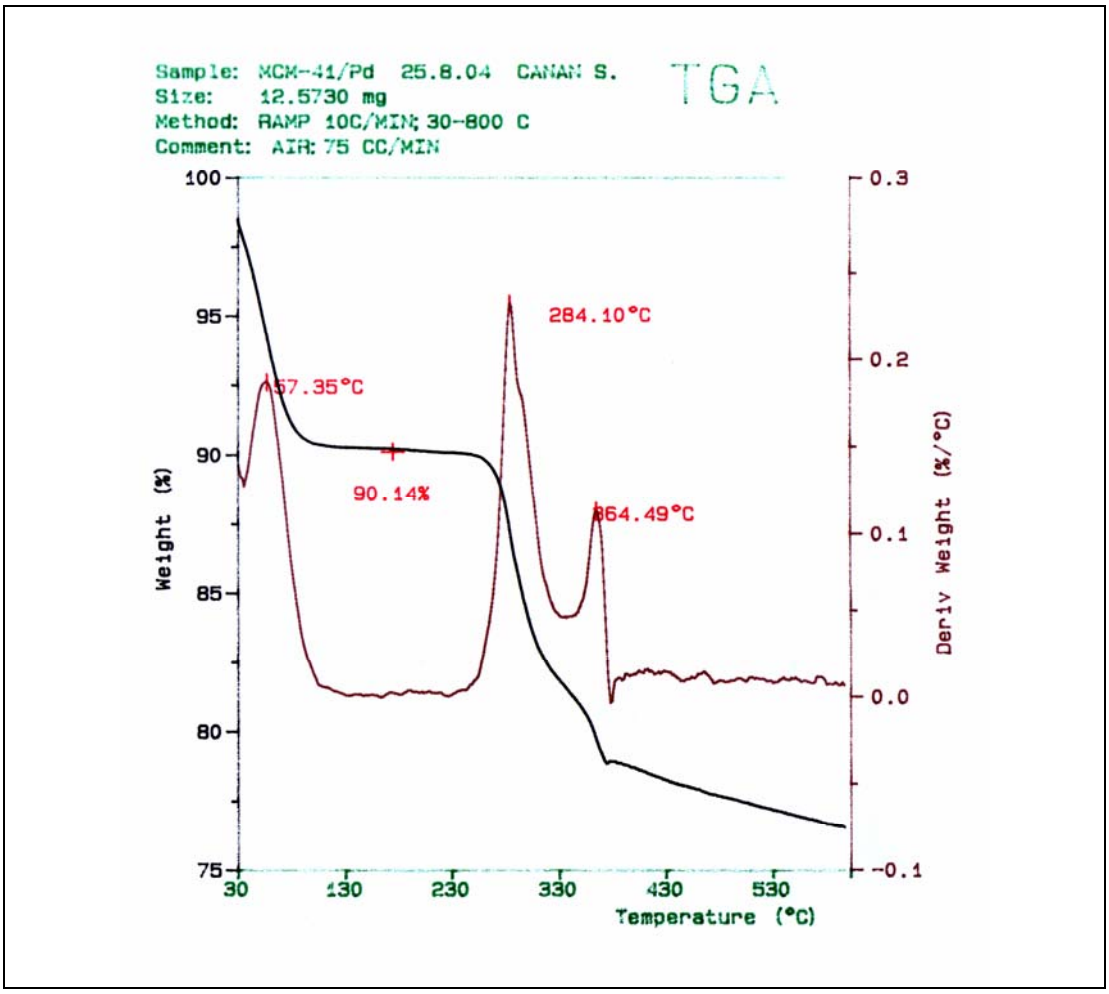

Figure 3.2.4. Thermal Gravimetric Analysis (TGA) for typical Pd-MCM-41 sample

f. Reduction

Calcined samples were swept with nitrogen gas at 200 ^{o}C and then reduced at the same temperature in a flow of hydrogen gas for two hours. Both calcined and reduced products were characterized by XRD, EDS, XPS and BET analyses.

In the synthesis procedure, Pd/Si atomic ratio was varied from 0.011 to 0.064 in the synthesis solution (Pd/Si wt ratio beween 0.04 and 0.24).

3.3. SYNTHESIS OF Pd@MCM-41 BY IMPREGNATION PROCEDURE

In the preparation of Pd@MCM-41 nanocomposite materials a procedure similar to the one used by Fukuoka et al. [50] was used.

3.3.1. Reagents

Reagents used in the synthesis of Pd/MCM-41 are given below;

- MCM-41 material
- Deionized water
- Palladium chloride, $PdCl_2$, FW 177.3, Sigma
- HCl, conc.

3.3.2. Procedure

Basic steps of Pd@MCM-41 synthesis is given in Figure 3.3.1.

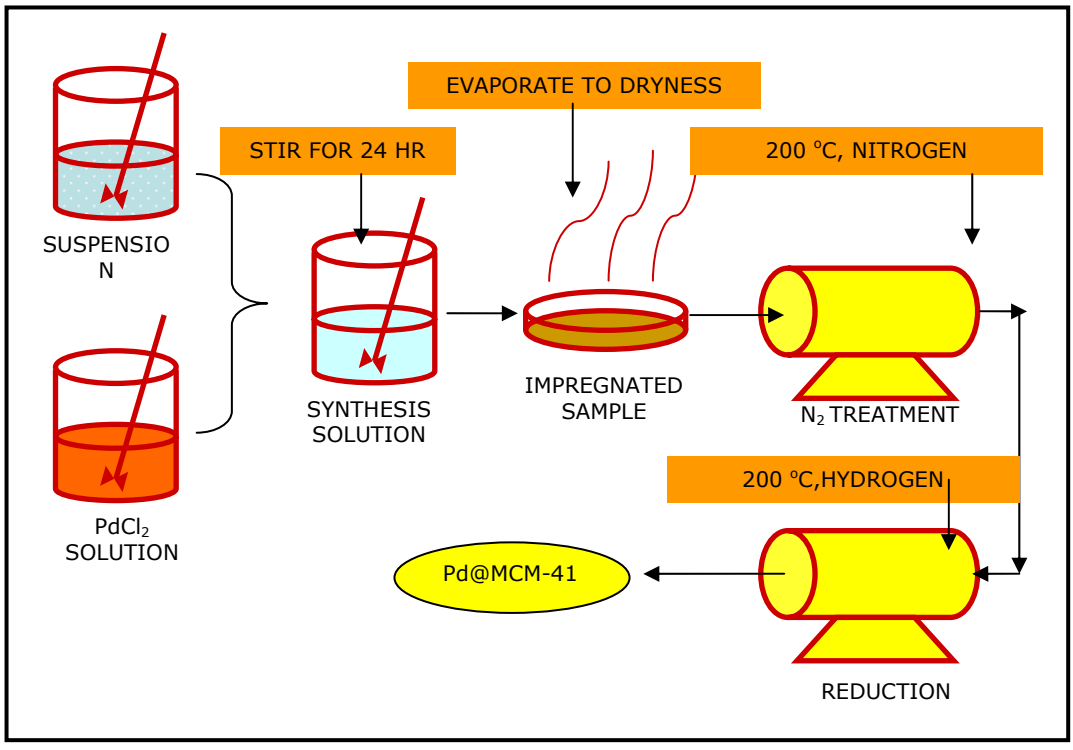

Figure 3.3.1. Synthesis steps of Pd nanoparticles inside MCM-41

a. Host Material

MCM-41 materials synthesized following the procedure described in Chapter 3.1 were used as host materials for palladium nanoparticles. [MCM-41(2)] and [MCM-41(3)] were used for this purpose. MCM-41 samples were dried under vacuum at 200 ^{o}C for 2 hours before used as hosts.

b. Palladium Solution

$PdCl_2$ was dissolved in concentrated HCl and the solution was evaporated to dryness to give H_2PdCl_4. The resudual was dissolved in water.

c. Impregnation

MCM-41 was suspended in water. The solution of palladium was added to the suspension of MCM-41. The mixture was stirred for 24 hr, evaporated to dryness, and dried under vacuum for 24 h.

d. Reduction

The impregnated sample, H_2PdCl_4-MCM-41 was purged with N_2 flow (35-40 ml min^{-1}) at 200 ^{o}C for 2 h. The treated sample was reduced in H_2 flow at 200 ^{o}C for 2 h. Finally, N_2 was treated for 5 minutes.

3.4. MATERIAL CHARACTERIZATION

X-ray diffraction (XRD), nitrogen physisorption, energy dispersive spectroscopy (EDS), scanning electron microscopy (SEM), transmission electron microscopy (TEM), X-ray photoelectron spectroscopy (XPS) and temperature programmed reduction (TPR) were employed for the characterization of the prepared material.

3.4.1. X-Ray Diffraction (XRD)

X-ray diffraction for the identification of the crystalline phases was performed by Rigaku D/MAX2200 diffractometer in Metallurgical and Materials Engineering at METU.

3.4.2. Nitrogen Physisorption

Surface area (BET, BJH) and pore structure information were obtained by the nitrogen adsorption technique. These measurements were performed by Quantachrome Autosorb 1C at Gazi University and by Micromeritics ASAP 2000 at METU.

Materials were prepared for the analyses by drying under vacuum overnight at 110 ^{o}C.

3.4.3. Energy Dispersive Spectroscopy (EDS)

Chemical compositions of the synthesized materials were measured by the JEOL 6400 apparatus at METU. Samples were coated with gold for the analyses.

3.4.4. Scanning Electron Microscopy (SEM)

SEM images were obtained from Metallurgical and Materials Engineering of METU, Sabanci University and Tubitak Marmara Research Center.

3.4.5. X-ray Photoelectron Spectroscopy (XPS)

The XPS spectra of Pd-MCM-41 and Pd@MCM-41 materials before and after H_2-reduction were obtained. The XPS measurements were performed with the SPECS instrument at the Central Laboratories in METU. The analyses were also made after ion bombardment (Ar^+) at 5000 eV for 2 min. The binding energy of the C is at 284.6 eV was taken as reference in the XPS measurements.

3.4.6. Temperature Programmed Reduction (TPR)

The TPR experiments with H_2 were carried out in the experimental set-up given in Figure 3.4.1. 0.2 g material samples were used in the analysis. The inlet total flow was 50 cm^3/min with a composition of 5% H_2 in He.

The experimental set-up consists of adsorbate (H_2) and diluent (He) gas cylinders joined to a differential fixed-bed reactor placed into a temperature-controlled furnace and a mass spectrometer connected on line to the outlet stream leaving the reactor for the simultaneous analysis of the products. The scheme of the experimental set-up is shown in Figure 3.4.1. A quartz tube with 73 cm length and 17 mm inside diameter was used to place the powder catalysts inside within quartz wool. The catalyst part was 1.5-2 cm in length. The flow rate of He was measured by flowmeter (Aalborg model GFM171) and that of H2 by rotameter (Cole-Parmer). Figure 3.4.2 presents the photograph of the set-up.

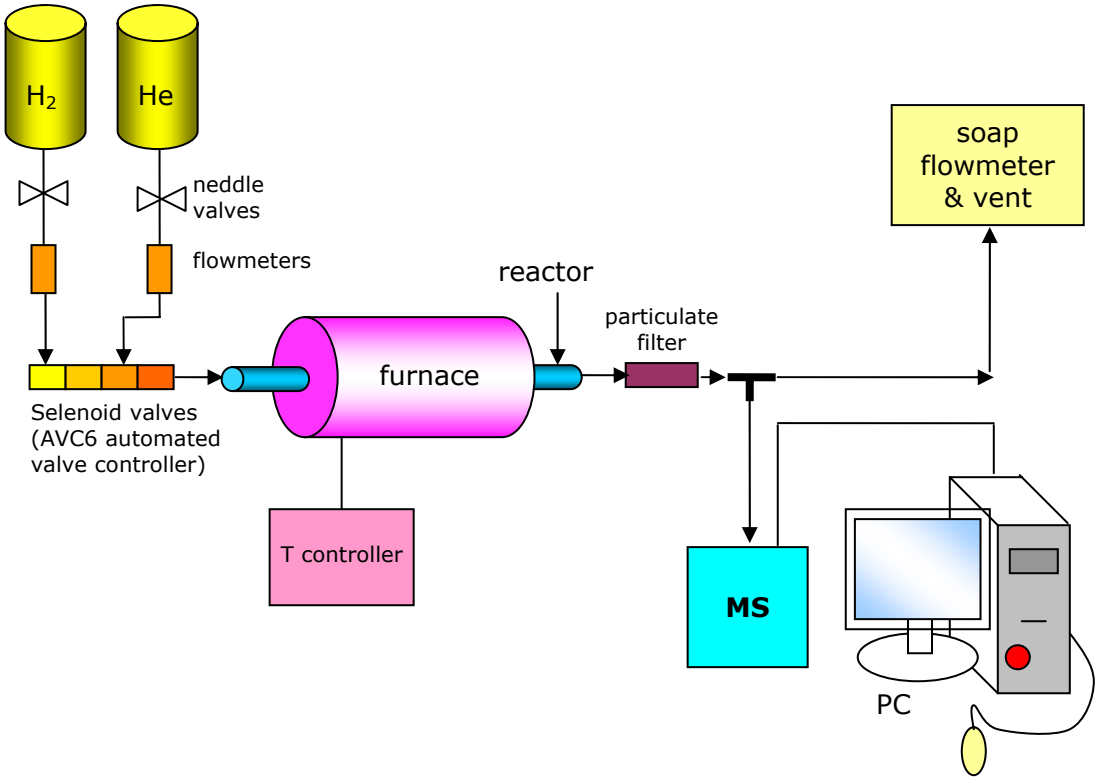

Figure 3.4.1. Experimental set-up for TPR studies

Figure 3.4.2. Photograph of experimental set-up

The mass spectrometer which was used in the system is 'Hiden Analytical HPR20 Gas Analysis System'. Its basic system comprises an ultra-high vacuum (UHV) housing, inlet system, turbo molecular pump and gauges. The inlet system is by-pass pumped and has a heated capillary sampling line.

The QIC (Quartz Inert Capillary) fast sampling capillary inlet of the system provides a dynamic method of sampling of the gases by the mass spectrometer. Two pressure reduction stages are employed to reduce the sample pressure to an acceptable level for the operation of the mass spectrometer ion source. In the first stage, the sample gas to be analysed is drawn down the silica capillary by the sample bypass pumping line. The sample gas which exists the capillary at low pressure and high velocity impinges on a platinum orifice providing the second stage pressure reduction. The flow then directly enters the mass spectrometer ion source. Continuous heating of the inlet capillary, orifice and sample bypass regions minimizes the condensation of vapors and the adsorption of the sample gas. The pressure at the capillary/orifice interface

depends on the sample bypass line pumping speed which is adjusted by the sample bypass control valve [63].

The system also has the AVC6 Automated Valve Controller which provides the control of four solenoid valves. In the temperature programmed desorption experiment, these solenoid valves were used as a mixing chamber for the gases in the system.

CHAPTER 4

RESULTS AND DISCUSSION

4.1. CHARACTERIZATION OF MCM-41 SAMPLES

MCM-41 samples were synthesized according to the procedure described in Chapter 3.1. Samples were characterized by X-ray diffraction (XRD), nitrogen adsorption, scanning electron microscopy (SEM) and energy dispersive spectroscopy (EDS) techniques. Although several and reproducible MCM-41 materials have been synthesized, only four of the characterized MCM-41 samples are presented and discussed (Table 4.1.1).

Table 4.1.1. Performed characterizations for MCM-41 samples

Sample	Date of Synthesis	XRD Analysis	BET Analysis	SEM/EDS Analysis
[MCM-41(2)]	14/07/2004	✓	✓	-
[MCM-41(3)]	15/07/2004	✓	✓	✓
[MCM-41(4)]	05/09/2004	✓	-	-
[MCM-41(5)]	15/06/2005	✓	-	-

4.1.1. X-Ray Diffraction (XRD) Analysis

XRD provides direct information of the pore structure of the materials. For mesoporous materials, the diffraction patterns only have reflection peaks in the low-angle range, meaning 2θ less than 10. No reflections are seen at higher angles. It has thereby been concluded that the pore walls mainly are amorphous. The ordering lies in the pore structure, and the low-angle diffraction peaks can be indexed according to different lattices [3]. From d_{100} value, calculation of parameter a in a hexagonal lattice is done by using the formula

$$a = 2 \times d_{100} / \sqrt{3} \qquad (4.1)$$

Unit cell parameter a and d_{100} are shown in Figure 4.1.1. Pore wall thickness δ can be calculated from the formula given below [57]

$$\delta = a - 2 \times r \qquad (4.2)$$

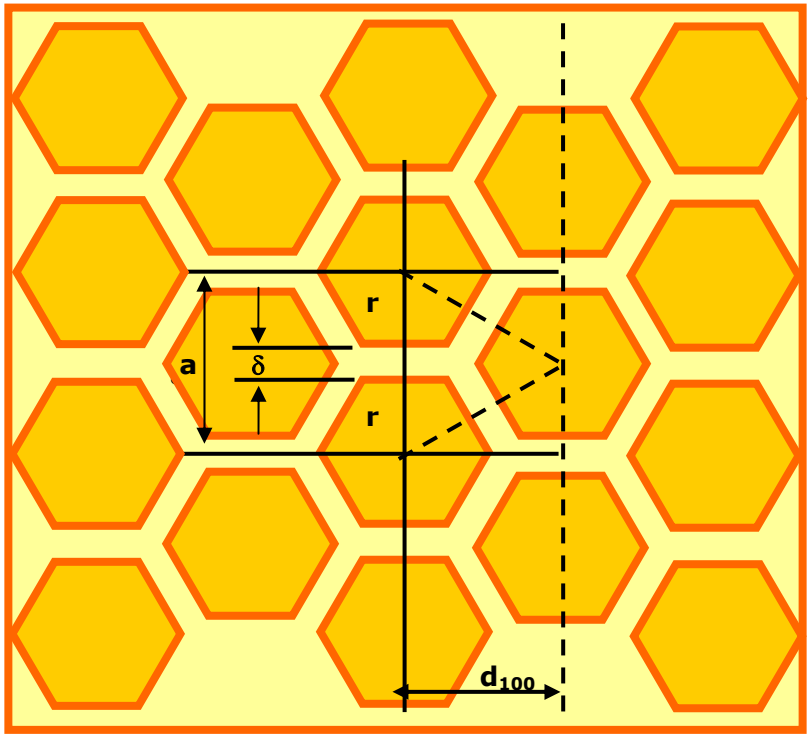

Figure 4.1.1. Schematical representation of pores of MCM-41 (adapted from [56])

Figure 4.1.2 shows the XRD pattern of the [MCM-41 (5)]. XRD spectrum of the sample displayed a sharp (100) peak and three reflections, demonstrating that those samples have a two-dimensional hexagonal structure. Reflection angles and d-spacings for different MCM-41 materials are given in Table 4.1.2. Exactly the same XRD patterns are obtained from different syntheses.

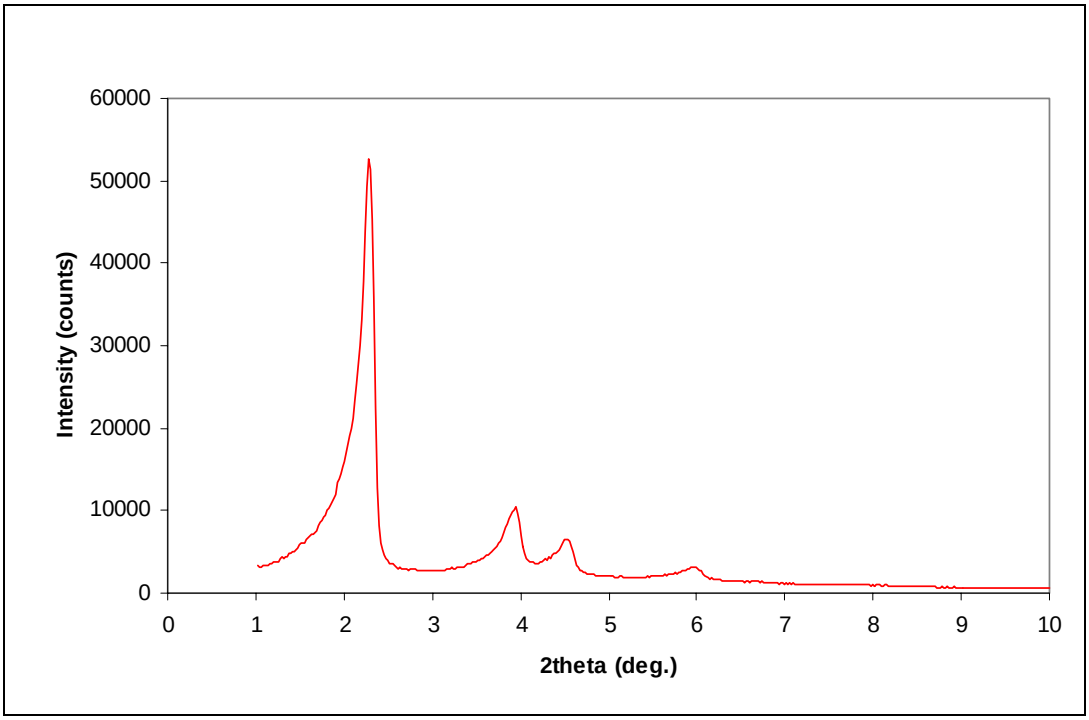

Figure 4.1.2. XRD pattern of [MCM-41(5)]

A typical MCM-41 material synthesized should have a major peak at 2.49° and three reflections corresponding to 4.27°, 4.93° and 6.50° [26]. Despite the difficulty in seeing the last reflection in the XRD pattern, the 2θ values obtained for the synthesized samples and the expected 2θ values match very well. Sharp and noise-free peaks of the MCM-41 sample indicate a successful synthesis of the desired structure.

Table 4.1.2. XRD results and d-spacings of synthesized MCM-41 structures

Sample	hlk	d-value (nm)	2θ (deg.)
[MCM-41 (2)]	100	3.60	2.455
	110	2.11	4.190
	200	1.85	4.775
	210	1.42	6.230
[MCM-41 (3)]	100	3.61	2.445
	110	2.12	4.155
	200	1.83	4.830
	210	1.41	6.265
[MCM-41 (4)]	100	3.65	2.420
	110	2.11	4.180
	200	1.84	4.810
	210	1.39	6.370
[MCM-41 (5)]	100	3.87	2.280
	110	2.25	3.920
	200	1.95	4.520
	210	1.48	5.980

4.1.2. SEM/EDS Analysis

Energy Dispersive Spectrum (EDS) of sample [MCM-41(3)] is given in Figure 4.1.3. Silicium and oxygen peaks were observed clerly from EDS pattern.

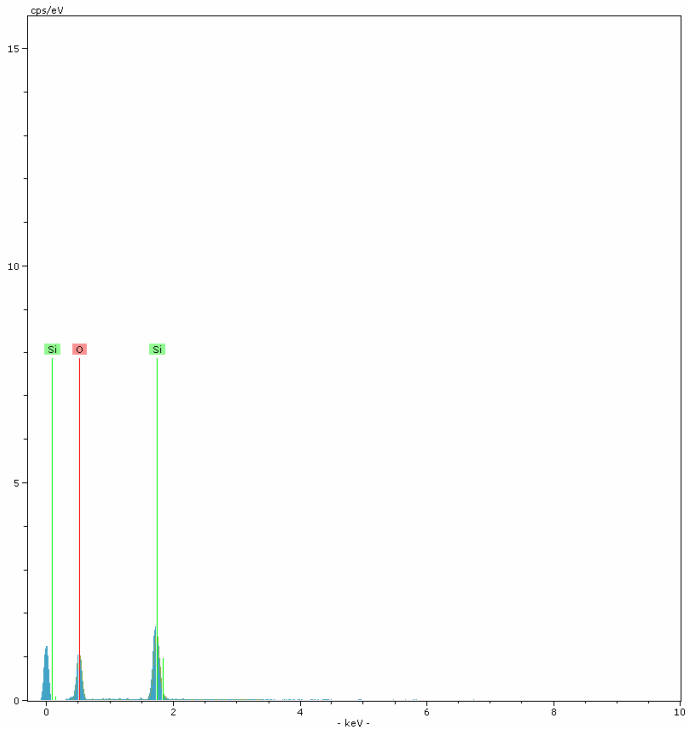

Figure 4.1.3. Energy Dispersive Spectrum (EDS) of [MCM-41(3)] sample

Elemental analysis obtained from EDS is given in Table 4.1.3. EDS analysis gives oxygen atomic concentration as 68.97% and that of silicium as 31.03%. These results proved that the structure of the synthesize material was in SiO_2 form.

Table 4.1.3. EDS Analysis of [MCM-41(3)]

Element	Weight %	Atomic %
O	55.87	68.97
Si	44.13	31.03

Scanning electron microscopy (SEM) images of the sample [MCM-41(3)] were given in Figure 4.1.4.

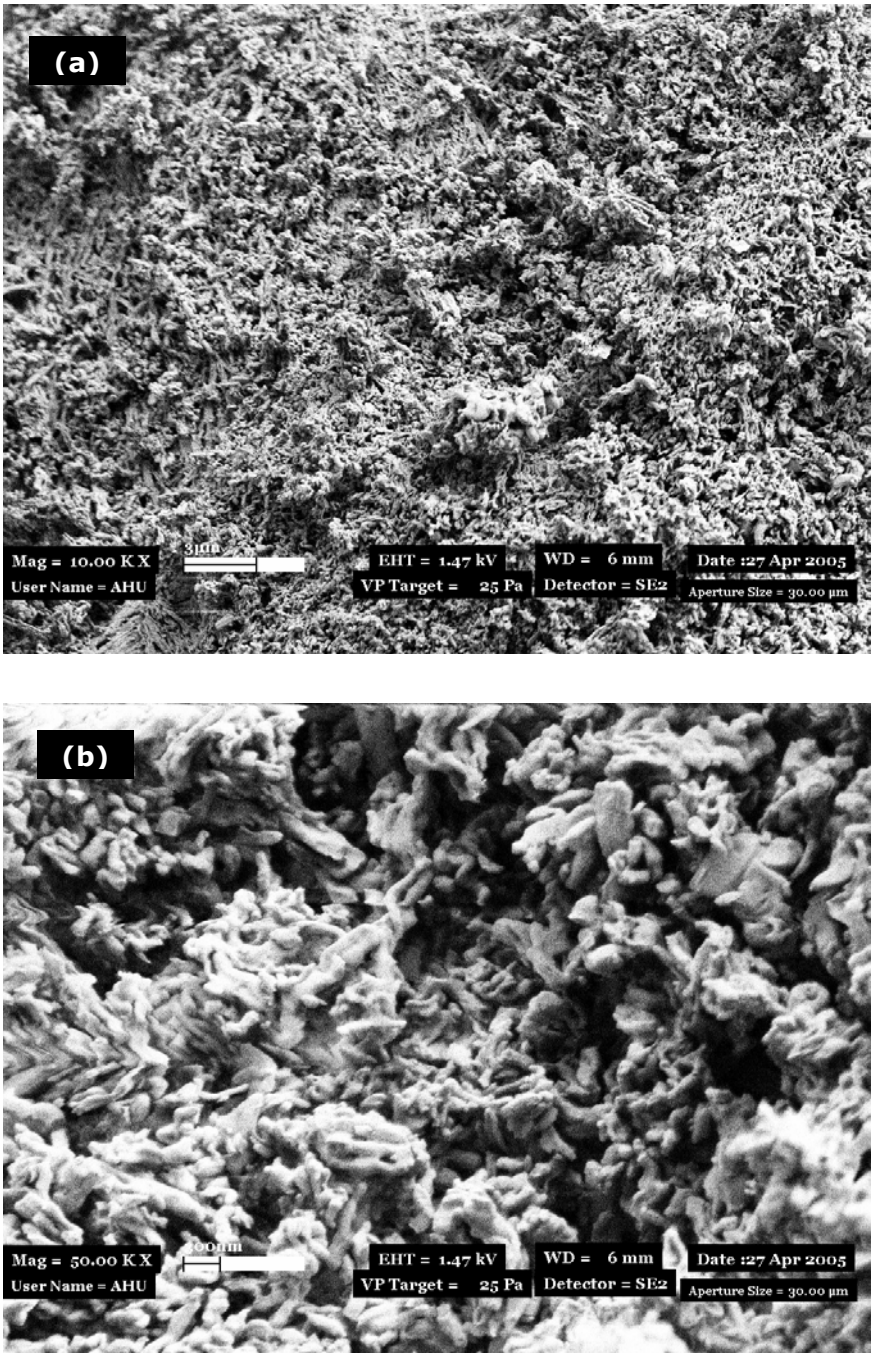

Figure 4.1.4. SEM images of [MCM-41(3)] (a) magnified 10000 times, (b) magnified 50000 times

4.1.3. Nitrogen Physisorption Analysis

The BET surface areas, the BJH adsorption pore diameters and the BJH adsorption and desorption pore volumes of the synthesized MCM-41 materials

were obtained using their nitrogen adsorption and desorption isotherms. Nitrogen adsorption experiments of MCM-41 samples were performed by Micromeritics ASAP 2000 in Middle East Technical University Chemical Engineering Department.

BET plot and nitrogen adsorption-desorption isotherm of [MCM-41(3)] are given in Figures 4.1.5 and 4.1.6, respectively. The nitrogen adsorption isotherm of the product obtained following described synthesis route, [MCM-41(3)], showed a typical Type IV isotherm, as described by the IUPAC classification (Figure 4.1.6).

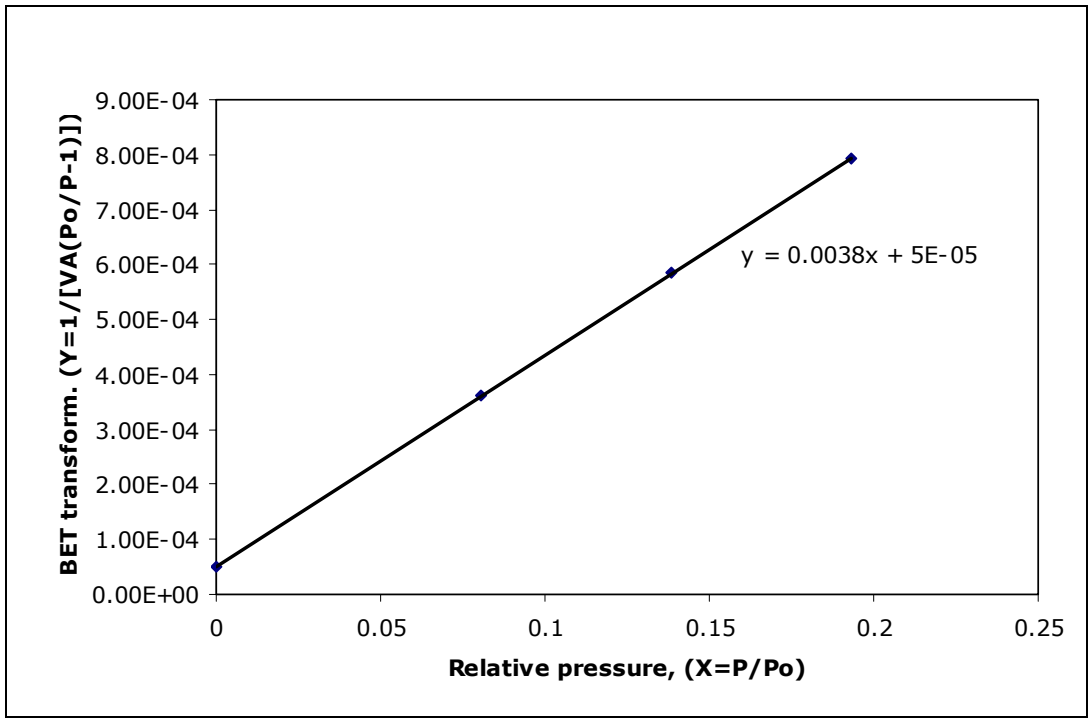

Figure 4.1.5. BET plot of [MCM-41(3)]

BET, BJH and single point surface areas of synthesized MCM-41 materials are listed in Table 4.1.4. Table 4.1.5 gives single point and BJH pore volume values of MCM-41 samples. It is clearly seen from Table 4.1.4 that high surface area MCM-41 could be synthesized. Pore volumes are high enough to use the materials as hosts.

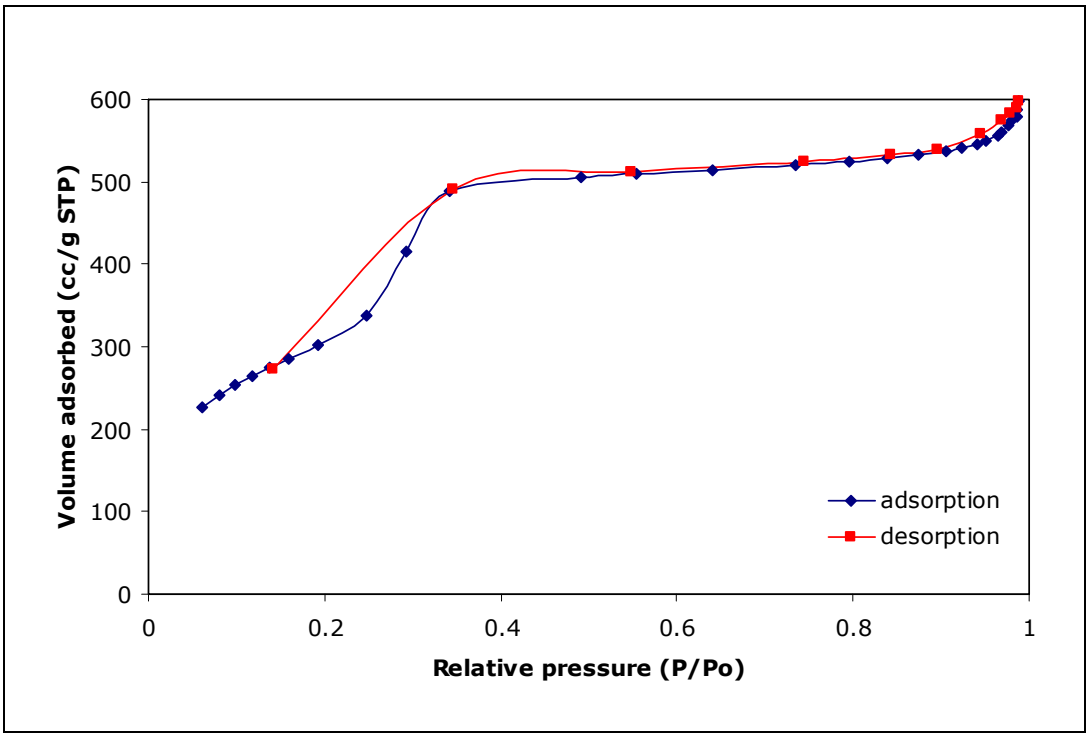

Figure 4.1.6. Nitrogen adsorption-desorption isotherm of [MCM-41(3)]

Table 4.1.4. Surface areas of synthesized MCM-41 samples

Sample	BET Surface Area (m^2/g)	BJH Adsorption Surface Area (m^2/g)	BJH Desorption Surface Area (m^2/g)	Single Point Surface Area at P/P_o 0.19 (m^2/g)
MCM-41(2)	1076.3	1434.3	1944.1	1026.3
MCM-41(3)	1123.3	1457.8	1823.7	1061.2

In Table 4.1.6, pore diameter values for MCM-41 samples are listed. All the samples synthesized have pore sizes in the mesoporous range. Pore size distribution curves for adsorption and desorption for the sample [MCM-41 (3)] are given in Figure 4.1.7. As shown in the figure, pore size distribution of MCM-41 is very narrow.

Table 4.1.5. Pore volumes of synthesized MCM-41 samples

Sample	Single Point Total Pore Volume at P/Po 0.9831 (cc/g)	BJH Adsorption Pore Volume (cc/g)	BJH Desorption Pore Volume (cc/g)
[MCM-41(2)]	0.91	1.03	1.02
[MCM-41(3)]	0.90	1.03	1.03

Table 4.1.6. Pore diameters of synthesized MCM-41 samples

Sample	Average Pore Diameter (nm)	BJH Adsorption Average Pore Diameter (nm)	BJH Desorption Average Pore Diameter (nm)
[MCM-41(2)]	3.39	2.87	2.10
[MCM-41(3)]	3.19	2.83	2.26

By using nitrogen adsorption analysis and X-ray diffraction analysis, pore wall thickness of the samples were calculated. Pore wall characteristics of synthesized MCM-41 samples are given in Table 4.1.7.

Table 4.1.7. Pore wall properties of synthesized MCM-41 samples

Sample	$d_{(100)}$ (nm)	Lattice Parameter	BJH Pore Diameter d_{pore} (nm)	Pore Wall Thick. δ (nm)
[MCM-41(2)]	3.60	4.16	2.87	1.29
[MCM-41(3)]	3.61	4.17	2.83	1.34

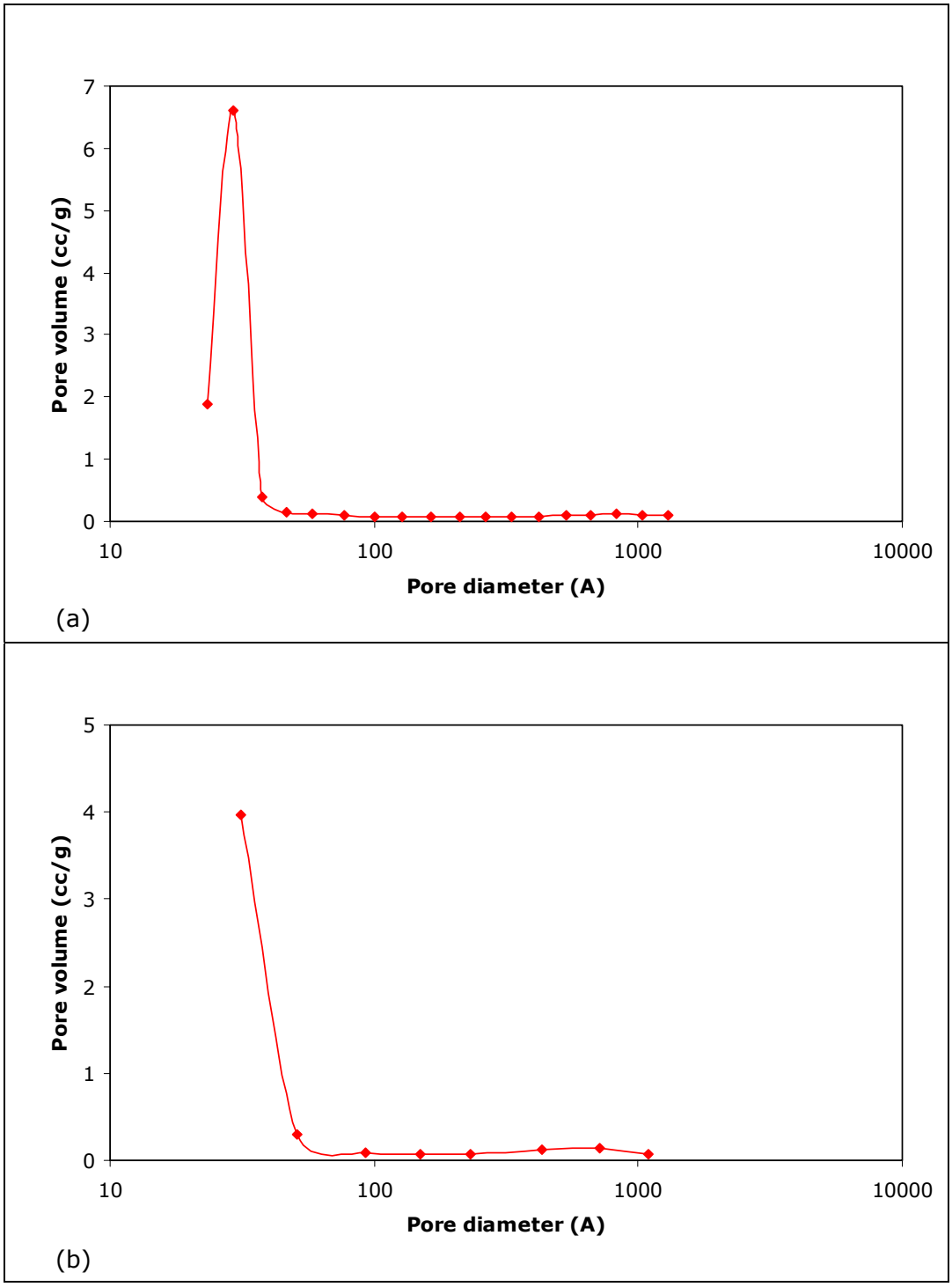

Figure 4.1.7. Pore size distribution of [MCM-41(3)] (a) BJH adsorption pore size distribution, (b) BJH desorption pore size distribution

4.2. CHARACTERIZATION OF Pd-MCM-41 SAMPLES SYNTHESIZED BY DIRECT HYDROTHERMAL SYNTHESIS

Pd-MCM-41 samples were prepared according to the procedure described in Chapter 3.2. Pd/Si atomic ratio was varied from 0.011 to 0.064 in the synthesis solution (Pd/Si weight ratio between 0.04 and 0.24), so the effect of amount of Pd loading was examined. Also, the synthesis conditions of Pd/MCM-41 nanocomposites synthesized by direct hydrothermal synthesis technique were discussed. For this purpose, syntheses at acidic and basic conditions and syntheses with different palladium precursors were performed. In Chapter 4.2.1 fully characterized Pd-MCM-41 sample is presented. Effects of palladium loading, pH and palladium source onto the modified structure are discussed in Chapters 4.2.2, 4.2.3 and 4.2.4, respectively. Table 4.2.1 summarizes the samples synthesized by following direct hydrothermal synthesis procedure and the characterization techniques used in the analysis of all samples.

Table 4.2.1. Characterization techniques used for Pd-MCM-41 samples synthesized by following direct hydrothermal synthesis procedure

Sample	Date of Synt.	XRD	BET	EDS	SEM	TEM	XPS
[Pd-MCM-41(1)]	01/08/2004	✓	✓	✓	✓	-	-
[Pd-MCM-41(2)]	06/09/2004	✓	✓	✓	✓	✓	✓
[Pd-MCM-41(5)]	04/09/2004	✓	✓	✓	✓	-	-
[Pd-MCM-41(6)]	11/11/2004	✓	✓	✓	✓	-	-
[Pd-MCM-41(7)]	12/11/2004	✓	✓	✓	✓	-	-
[Pd-MCM-41(8)]	15/11/2004	✓	✓	✓	✓	-	-
[Pd-MCM-41(9)]	19/02/2005	✓	✓	✓	✓	-	-

4.2.1. Characterization of Pd-MCM-41 Nanocomposite Material with the highest Pd/Si ratio [Pd-MCM-41(2)]

[Pd-MCM-41(2)] is the nanocomposite material which has the highest amount of palladium among the synthesized samples.

During the experiment Pd/Si weight ratio was adjusted to 0.24 in the synthesis solution. Synthesis pH was 11 and the palladium source was $PdCl_2$. For obtaining Pd/Si ratio as 0.24, 0.6899 grams of $PdCl_2$ was dissolved in 25 ml deionized water. After addition of 35 drops of HCl, at 60 ^oC, $PdCl_2$ was dissolved and stirred for 1 hour. This solution was added to the synthesis solution of MCM-41 as described in Chapter 3.2. The color of the synthesis solution was orange, but after hydrothermal synthesis, color was turned to palladium black. After calcination of the sample, sample's color turned to brown due to oxidation of palladium and following the reduction procedure the color covers its palladium black state.

Before and after reduction steps, [Pd-MCM-41(2)] was characterized by X-ray diffraction (XRD), nitrogen physisorption, transmission electron microscopy (TEM), scanning electron microscopy (SEM), energy dispersive spectroscopy (EDS) and X-ray photoelectron spectroscopy (XPS).

4.2.1.1. X-Ray Diffraction (XRD) Analysis

The XRD pattern of the [Pd-MCM-41(2)] material prepared by the direct hydrothermal synthesis procedure, following the basic route, clearly showed the characteristic Bragg peaks of MCM-41 structure corresponding to $d_{(100)}$ and the three reflections. In Table 4.2.2 characteristic Bragg peaks are given for both the calcined and the reduced samples. Figure 4.2.1 displays the XRD patterns of [Pd-MCM-41(2)] after calcination and after reduction steps.

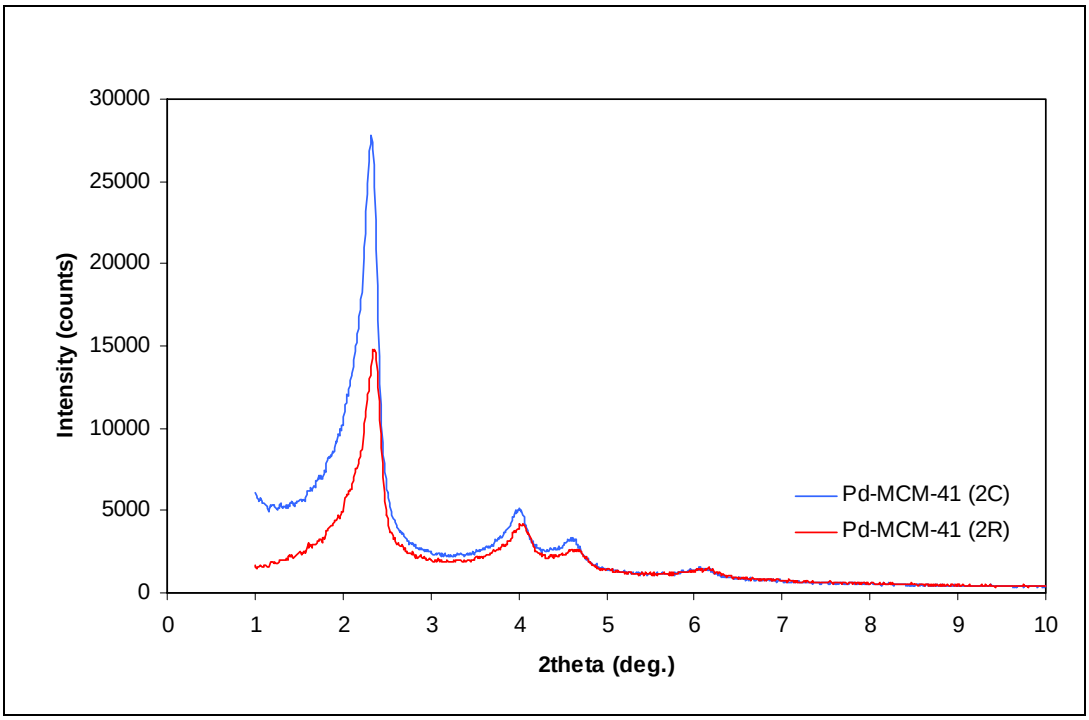

Figure 4.2.1. XRD pattern of [Pd-MCM-41(2)] (calcined and reduced samples)

Table 4.2.2. XRD results and d-spacings of [Pd-MCM-41 (2)]

Sample	hlk	$d_{(100)}$ (nm)	Angle (2theta)
[Pd-MCM-41(2C)] (calcined sample)	100	3.80	2.320
	110	2.21	4.000
	200	1.92	4.610
	210	1.45	6.080
[Pd-MCM-41(2R)] (reduced sample)	100	3.77	2.350
	110	2.19	4.040
	200	1.89	4.660
	210	1.46	0.060

4.2.1.2. Scanning Electron Microscopy (SEM) Analysis

SEM analyses of [Pd-MCM-41(2)] samples were performed in Sabanci University. Images with different magnifications are given in Figure 4.2.2.

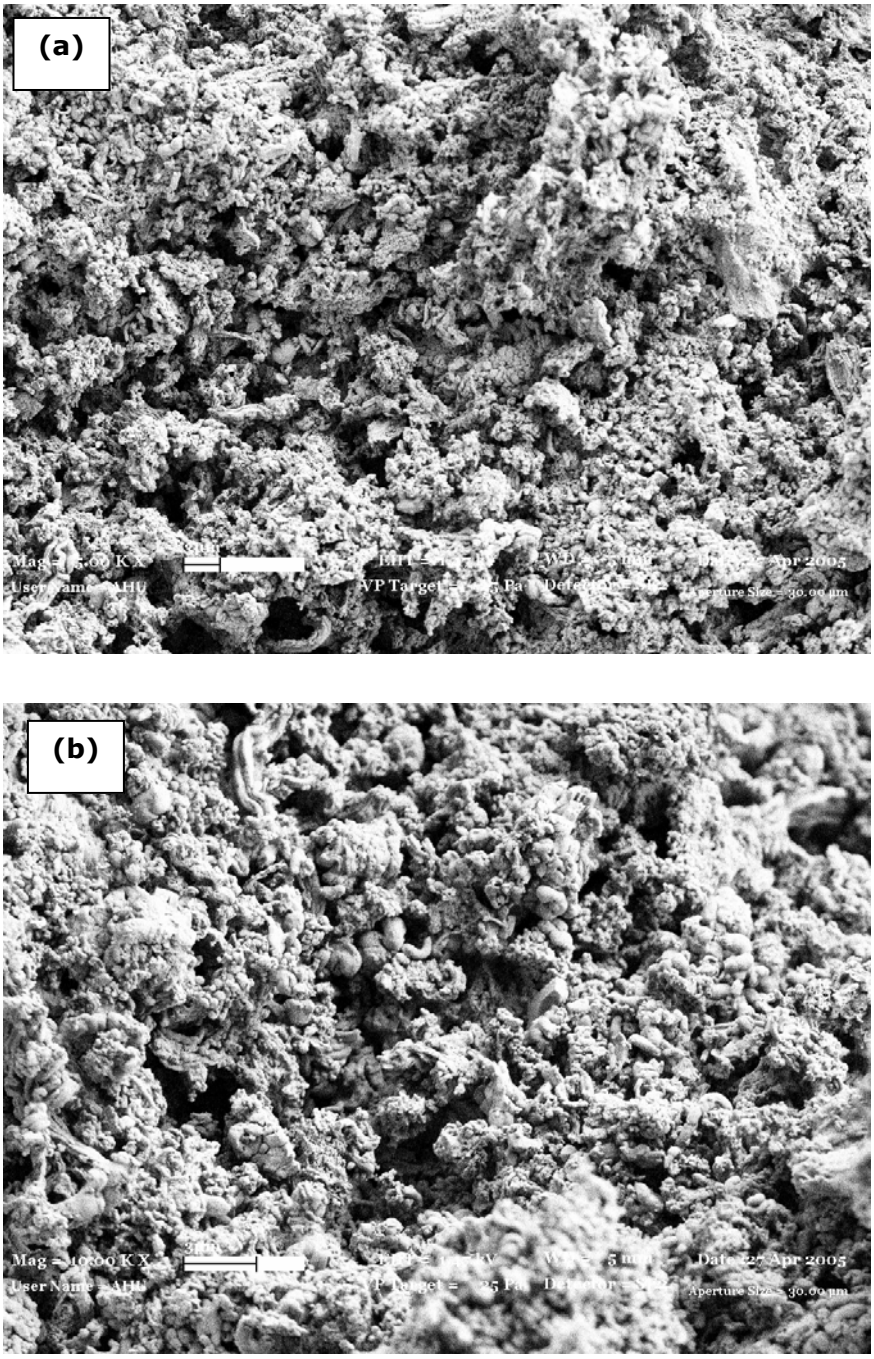

Figure 4.2.2. SEM images of [Pd-MCM-41(2R)]

4.2.1.3. Transmission Electron Microscopy (TEM) Analysis

Transmission electron microscopy (TEM) images of the sample [Pd-MCM-41 (2C)] are shown in Figure 4.2.3. Palladium grains within the MCM-41 structure are seen in these images.

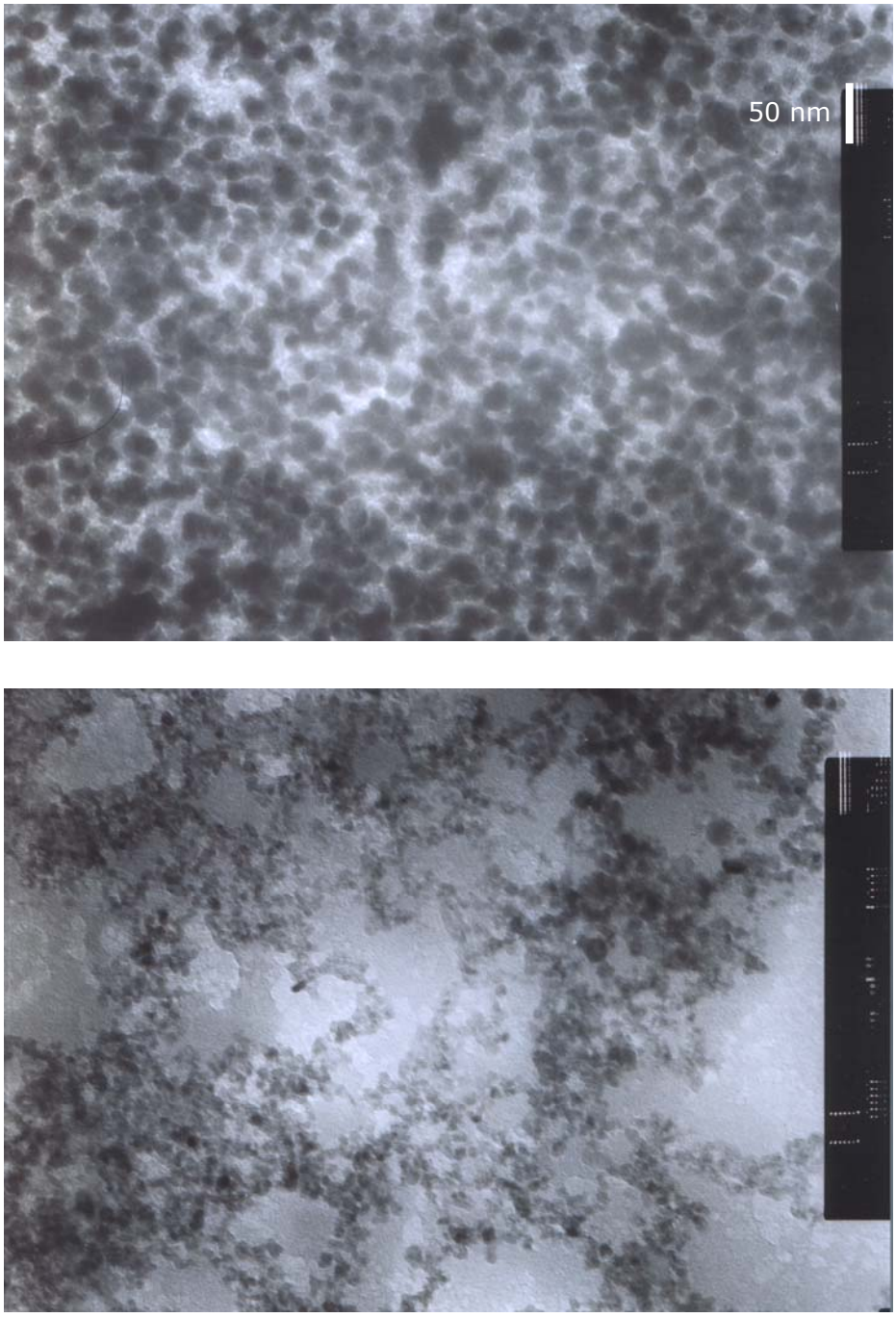

Figure 4.2.3. TEM images of [Pd-MCM-41(2C)]

4.2.1.4. Nitrogen Physisorption Analysis

Nitrogen adsorption-desorption isotherms of [Pd-MCM-41(2)] are given in Figure 4.2.4 for both calcined and reduced samples. Analyses for calcined and reduced samples were taken from different sorption analyzers, that is the reason of small differences in the adsorption isotherms given in Figure 4.2.4.

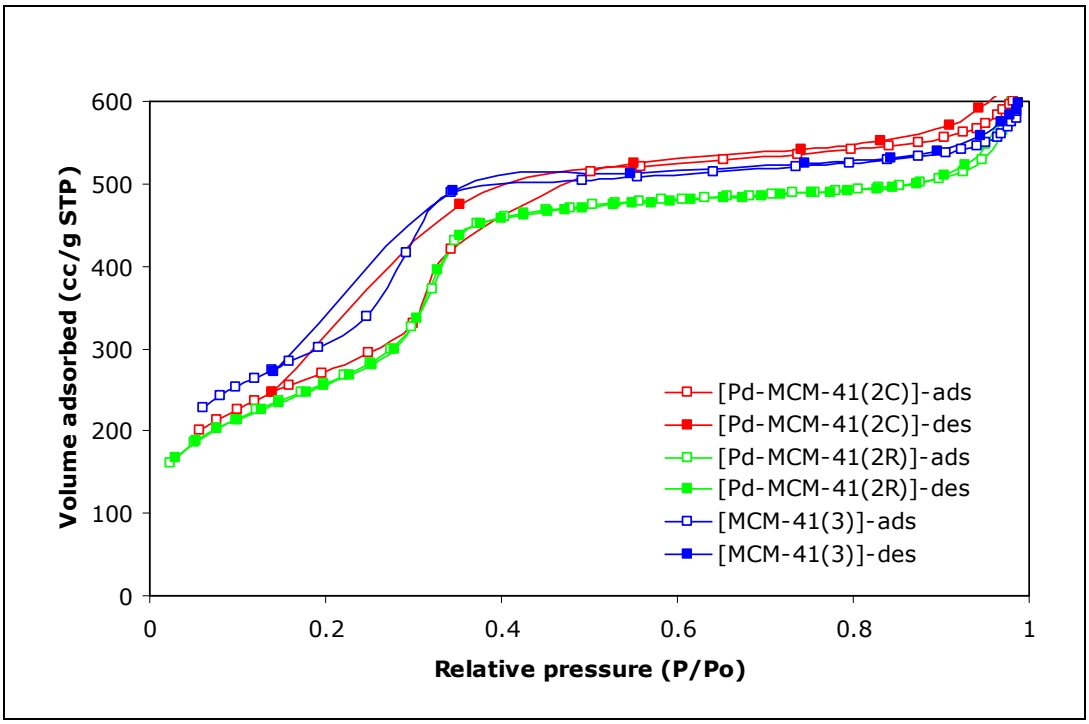

Figure 4.2.4. Nitrogen adsorption-desorption isotherm of [Pd-MCM-41(2C)] and [Pd-MCM-41(2R)]

Nitrogen adsorption-desorption isotherms of [Pd-MCM-41(2C)] and [Pd-MCM-41(2R)] are similar, they showed typical Type IV isotherm.

Surface area, pore volume and pore size data for [Pd-MCM-41(2C)] and [Pd-MCM-41(2R)] materials are given in Tables 4.2.3, 4.2.4 and 4.2.5, respectively.

Table 4.2.3 summarizes BET, BJH and single point surface areas. It is interesting to observe that surface areas of [Pd-MCM-41(2C)] and [Pd-MCM-41(2R)] materials are as high as MCM-41.

Table 4.2.3. Surface area of [Pd-MCM-41 (2)] sample

Sample	BET Surface Area (m^2/g)	BJH Adsorption Surface Area (m^2/g)	BJH Desorption Surface Area (m^2/g)	Single Point Surface Area at P/P_o 0.19 (m^2/g)
[MCM-41 (3)]	1123	1458	1824	1061
[Pd-MCM-41 (2C)]	1000	1347	1860	947
[Pd-MCM-41 (2R)]	999.2	1327	1282	897.2

Table 4.2.4. Pore volume of [Pd-MCM-41 (2)] sample

Sample	Single Point Total Pore Volume at P/Po 0.98 (cc/g)	BJH Adsorption Pore Volume (cc/g)	BJH Desorption Pore Volume (cc/g)
[MCM-41 (3)]	0.90	1.03	1.03
[Pd-MCM-41 (2C)]	0.93	1.03	1.04
[Pd-MCM-41 (2R)]	0.87	1.11	1.10

As shown in Table 4.2.5, increase was observed in the pore sizes by the incorporation of high amounts of palladium. The pore wall thickness values "δ", evaluated from $\delta=(a- d_p)$ were found to be about the same for MCM-41 and Pd incorporated material which was prepared by the basic direct hydrothermal synthesis route (Table 4.2.6).

Table 4.2.5. Pore diameter of [Pd-MCM-41 (2)] sample

Sample	Average Pore Diameter (nm)	BJH Adsorption Average Pore Diameter (nm)	BJH Desorption Average Pore Diameter (nm)
[MCM-41 (3)]	3.195	2.831	2.261
[Pd-MCM-41 (2C)]	3.721	3.069	2.235
[Pd-MCM-41 (2R)]	3.468	2.782	2.670

Table 4.2.6. Pore wall characteristics of [Pd-MCM-41 (2)]

Sample	$d_{(100)}$ (nm)	Lattice Parameter	BJH Pore Diameter d_p (nm)	Pore Wall Thick. δ (nm)
[MCM-41 (3)]	3.61	4.17	2.83	1.34
[Pd-MCM-41 (2C)]	3.80	4.39	3.07	1.32
[Pd-MCM-41 (2R)]	3.76	4.34	2.78	1.56

Reduction step is expected to cause changes in the XRD and XPS spectra. XPS will be discussed later, but we clearly observed in section 4.2.1.1 that XRD pattern was not destroyed after reduction.

BJH pore size distribution curves for [Pd-MCM-41(2C)], [Pd-MCM-41(2R)] and [MCM-41(3)] are plotted in Figure 4.2.5. [Pd-MCM-41(2C)] gives slightly wider pore size distribution than that of pure MCM-41.

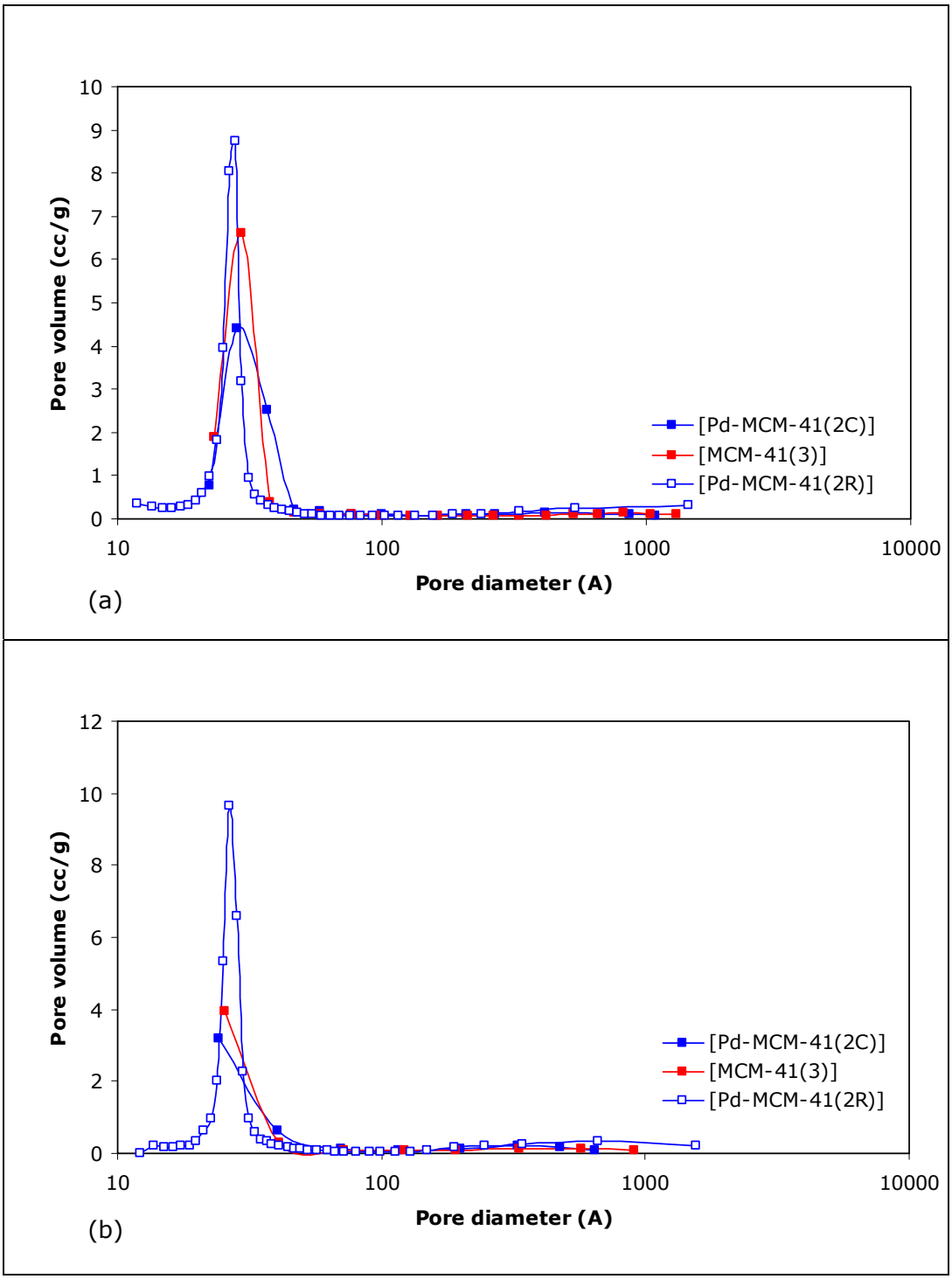

Figure 4.2.5. Pore size distribution curves of [Pd-MCM-41(2C)] (a) BJH adsorption pore size distribution, (b) BJH desorption pore size distribution

4.2.1.5. Energy Dispersive Spectroscopy (EDS) Analysis

Energy dispersive spectra (EDS) of calcined and reduced forms of [Pd-MCM-41(2)] are given in Figure 4.2.6.

Bulk composition of the nanocomposite material was determined by qualitative EDS analysis. Chemical composition of the sample [Pd-MCM-41(2)] is given in the Table 4.2.7 for both calcined and reduced forms. It is interesting to obtain Pd/Si weight ratio as 0.45 from EDS analysis while it was adjusted as 0.24 during the synthesis. It can be concluded that all palladium was incorporated into the structure but some of the silisium was not.

Table 4.2.7. EDS analysis of [Pd-MCM-41(2)]

Sample	Element	Weight Conc. (%)	Atom Conc. (%)	Pd/Si Ratio	
				Weight	Atomic
[Pd-MCM-41 (2C)]	Pd	29.55	9.97	0.42	0.11
	Si	70.45	90.03		
[Pd-MCM-41 (2R)]	Pd	31.15	10.81	0.45	0.12
	Si	68.85	89.19		

Pd/Si ratio values were obtained by dividing concentration of palladium to the concentration of silicium directly. Hence, Pd/Si weight ratio of the calcined sample is 29.55/70.45=0.42.

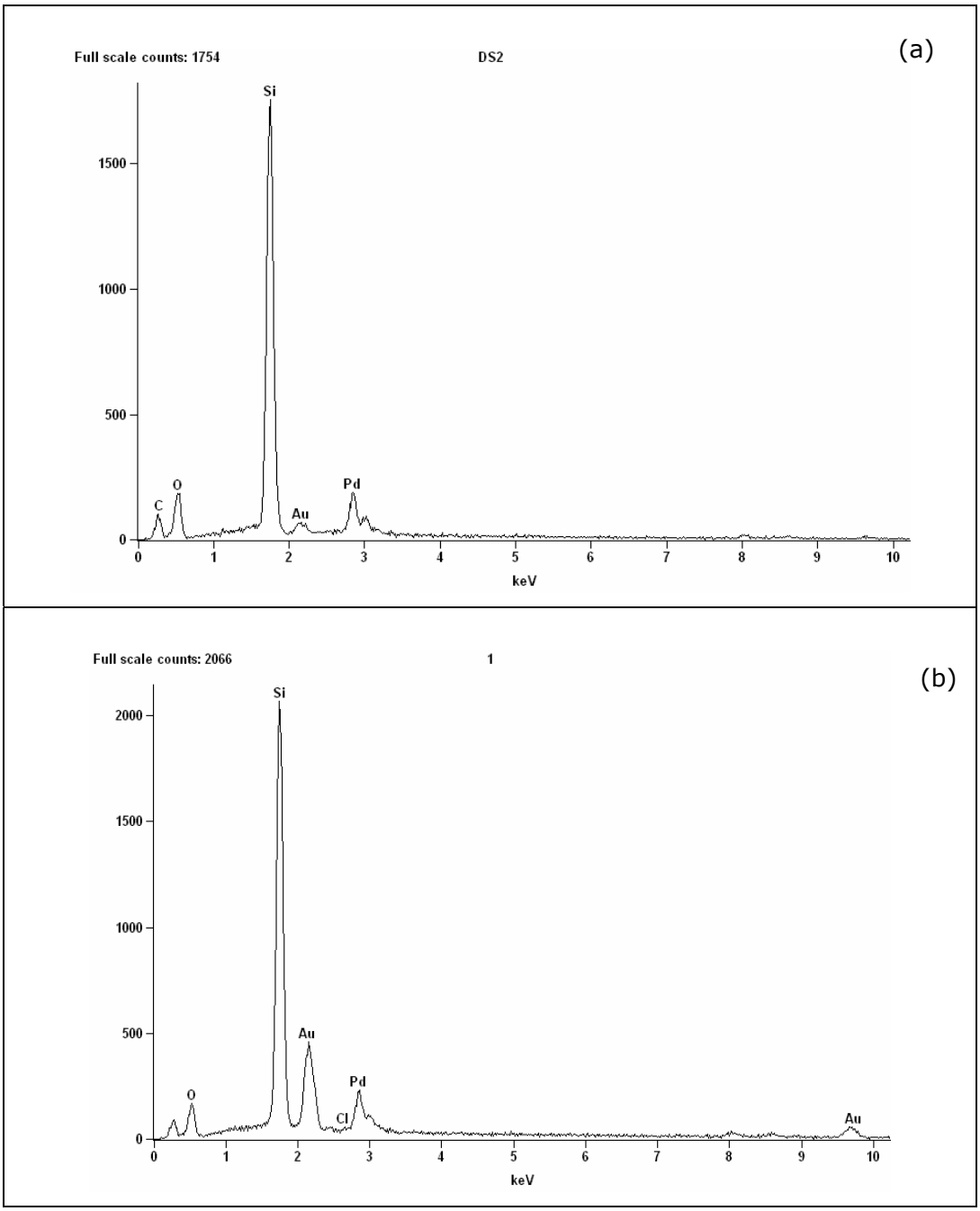

Figure 4.2.6. Energy dispersive spectrum (EDS) of [Pd-MCM-41(2)] (a) for calcined sample [Pd-MCM-41(2C)], (b) for reduced sample [Pd-MCM-41(2R)]

4.2.1.6. X-Ray Photoelectron Spectroscopy (XPS) Analysis

The XPS analysis of the calcined [Pd-MCM-41(2C)] and the reduced [Pd-MCM-41(2R)] materials showed the characteristic Pd $3d_5$ bands at 336.0 and 335.6 eV, respectively. For PdO and Pd, XPS bands are expected at 336.3 eV and 335.1 eV, respectively [62] (Figure 4.2.7). These results indicated reduction of palladium oxide during the treatment of the calcined material with hydrogen gas at 200 ^{o}C. This is more clearly seen from the differences of photoelectron binding energy differences of O 1s and Pd $3d_5$ ΔO-Pd of the calcined and the reduced materials. For these two cases ΔO-Pd values were 196.8 eV and 197.2 eV, respectively. This difference was expected as 196.2 eV and 197.4 eV, for Pd and PdO, respectively. For both [Pd-MCM-41(2C)] and [Pd-MCM-41(2R)], the characteristic photoelectron binding energy of Si 2p were observed at 103.2 eV.

Table 4.2.8. Surface composition of [Pd-MCM-41(2)] from XPS quantification

Sample	Element	Atom Conc. (%)	Pd/Si Ratio
[Pd-MCM-41(2C)]	C	7.5	0.05
	O	61.4	
	Si	29.5	
	Pd	1.5	
[Pd-MCM-41(2R)]	C	6.9	0.12
	O	66.0	
	Si	24.3	
	Pd	2.8	

By qualitative XPS analysis, EDS analysis was also supported.

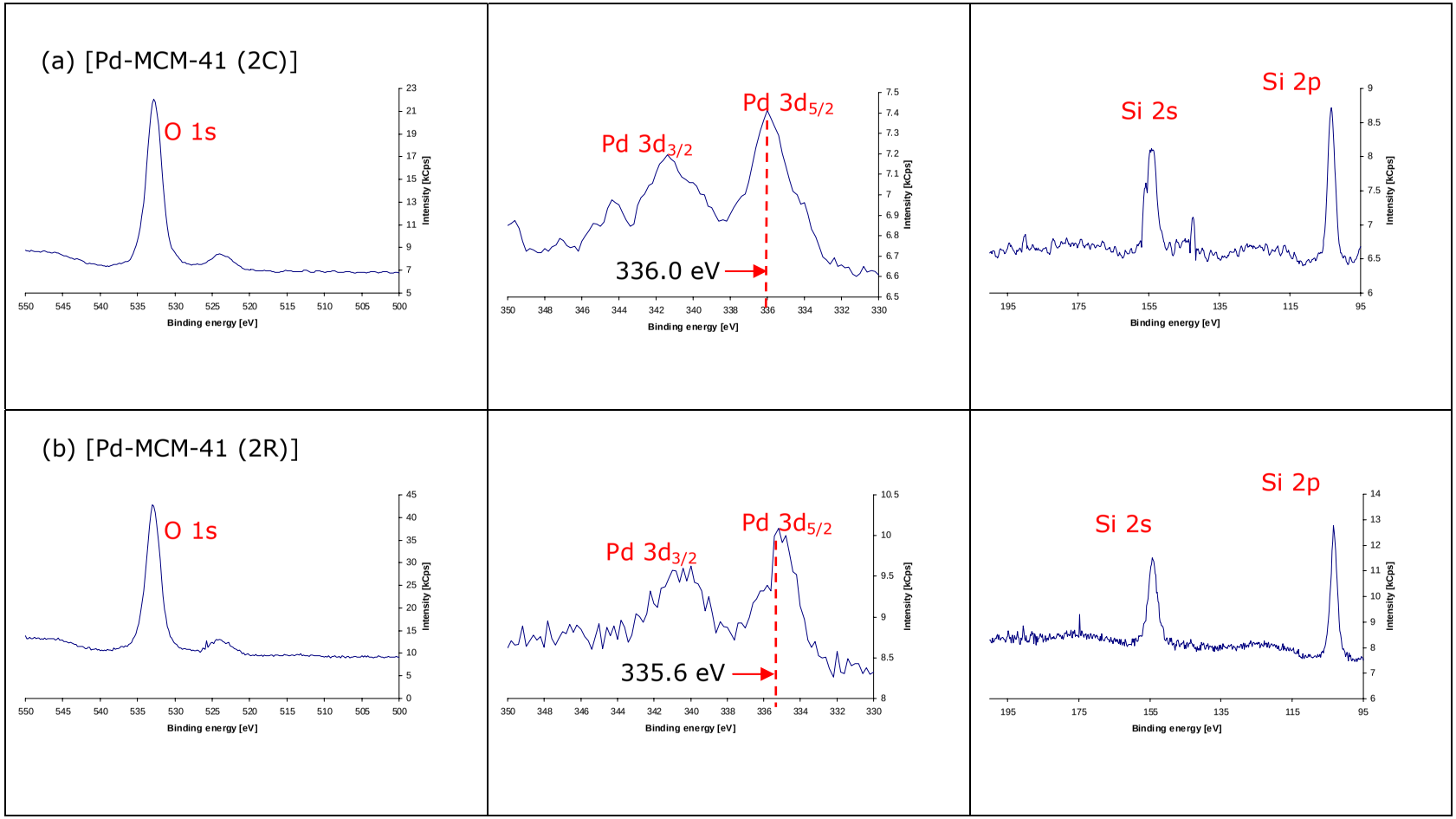

Figure 4.2.7. X-ray photoelectron spectra of calcined [Pd-MCM-41 (2C)] and reduced [Pd-MCM-41 (2R] materials

4.2.1.7. Temperature Programmed Reduction (TPR) Analysis

Temperature programmed reduction (TPR) analysis was performed using 5% hydrogen gas in helium in the reaction system described in Chapter 3.4.

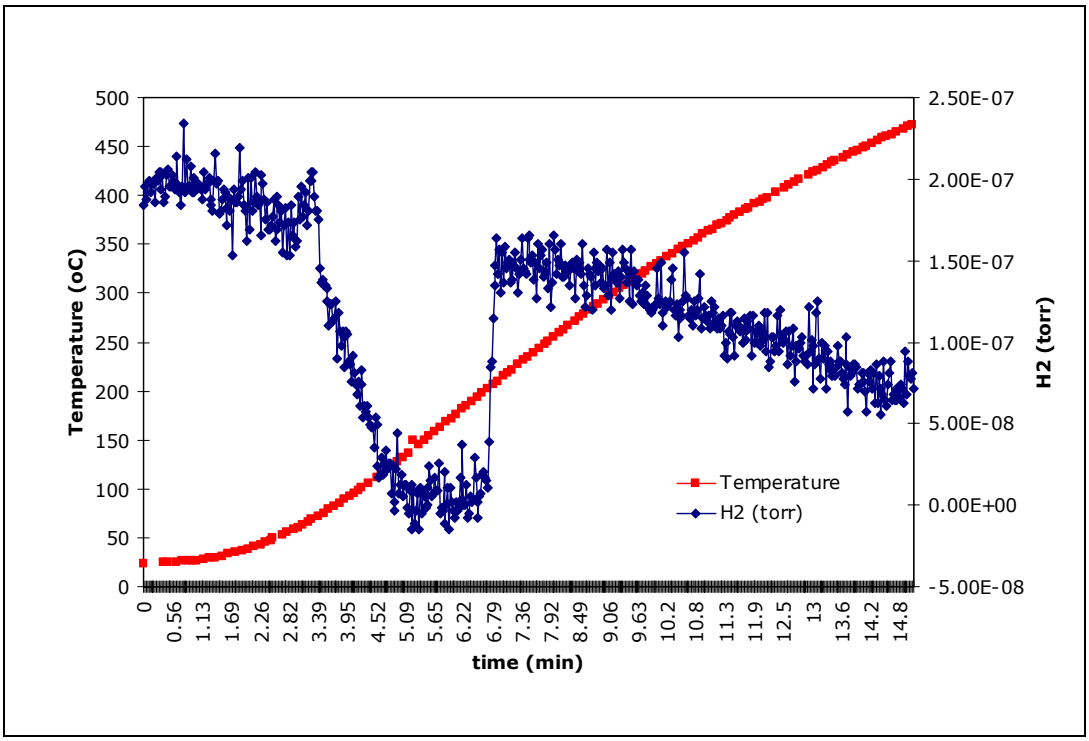

Figure 4.2.8. Temperature programmed reduction (TPR) profile of [Pd-MCM-41(2C)]

The TPR profile of [Pd-MCM-41 (2)] is shown in Figure 4.2.8. As it can be seen from the decrease of H_2, the [Pd-MCM-41(2C)] material started to show a reduction peak at about 80 ^oC with a maximum H_2 consumption at about 172 ^oC. Reduction was completed below 200 ^oC. Increasing temperature up to 565 ^oC did not cause any further reduction in the sample. From the temperature programmed reduction profile, it is clearly seen that 200 ^oC is sufficient to reduce all the palladium.

The H_2 consumption of this run was calculated as $2.3x10^{-4}$ gmol H_2 from the curve of Figure 4.2.8. The calculations are given below.

H_2 consumption= $C_{total} Q \int_{t_1}^{t_2} (y_{H_{20}} - y_{H_2}) dt$

Here, Q is the volumetric flow rate, C_{total} is the total concentration and y_{H_2} the mole fraction of H_2.

$$y_{H_{20}} = 0.05$$

Therefore,

$$y_{H_2} = \alpha h_{H_2} = \left(\frac{y_{H_{20}}}{h_{H_{20}}} \right) h_{H_2}$$

Here, α is the calibration factor, h_{H_2}, $h_{H_{20}}$ are readings at any time and time equal to zero in the ordinate of Figure 4.2.8.

H_2 consumption= $C_{total} Q \frac{0.05}{h_{H_{20}}} \int_{t_1}^{t_2} (h_{H_{20}} - h_{H_2}) dt$

By using Mathematica, $\int_{t_1}^{t_2} (h_{H_{20}} - h_{H_2}) dt = 4.97 \times 10^{-7}$

$$C_{total} = \frac{P}{RT} = 4.1 \times 10^{-5} mol / cm^3$$

$$Q = 50 cm^3 / \min$$

H_2 consumed with [Pd-MCM-41(2C)] = 2.55x10^{-4} mol H_2

H_2 consumed per g of [Pd-MCM-41(2)] = 12.7x10^{-4}mol H_2/g of [Pd-MCM-41(2)]

Since palladium weight percentage is 15.8% in the sample;

0.2 g material x (0.158) g Pd/g material = 0.0316 g Pd

It corresponds to $2.98x10^{-4}$ mol palladium.

Consumed H_2 and amount of palladium have the same order of magnitude.

Results showed that about 85% of PdO was reduced to Pd during the reduction by hydrogen.

4.2.2. Effect of Pd Loading in tne Synthesis of Pd-MCM-41 Samples

For the examination the effect of palladium loading, a set of experiments were performed. [Pd-MCM-41(5)], [Pd-MCM-41(9)] and [Pd-MCM-41(2)] samples were prepared by the same procedure, only the difference is amount of Pd added. Synthesis conditions are given in Table 4.2.9.

Table 4.2.9. Synthesis conditions of synthesized Pd-MCM-41 samples with different Pd/Si ratios

Sample	Pd Source	Amount of Pd source added (g)	pH	Pd/Si Weight Ratio	Pd/Si Atomic Ratio
MCM-41	-	0	11.0	0	0
[Pd-MCM-41 (5)]	$PdCl_2$	0.1446	11.0	0.04	0.01
[Pd-MCM-41 (9)]	$PdCl_2$	0.4022	11.0	0.12	0.03
[Pd-MCM-41 (2)]	$PdCl_2$	0.6899	11.0	0.24	0.06

X-ray diffraction patterns of the Pd/MCM-41 samples synthesized with different palladium loadings are plotted in Figure 4.2.9. Same XRD patterns were obtained for all the samples, the only difference is the decrease of intensity by increasing palladium addition. For a comparison XRD pattern of pure MCM-41 was plotted on the same figure. From this figure it is clearly seen that hexagonal

structure of MCM-41 was not destroyed by palladium incorporation up to Pd/Si weight ratio of 0.42.

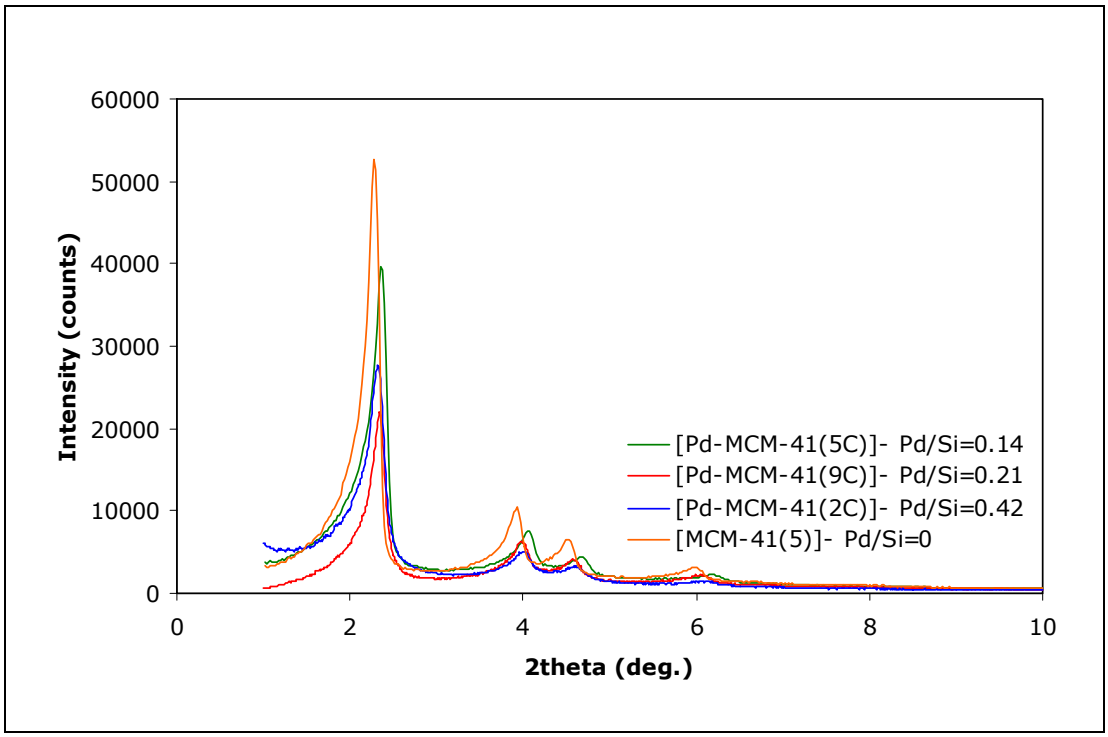

Figure 4.2.9. XRD patterns of Pd-MCM-41 samples with different Pd/Si ratios

SEM images of the samples [Pd-MCM-41(5R)] and [Pd-MCM-41(9R)] are shown on Figure 4.2.10. with a magnification of 5000 times, particles could be seen clearly. It is observed that increase of palladium incorporation did not affect the morphology of the final product to be obtained, i.e. nearly same particle sizes were obtained from these two syntheses.

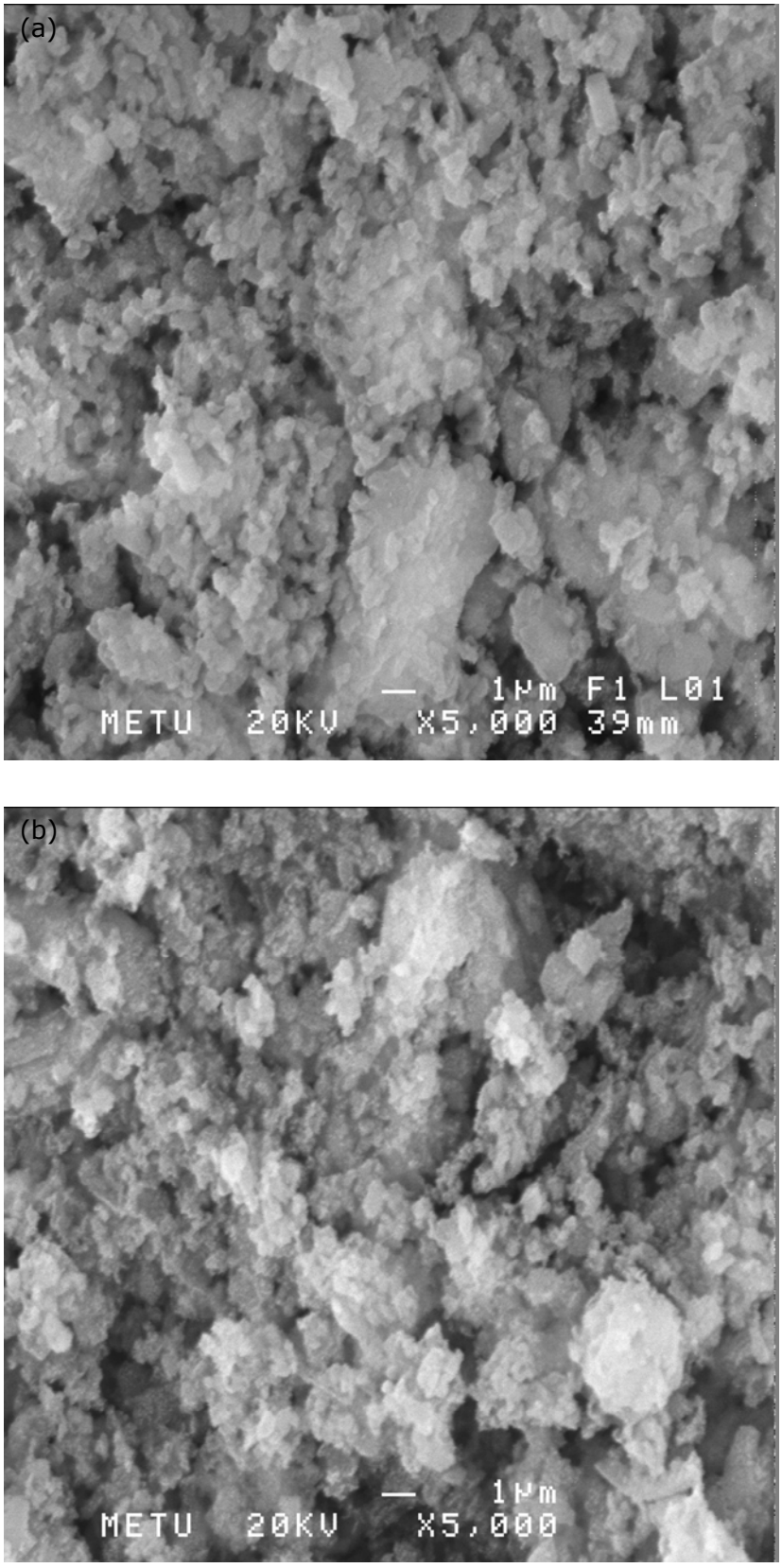

Figure 4.2.10. SEM images of (a) [Pd-MCM-41(5R)] and (b) [Pd-MCM-41(9R)]

Nitrogen adsorption-desorption isotherms of the samples [Pd-MCM-41(5)], [Pd-MCM-41(9)] and [Pd-MCM-41(2)] were plotted in Figure 4.2.11 for their calcined forms. Similar isotherms were obtained for all the samples. [Pd-MCM-41(2)] and [Pd-MCM-41(9)] are more comparable because physisorption analyses of these two samples were performed in the same physisorption apparatus. Physisorption analysis of [Pd-MCM-41(5)] was carried out with Autosorb 1C.

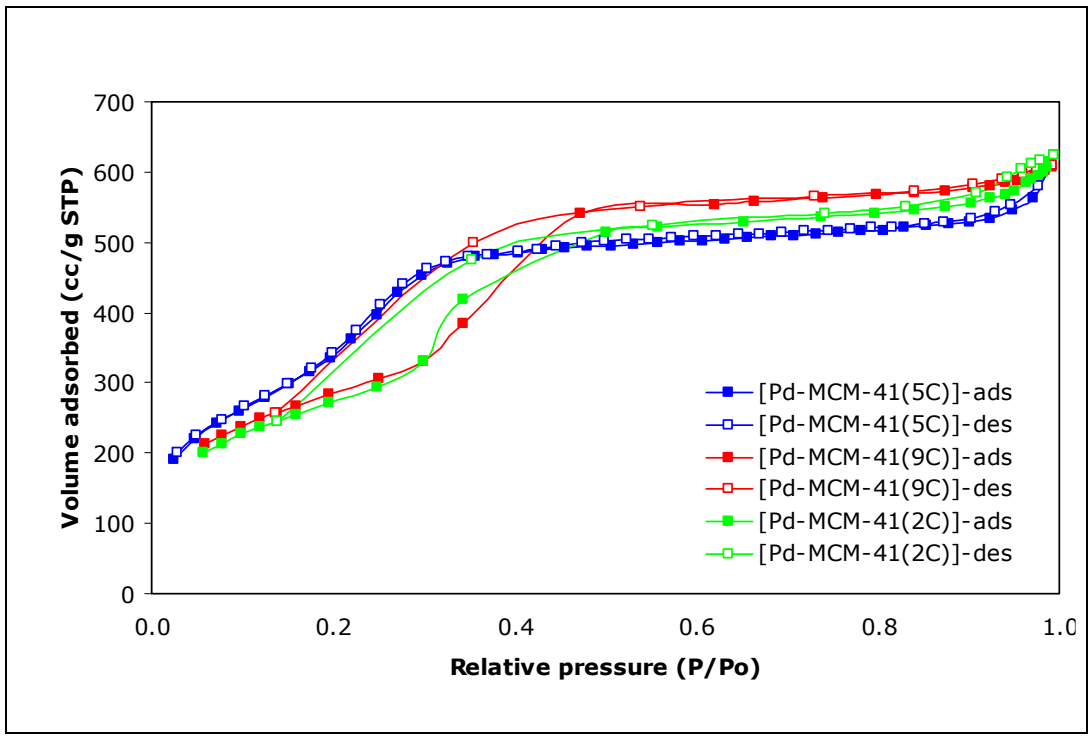

Figure 4.2.11. Nitrogen adsorption-desorption isotherms of Pd-MCM-41 samples with different palladium loadings

In Table 4.2.9 BET, BJH and single point surface area values for Pd-MCM-41 samples with different palladium loadings were listed. Surface area decreases slightly with increasing palladium addition. Surface areas of synthesized Pd-MCM-41 samples with all palladium compositions have surface areas as high as being in pure MCM-41. When [Pd-MCM-41(9)] and [Pd-MCM-41(2)] were compared, it is interesting to see that doubling the Pd/Si weight ratio did not affect the surface area of the final product. By nitrogen adsorption-desorption

analysis, it is concluded that palladium is incorporated into the walls of MCM-41, and does not close the pores.

Table 4.2.10. Surface areas of synthesized Pd-MCM-41 samples with different Pd/Si ratios

Sample	BET Surface Area (m^2/g)	BJH Adsorption Surface Area (m^2/g)	BJH Desorption Surface Area (m^2/g)	Single Point Surface Area at P/P_o 0.19 (m^2/g)
[MCM-41 (3)]	1123	1458	1824	1061
[Pd-MCM-41 (5C)]	1483	1736	1703	1173
[Pd-MCM-41 (9C)]	1040	1322	1970	990
[Pd-MCM-41 (9R)]	1051	1408	1404	939.7
[Pd-MCM-41 (2C)]	1000	1347	1860	947
[Pd-MCM-41 (2R)]	999.2	1327	1282	897.2

Trend of BET surface area of the samples with increasing palladium amount incorporated in the structure is shown in a plot in Figure 4.2.13.a.

Pore size distributions of the synthesized samples were also compared in Figure 4.2.12. It is observed that [Pd-MCM-41(5)] has a narrower pore size distribution. Increase of incorporated palladium amount gave slightly wider pore size distribution curves. Average pore sizes obtained by using BET and BJH techniques for the samples under discussion are also listed in Table 4.2.11. Table 4.2.12 gives the pore volume values of the samples. Comparison of samples [Pd-MCM-41(5)], [Pd-MCM-41(9)] and [Pd-MCM-41(2)] points out that increasing the amount of palladium in the nanocomposite structure results increase in pore size of the materials. Change in pore size with increasing palladium amount was also shown in Figure 4.2.13.b.

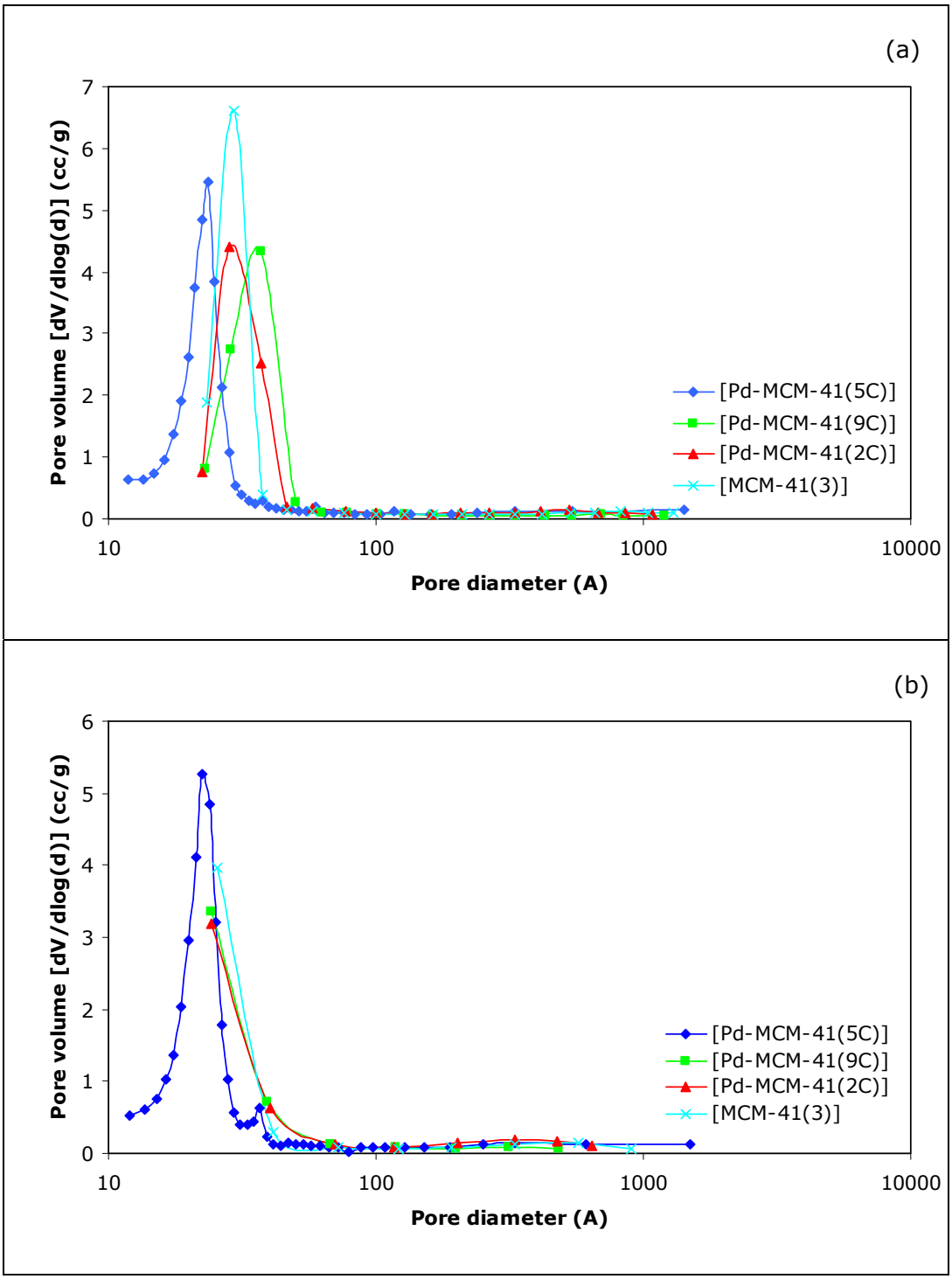

Figure 4.2.12. Pore size distribution curves for Pd-MCM-41 samples with different Pd loadings (a) BJH adsorption pore size distribution, (b) BJH desorption pore size distribution

Table 4.2.11. Pore sizes of Pd-MCM-41 samples having different Pd/Si ratios

Sample	Average Pore Diameter (nm)	BJH Adsorption Average Pore Diameter (nm)	BJH Desorption Average Pore Diameter (nm)
[MCM-41 (3)]	3.19	2.83	2.26
[Pd-MCM-41 (5C)]	2.34	2.36	2.25
[Pd-MCM-41 (9C)]	3.61	3.11	2.08
[Pd-MCM-41 (9R)]	3.27	2.78	2.82
[Pd-MCM-41 (2C)]	3.72	3.07	2.23
[Pd-MCM-41 (2R)]	3.47	2.78	2.67

Table 4.2.12. Pore volumes of Pd-MCM-41 samples having different Pd/Si ratios

Sample	Single Point Total Pore Volume at P/Po 0.98 (cc/g)	BJH Adsorption Pore Volume (cc/g)	BJH Desorption Pore Volume (cc/g)
[MCM-41 (3)]	0.90	1.03	1.03
[Pd-MCM-41 (5C)]	0.87	1.07	1.06
[Pd-MCM-41 (9C)]	0.94	1.03	1.02
[Pd-MCM-41 (9R)]	0.86	1.06	1.06
[Pd-MCM-41 (2C)]	0.93	1.03	1.04
[Pd-MCM-41 (2R)]	0.87	1.11	1.10

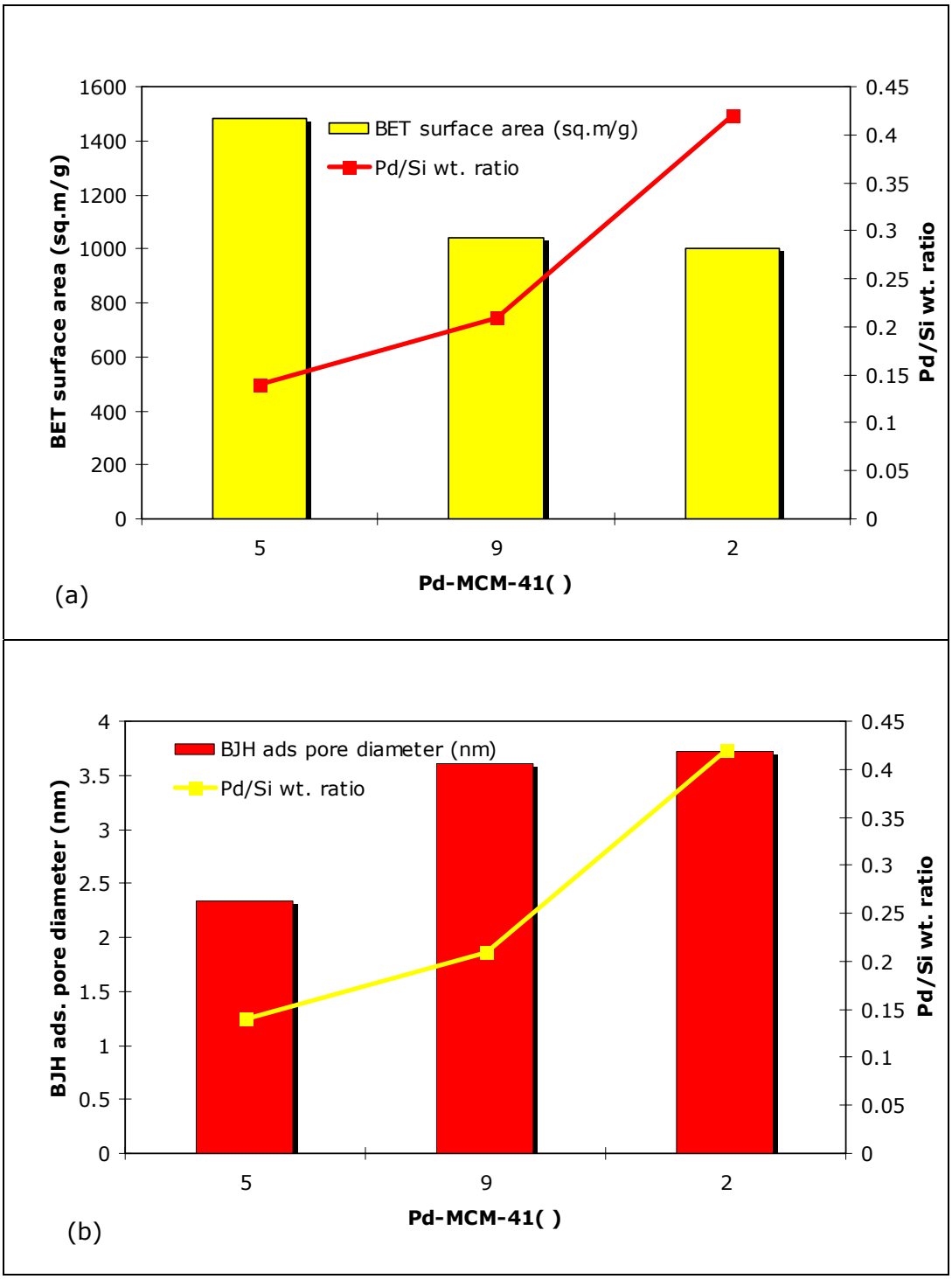

Figure 4.2.13. Trends of (a) surface area, (b) pore diameter with changing Pd/Si wt. ratio

Table 4.2.13. Pore wall characteristics of Pd-MCM-41 samples having different Pd/Si ratios

Sample	$d_{(100)}$ (nm)	Lattice Parameter	BJH Pore Diameter d_p (nm)	Pore Wall Thick. δ (nm)
[MCM-41 (3)]	3.61	4.17	2.83	1.34
[Pd-MCM-41 (5C)]	3.46	4.00	2.37	1.63
[Pd-MCM-41 (9C)]	3.79	4.38	3.11	1.27
[Pd-MCM-41 (9R)]	3.74	4.32	2.80	1.52
[Pd-MCM-41 (2C)]	3.80	4.39	3.07	1.32
[Pd-MCM-41 (2R)]	3.76	4.34	2.79	1.55

Pore wall thickness of the samples with different amounts of palladium loadings are listed in Table 4.2.13. Physisorption analyses of the samples [MCM-41(3)], [Pd-MCM-41(9C)] and [Pd-MCM-41(2C)] were performed by using Micromeritics analyzer and that of remaining others in Table 4.2.13 were performed by Autosorb analyzer. According to this separation, comparing [MCM-41(3)], [Pd-MCM-41(9C)] and [Pd-MCM-41(2C)] with each other show that incorporation of palladium into the MCM-41 structure does not affect the pore wall thickness of the samples.

In order to obtain information about the success of palladium incorporation into the structure, EDS analyses for all the samples were performed. Table 4.2.14 gives palladium and silicium concentrations and Pd/Si weight and atomic ratios for the materials [Pd-MCM-41(5)], [Pd-MCM-41(9)] and [Pd-MCM-41(2)] for calcined and reduced forms.

Table 4.2.14. EDS analyses of the Pd-MCM-41 samples having different Pd loadings

Sample	Element	Weight Conc. (%)	Atom Conc. (%)	Pd/Si Ratio	
				Weight	Atomic
[Pd-MCM-41 (5C)]	Pd	12.07	3.51	0.14	0.04
	Si	86.69	95.41		
[Pd-MCM-41 (5R)]	Pd	14.95	4.43	0.18	0.05
	Si	85.05	95.57		
[Pd-MCM-41 (9C)]	Pd	17.23	5.21	0.21	0.06
	Si	82.77	94.79		
[Pd-MCM-41 (9R)]	Pd	18.59	5.69	0.23	0.06
	Si	81.41	94.31		
[Pd-MCM-41 (2C)]	Pd	29.55	9.97	0.42	0.11
	Si	70.45	90.03		
[Pd-MCM-41 (2R)]	Pd	30.95	10.58	0.45	0.12
	Si	68.93	89.30		

Table 4.2.14 tells us that palladium incorporates into the structure more effectively at low concentrations. For [Pd-MCM-41(5)], Pd/Si weight ratio obtained from EDS analysis is 3.5 fold of its value in the synthesis solution. However, it is 1.75 and 1.88 fold for [Pd-MCM-41(9)] and [Pd-MCM-41(2)], respectively.

EDS patterns of [Pd-MCM-41(5)] and [Pd-MCM-41(9)] materials are given in Figures 4.2.14 and 4.2.15, respectively.

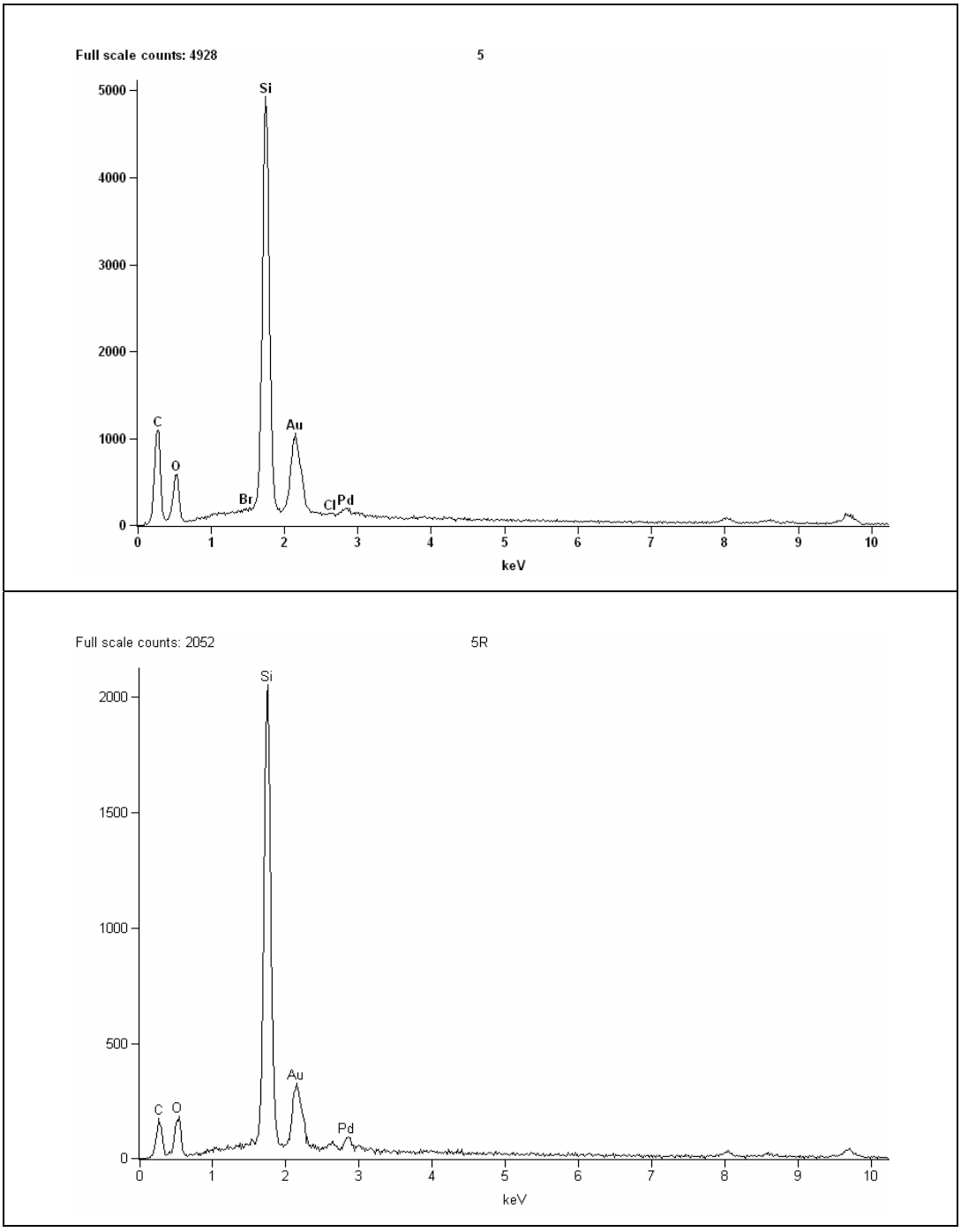

Figure 4.2.14. EDS patterns of [Pd-MCM-41(5)] (a) after calcination (b) after reduction

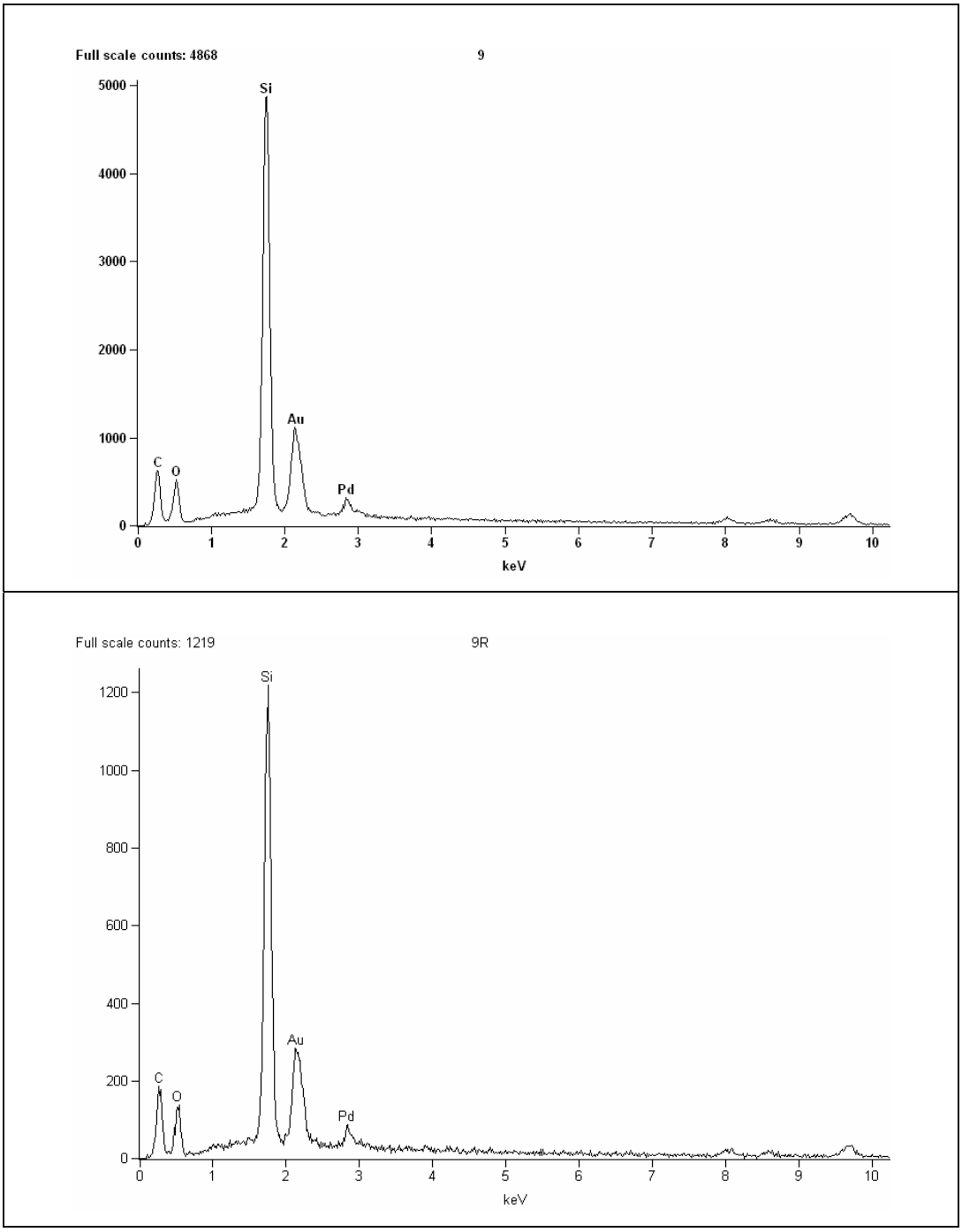

Figure 4.2.15. EDS patterns of [Pd-MCM-41(9)] (a) after calcination (b) after reduction

4.2.3. Effect of pH in the Synthesis of Pd-MCM-41 Samples

MCM-41 itself can be synthesized under acidic and basic conditions. For the synthesis of MCM-41 final pH of the synthesis solution must be under 2 or over 11 []. For the examination of effect of pH for palladium incorporated case, a set of experiments were performed. Synthesis conditions for samples of this set are listed in Table 4.2.15.

Table 4.2.15. Pd-MCM-41 samples synthesized under acidic and basic conditions

Sample	Pd Source	Amount of Pd source added (g)	pH	Pd/Si Weight Ratio	Pd/Si Atomic Ratio
[Pd-MCM-41 (6)]	$PdCl_2$	0.4022	1.5	0.12	0.03
[Pd-MCM-41 (9)]	$PdCl_2$	0.4022	11.0	0.12	0.03

The XRD patterns of the Pd incorporated mesoporous material [Pd-MCM41(6)] synthesized following an acidic direct hydrothermal synthesis route (solution pH=1.5) showed a much wider $d_{(100)}$ peak at a 2θ value of 2.32 (Figure 4.2.16) than the corresponding peak observed for the material synthesized following the basic route. For these two cases, the only difference is the pH of the solution during the hydrothermal synthesis. This wide band corresponds to a wide distribution of pore sizes. As it will be discussed later, this conclusion was also justified by the pore size distributions of the samples. The second, third and fourth characteristic XRD peaks MCM-41 at higher 2θ values could not be observed for this product. Although the structure of this product can not be considered as MCM-41, it was symbolized as [Pd-MCM-41(6)]. However, it is also a mesoporous Pd incorporated material.

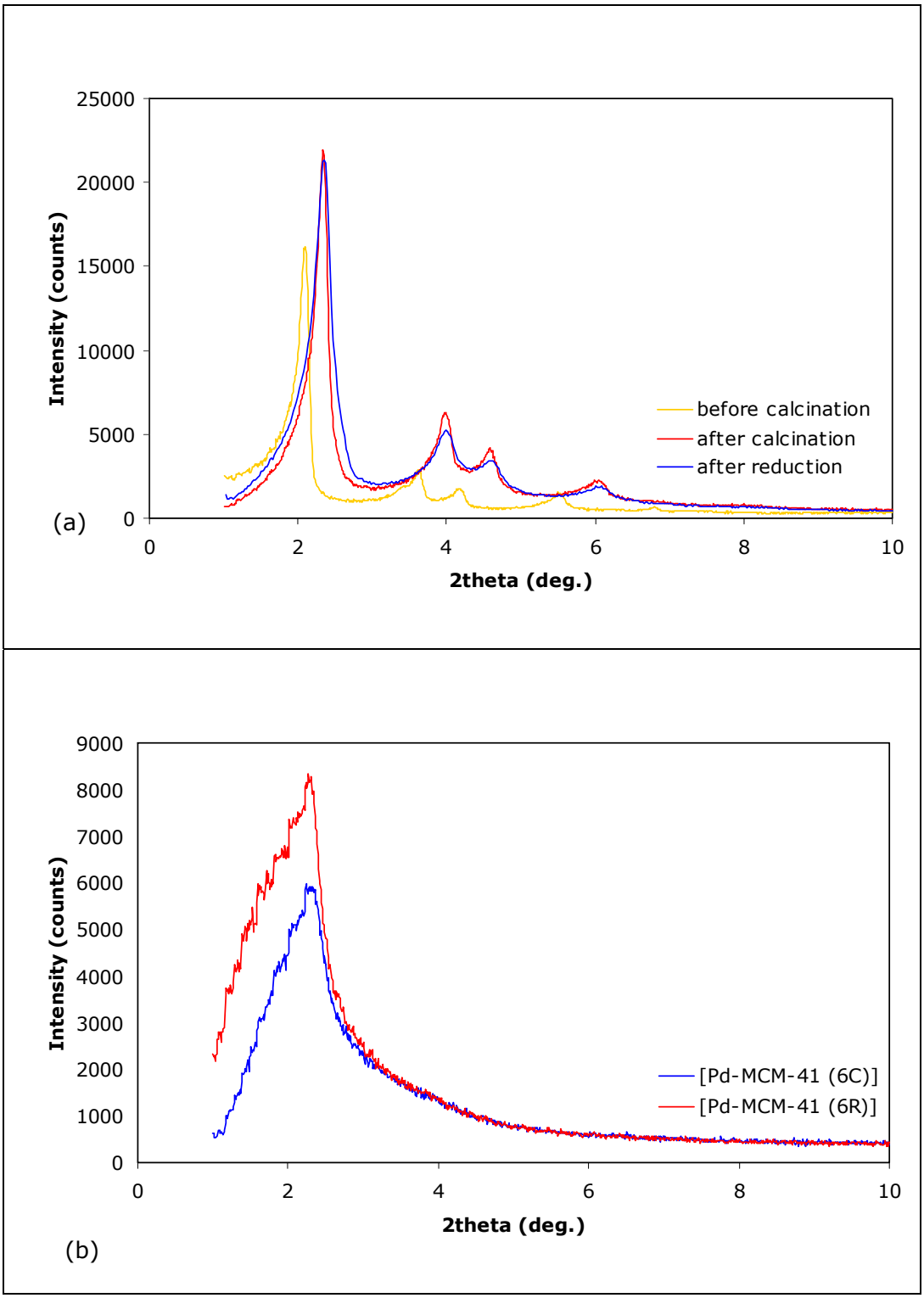

Figure 4.2.16. XRD patterns of Pd-MCM-41 materials prepared by direct hydrothermal synthesis with a Pd/Si wt ratio of 0.12 in the solution (a) Basic route (pH=11) (b) Acidic route (pH=1.5).

Although the surface area of this product was smaller (BET area=671 m^2/g) than the corresponding value of the product obtained following the basic route, it is still sufficiently high for many of the catalytic applications. In Table 4.2.16, surface area values of the materials synthesized under acidic and basic conditions were compared. Surface area of the basic synthesis was found to be approximately two folds of the acidic synthesis. Synthesis pH was found to be a key factor for proper mesoporous materials synthesis.

Table 4.2.16. Surface area of Pd-MCM-41 samples synthesized under acidic and basic conditions

Sample	BET Surface Area (m^2/g)	BJH Adsorption Surface Area (m^2/g)	BJH Desorption Surface Area (m^2/g)	Single Point Surface Area at P/P_o 0.19 (m^2/g)
[Pd-MCM-41 (6C)]	670.6	782.6	895.3	630.6
[Pd-MCM-41 (6R)]	693.9	807.2	945.8	652.6
[Pd-MCM-41 (9C)]	1039.9	1322.4	1969.9	990.3
[Pd-MCM-41 (9R)]	1051.0	1408.0	1404.0	939.7

The nitrogen adsorption isotherm of the product obtained following the basic route [Pd-MCM-41(9C)] showed a typical Type IV isotherm, as described by the IUPAC classification (Figure 4.2.17). Capillary condensation of nitrogen was observed at relative pressures between 0.30 and 0.35.

As shown in Figure 4.2.19, the pore size distributions of pure MCM-41 and Pd incorporated MCM-41 synthesized by the basic direct hydrothermal synthesis procedure are both very narrow. However, the pore size distribution of the Pd incorporated mesoporous material prepared following the acidic route, [Pd-MCM-41(6R)], is much wider, indicating the presence of pores having diameters up to 10 nm.

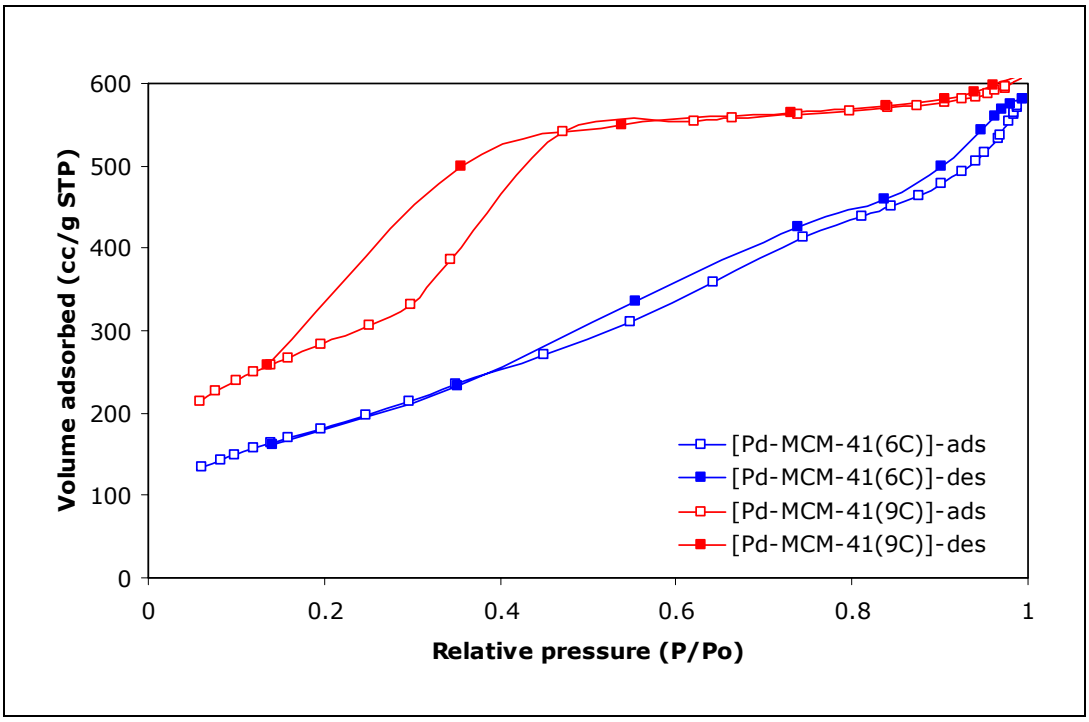

Figure 4.2.17. Nitrogen adsorption-desorption isotherms of the materials synthesized under acidic and basic conditions

Pore volumes of the samples synthesized for the examination of the effect of synthesis pH were given in Table 4.2.17. SEM images of [Pd-MCM-1(6)] were given in Figure 4.2.18. Particles with approximately 200 nm are observed from the images.

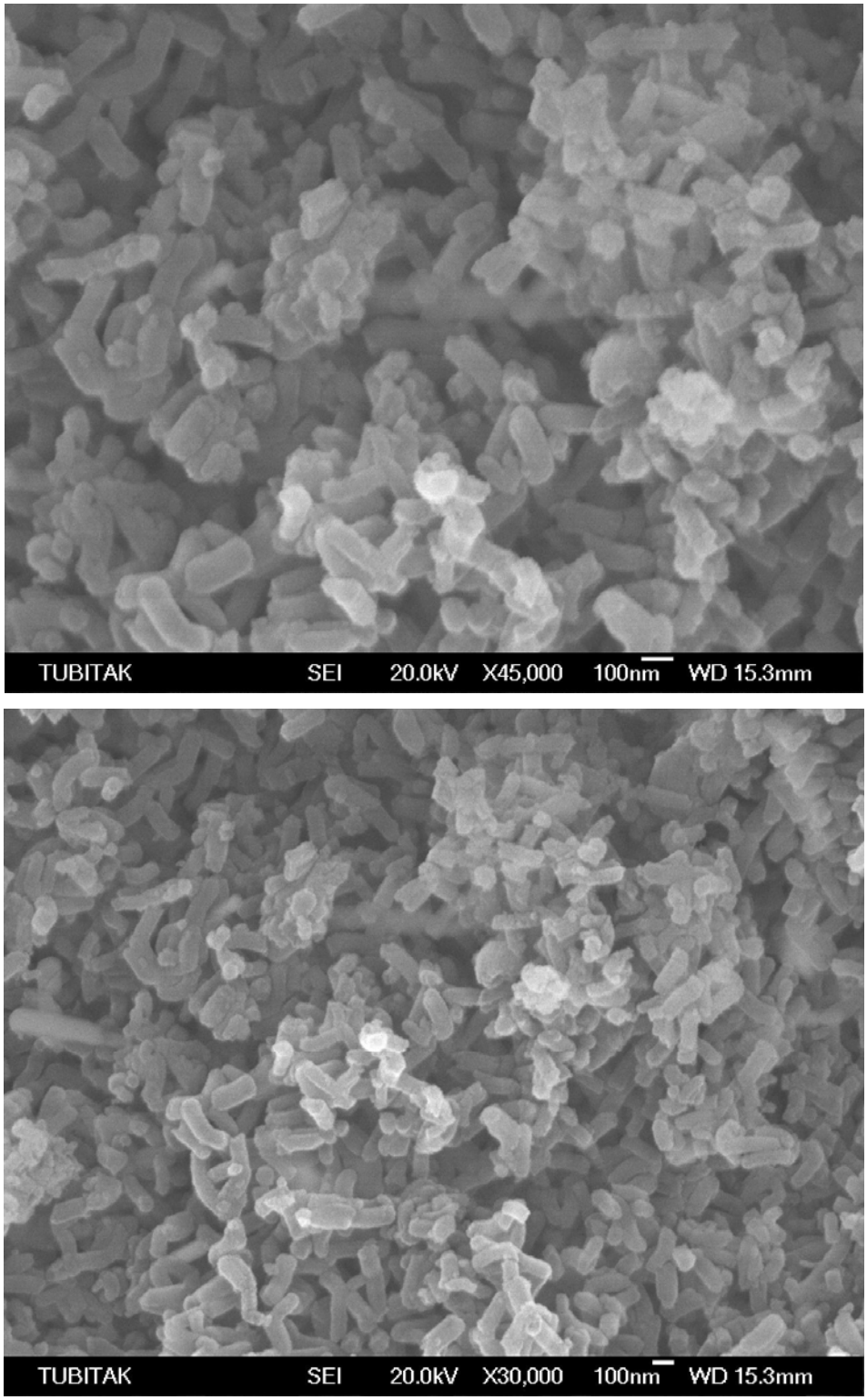

Figure 4.2.18. SEM images of [Pd-MCM-41(6)]

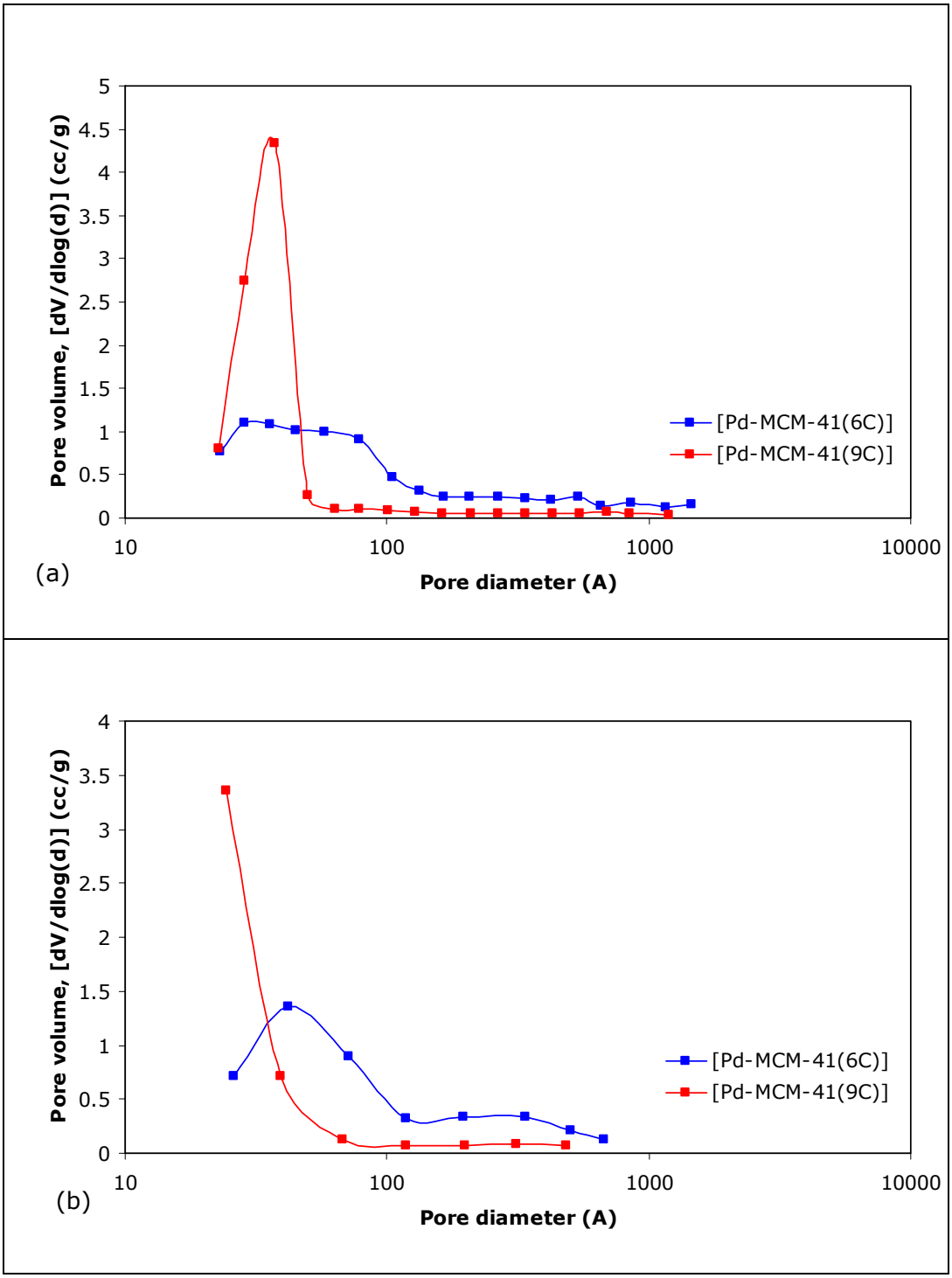

Figure 4.2.19. Pore size distribution curves for Pd-MCM-41 samples synthesized under acidic and basic conditions (a) BJH adsorption pore size distribution (b) BJH desorption pore size distribution

Table 4.2.17. Pore volumes of Pd-MCM-41 samples synthesized under acidic and basic conditions

Sample	Single Point Total Pore Volume at P/Po 0.98 (cc/g)	BJH Adsorption Pore Volume (cc/g)	BJH Desorption Pore Volume (cc/g)
[Pd-MCM-41 (6C)]	0.87	0.93	0.93
[Pd-MCM-41 (6R)]	0.92	1.00	1.00
[Pd-MCM-41 (9C)]	0.94	1.03	1.02
[Pd-MCM-41 (9R)]	0.86	1.06	1.06

Table 4.2.18. Pore diameters of Pd-MCM-41 samples synthesized under acidic and basic conditions

Sample	Average Pore Diameter (nm)	BJH Adsorption Average Pore Diameter (nm)	BJH Desorption Average Pore Diameter (nm)
[Pd-MCM-41 (6C)]	5.21	4.77	4.16
[Pd-MCM-41 (6R)]	5.30	4.95	4.24
[Pd-MCM-41 (9C)]	3.61	3.11	2.08
[Pd-MCM-41 (9R)]	3.27	2.78	2.82

Table 4.2.19. Pore wall characteristics of Pd-MCM-41 samples synthesized under acidic and basic conditions

Sample	$d_{(100)}$ (nm)	Lattice Parameter	BJH Pore Diameter d_p (nm)	Pore Wall Thick. δ (nm)
[Pd-MCM-41 (6C)]	3.80	4.39	4.77	-
[Pd-MCM-41 (6R)]	3.87	4.47	4.95	-
[Pd-MCM-41 (9C)]	3.79	4.38	3.11	1.27
[Pd-MCM-41 (9R)]	3.74	4.32	2.80	1.52

Since the structure of [Pd-MCM-41(6)] is not hexagonal, pore wall thickness cannot be calculated.

EDS analysis showed that Pd was also successfully incorporated into the structure of this mesoporous product [Pd-MCM-41(6)]. The Pd/Si wt ratio was found as 0.17 in this product (Table 4.2.20). But it is clearly seen that, palladium incorporation was achieved with high efficiency under basic conditions. Pd/Si weight ratio obtained from EDS analysis is nearly two times of its value adjusted during the synthesis.

Table 4.2.20. EDS Analysis Pd-MCM-41 materials synthesized under acidic and basic conditions

Sample	Element	Weight Conc. (%)	Atom Conc. (%)	Pd/Si Ratio	
				Weight	Atomic
[Pd-MCM-41 (6C)]	Pd	14.31	4.22	0.17	0.04
	Si	85.69	95.78		
[Pd-MCM-41 (6R)]	Pd	15.10	4.50	0.18	0.05
	Si	83.63	94.37		
[Pd-MCM-41 (9C)]	Pd	17.23	5.21	0.21	0.06
	Si	82.77	94.79		
[Pd-MCM-41 (9R)]	Pd	18.59	5.69	0.23	0.06
	Si	81.59	94.31		

4.2.4. Effect of Palladium Source in the Synthesis of Pd-MCM-41 Samples Under Basic Conditions

In the synthesis of Pd-MCM-41 nanocomposite materials synthesized by direct hydrothermal synthesis technique, primarily $PdCl_2$ was used as palladium precursor. However, synthesis of [Pd-MCM-41] nanocomposites under basic conditions was very difficult by using $PdCl_2$ as the palladium source. $PdCl_2$ is slightly soluble in water and soluble in HCl. Adding HCl for dissolving $PdCl_2$, sharply decreases the final pH of the synthesis solution after the addition of palladium solution into the synthesis solution. To overcome this problem, it was decided to use different palladium precursors. K_2PdCl_4 and $Pd(NH_3)_4(NO_3)_2$ were tested for this purpose. For this set of experiments, all these materials were synthesized following the basic direct hydrothermal synthesis route and the Pd/Si wt. ratio was adjusted to 0.12 in the synthesis solution (Table 4.2.21).

Table 4.2.21. Pd-MCM-41 samples synthesized with different palladium precursors

Sample	Pd Source	Amount of Pd source added (g)	pH	Pd/Si Weight Ratio	Pd/Si Atomic Ratio
[Pd-MCM-41 (7)]	K_2PdCl_4	1.5016	11.0	0.12	0.03
[Pd-MCM-41 (8)]	$Pd(NH_3)_4(NO_3)_2$	13.4574	11.0	0.12	0.03
[Pd-MCM-41 (9)]	$PdCl_2$	0.4022	11.0	0.12	0.03

XRD spectra of all these materials showed the characteristic MCM-41 patterns with a sharp $d_{(100)}$ Bragg peak and the three reflections (Figure 4.2.20 and 4.2.21). XRD patterns were also compared in Figure 4.2.22.

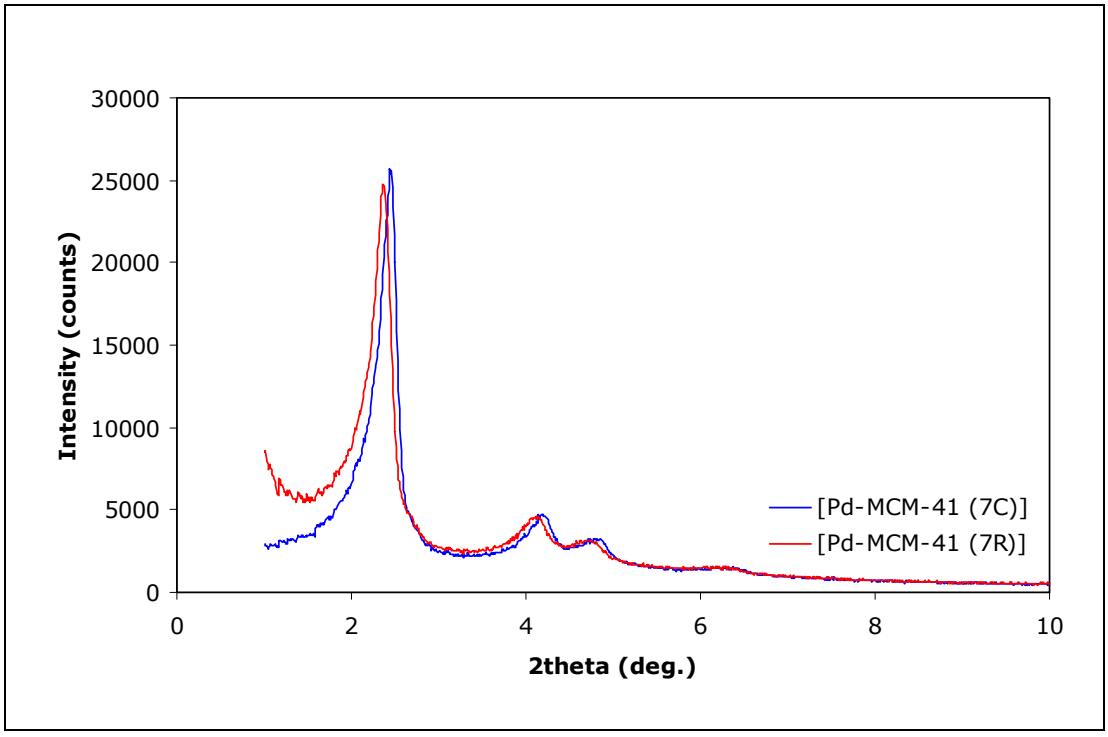

Figure 4.2.20. XRD pattern of [Pd-MCM-41(7)]

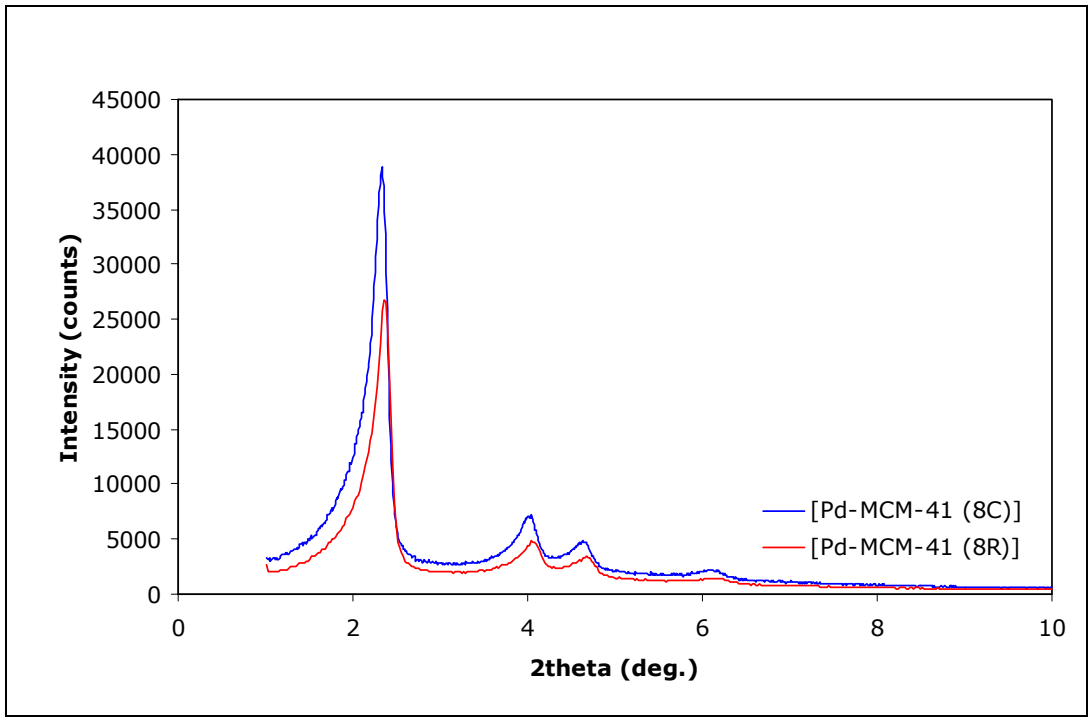

Figure 4.2.21. XRD pattern of [Pd-MCM-41(8)]

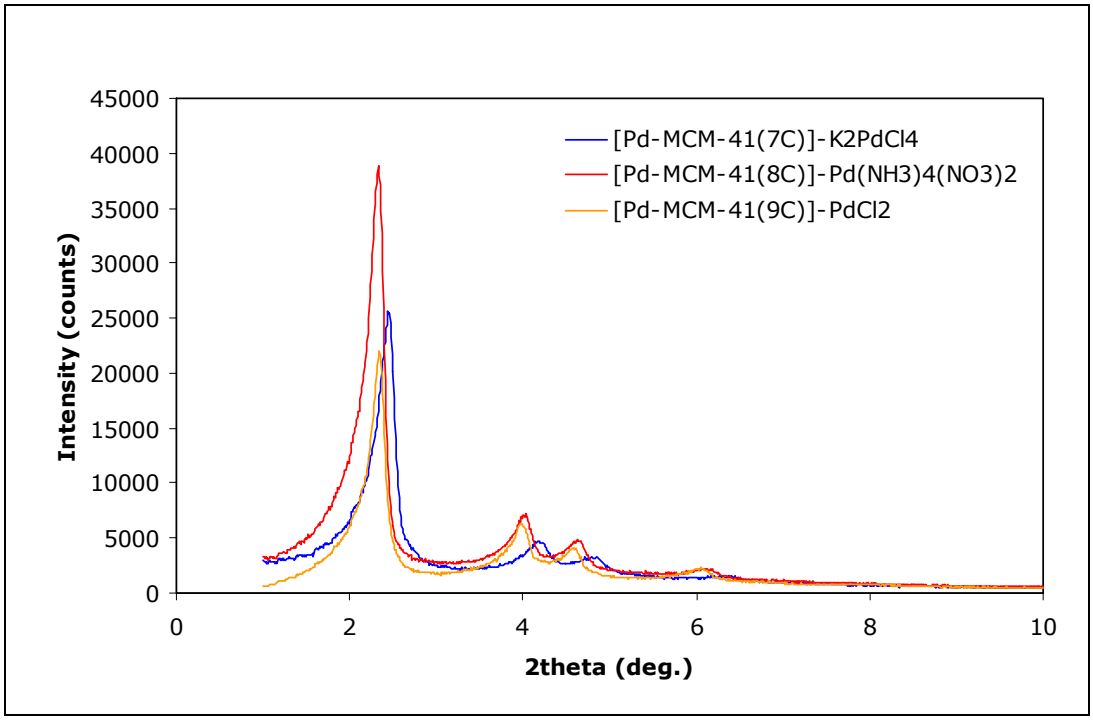

Figure 4.2.22. XRD patterns of Pd-MCM-41 samples synthesized by different palladium precursors

In all these cases, Pd was succesfully incorporated into the lattice without destroying the MCM-41 structure. As shown in Table 4.2.21, the highest Pd/Si wt ratio was obtained as 0.26 using K_2PdCl_4 as the Pd source.

In the case of using $Pd(NH_3)_4(NO_3)_2$ as the palladium source, incorporation of Pd into the MCM-41 lattice was lower than the other two Pd sources used in this work. Similarly, rather low incorporation of vanadium into the MCM-41 structure was observed with the ammonium salt of vanadium (ammonium vanadate) by Gucbilmez [30].

Table 4.2.22. EDS analysis of the Pd-MCM-41 samples synthesized with different Pd sources

Sample	Element	Weight Conc. (%)	Atom Conc. (%)	Pd/Si Ratio	
				Weight	Atomic
[Pd-MCM-41 (7C)]	Pd	20.62	6.42	0.26	0.07
	Si	79.38	93.58		
[Pd-MCM-41 (7R)]	Pd	18.69	5.72	0.23	0.06
	Si	81.31	94.28		
[Pd-MCM-41 (8C)]	Pd	12.32	3.58	0.14	0.04
	Si	87.68	96.42		
[Pd-MCM-41 (8R)]	Pd	15.62	4.66	0.19	0.05
	Si	84.38	95.34		
[Pd-MCM-41 (9C)]	Pd	17.23	5.21	0.21	0.06
	Si	82.77	94.79		
[Pd-MCM-41 (9R)]	Pd	18.59	5.69	0.23	0.06
	Si	81.41	94.31		

The BET surface area values of all these materials were close, being around 1050 m^2/g (Table 4.2.23). Also, the characteristic lattice parameter values were all around 4.35 nm.

Table 4.2.23. Surface areas of Pd-MCM-41 samples synthesized with different palladium sources

Sample	BET Surface Area (m^2/g)	BJH Adsorption Surface Area (m^2/g)	BJH Desorption Surface Area (m^2/g)	Single Point Surface Area at P/P_o 0.19 (m^2/g)
[Pd-MCM-41 (7C)]	1081.5	1436.7	1830.0	1018.8
[Pd-MCM-41 (7R)]	1091.3	1444.9	1808.8	1026.1
[Pd-MCM-41 (8C)]	1025.4	1373.4	1779.6	978.0
[Pd-MCM-41 (8R)]	1054.0	1423.0	1407.0	987.9
[Pd-MCM-41 (9C)]	1039.9	1322.4	1969.9	990.3
[Pd-MCM-41 (9R)]	1051.0	1408.0	1404.0	939.7

Nitrogen adsorption-desorption isotherms of the samples [Pd-MCM-41(7)] and [Pd-MCM-41(8)] were given in Figures 4.2.23.and 4.2.24, respectively. For a comparison, isotherms for all three samples synthesized with different palladium precursors were also shown in Figure 4.2.28. Figures 4.2.25 and 4.2.26 are the pore size distribution curves for [Pd-MCM-41(7)] and [Pd-MCM-41(8)] samples. In Figure 4.2.29, pore sizes of this set are compared and found that all the materials had narrow pore size distributions. [Pd-MCM-41(9)] has a relatively wider pore size distribution.

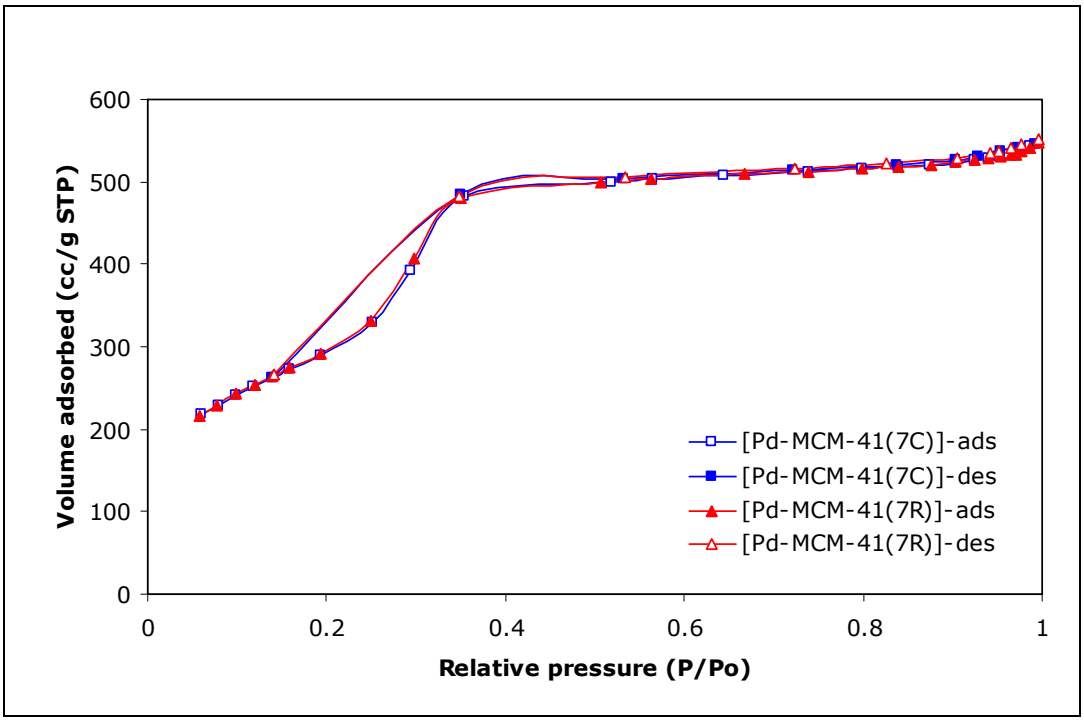

Figure 4.2.23. Nitrogen adsorption-desorption isotherm of [Pd-MCM-41(7)]

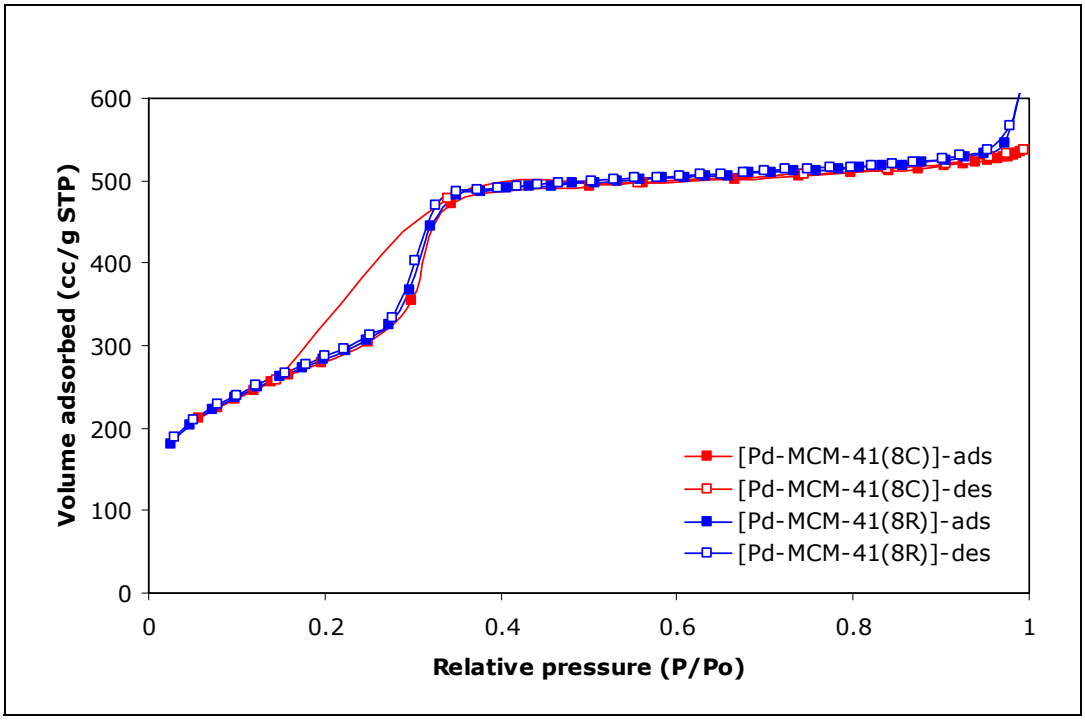

Figure 4.2.24. Nitrogen adsorption-desorption isotherm of [Pd-MCM-41(8)]

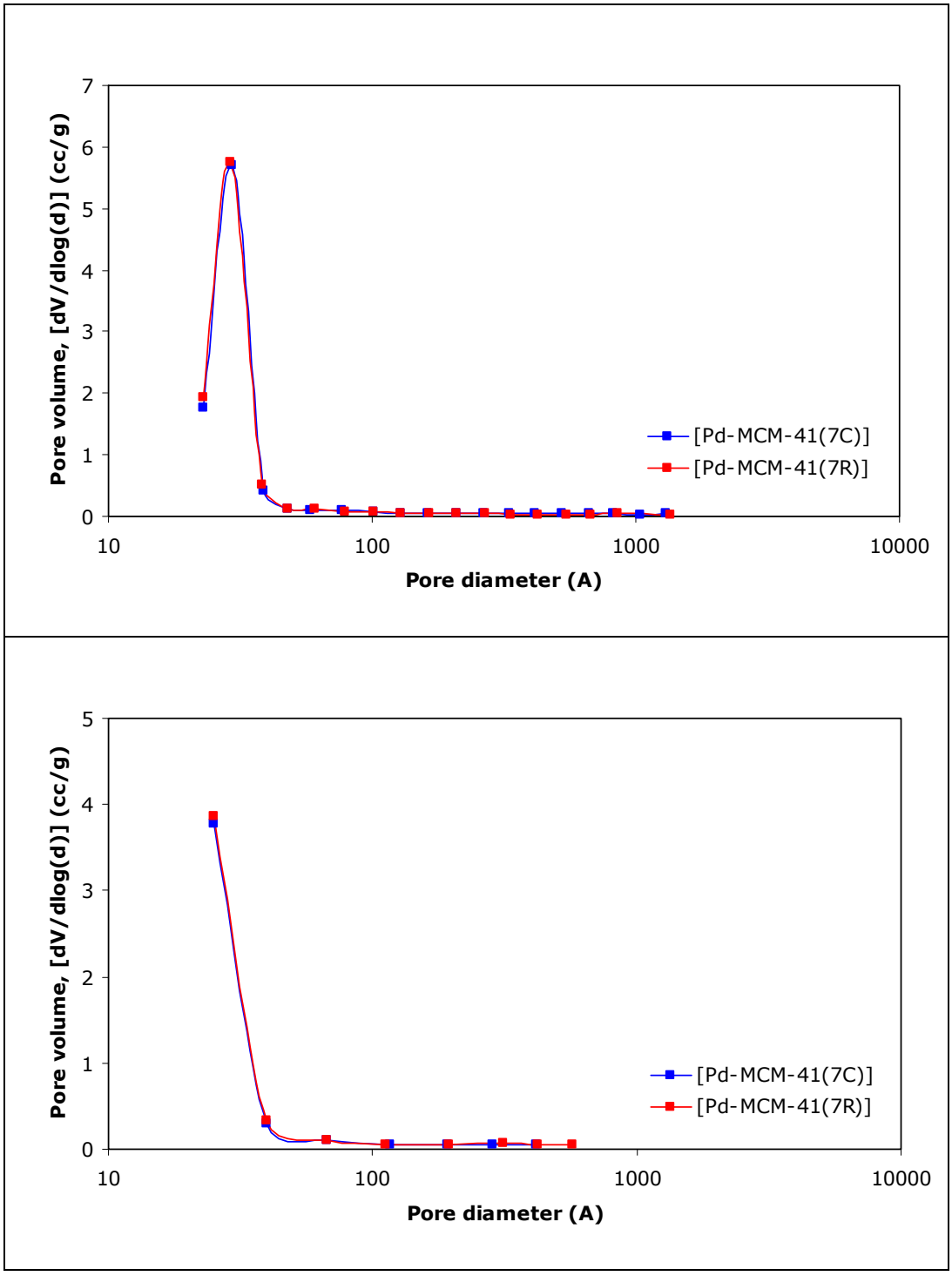

Figure 4.2.25. Pore size distribution curves for [Pd-MCM-41(7)] (a) BJH adsorption pore size distribution (b) BJH desorption pore size distribution

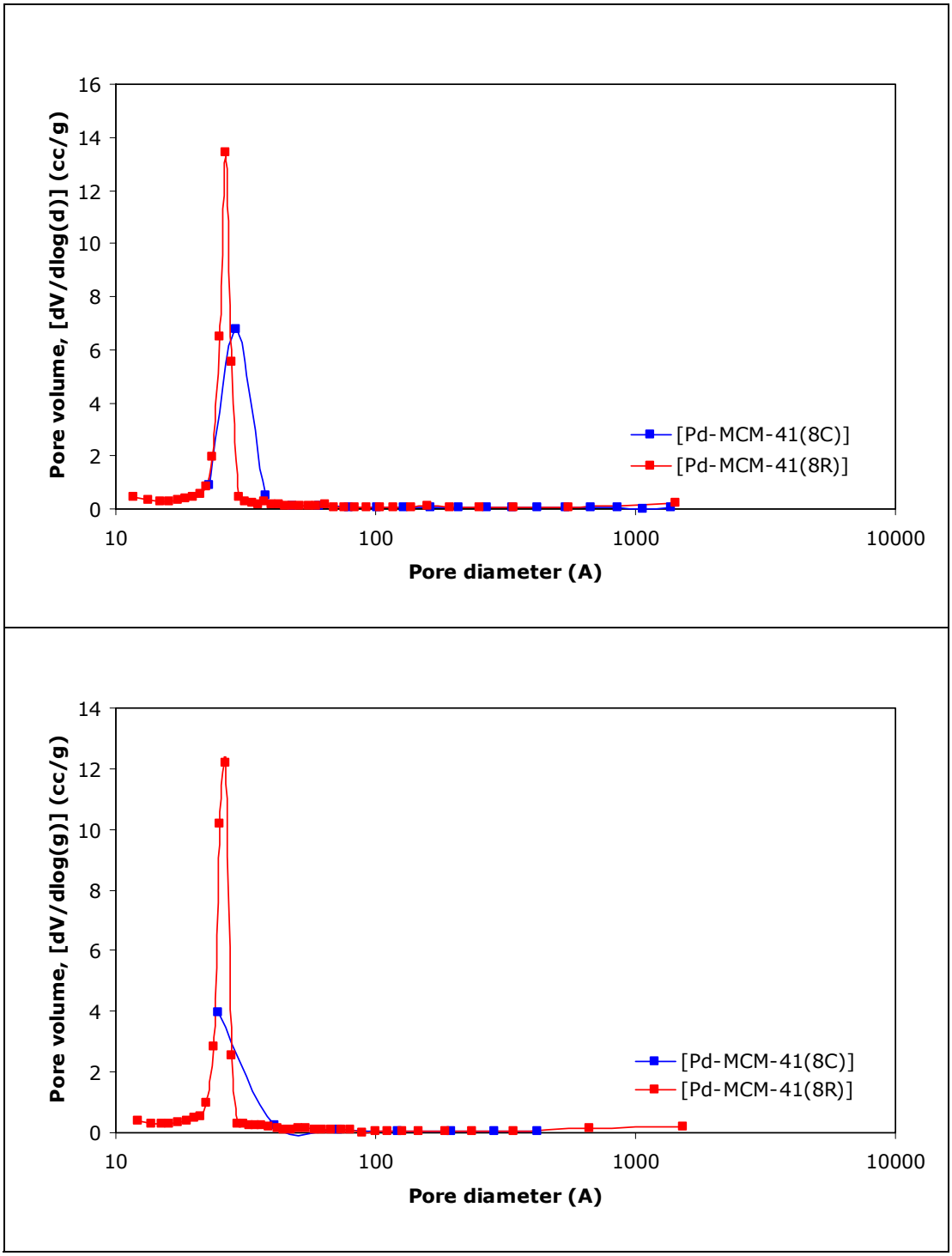

Figure 4.2.26. Pore size distribution curves for [Pd-MCM-41(8)] (a) BJH adsorption pore size distribution (b) BJH desorption pore size distribution

Table 4.2.24. Pore volumes of Pd-MCM-41 samples synthesized with different palladium sources

Sample	Single Point Total Pore Volume at P/Po 0.98 (cc/g)	BJH Adsorption Pore Volume (cc/g)	BJH Desorption Pore Volume (cc/g)
[Pd-MCM-41 (7C)]	0.835	0.952	0.947
[Pd-MCM-41 (7R)]	0.836	0.961	0.957
[Pd-MCM-41 (8C)]	0.823	0.931	0.933
[Pd-MCM-41 (8R)]	0.839	1.021	1.014
[Pd-MCM-41 (9C)]	0.939	1.029	1.025
[Pd-MCM-41 (9R)]	0.859	1.064	1.060

Pore volumes of the samples synthesized using different palladium sources were listed in Table 4.2.24.

Table 4.2.25 depicts that relatively smaller pore sizes could be obtained by using K_2PdCl_4 as the palladium source for the synthesis of Pd-MCM-41 nanocomposites. $Pd(NH_3)_4(NO_3)_2$ gives relatively thicker pore walls (Table 4.2.26).

Figure 4.2.27 displays SEM images of [Pd-MCM-41(7)] and [Pd-MCM-41(8)]. It is observed from the figures that surface morphology did not remain same when Palladium precursor was changed. Two samples have different particule sizes and shapes.

Table 4.2.25. Pore diameters of Pd-MCM-41 samples synthesized with different palladium sources

Sample	Average Pore Diameter (nm)	BJH Adsorption Average Pore Diameter (nm)	BJH Desorption Average Pore Diameter (nm)
[Pd-MCM-41 (7C)]	3.09	2.65	2.07
[Pd-MCM-41 (7R)]	3.07	2.66	2.12
[Pd-MCM-41 (8C)]	3.21	2.71	2.10
[Pd-MCM-41 (8R)]	3.18	2.63	2.66
[Pd-MCM-41 (9C)]	3.61	3.11	2.08
[Pd-MCM-41 (9R)]	3.27	2.78	2.82

Table 4.2.26. Pore wall characteristics of Pd-MCM-41 samples synthesized with different palladium sources

Sample	$d_{(100)}$ (nm)	Lattice Parameter	BJH Pore Diameter d_p (nm)	Pore Wall Thick. δ (nm)
[Pd-MCM-41 (7C)]	3.62	4.18	2.65	1.53
[Pd-MCM-41 (7R)]	3.72	4.30	2.66	1.64
[Pd-MCM-41 (8C)]	3.77	4.35	2.71	1.64
[Pd-MCM-41 (8R)]	3.74	4.32	2.64	1.68
[Pd-MCM-41 (9C)]	3.79	4.38	3.11	1.27
[Pd-MCM-41 (9R)]	3.74	4.32	2.80	1.52

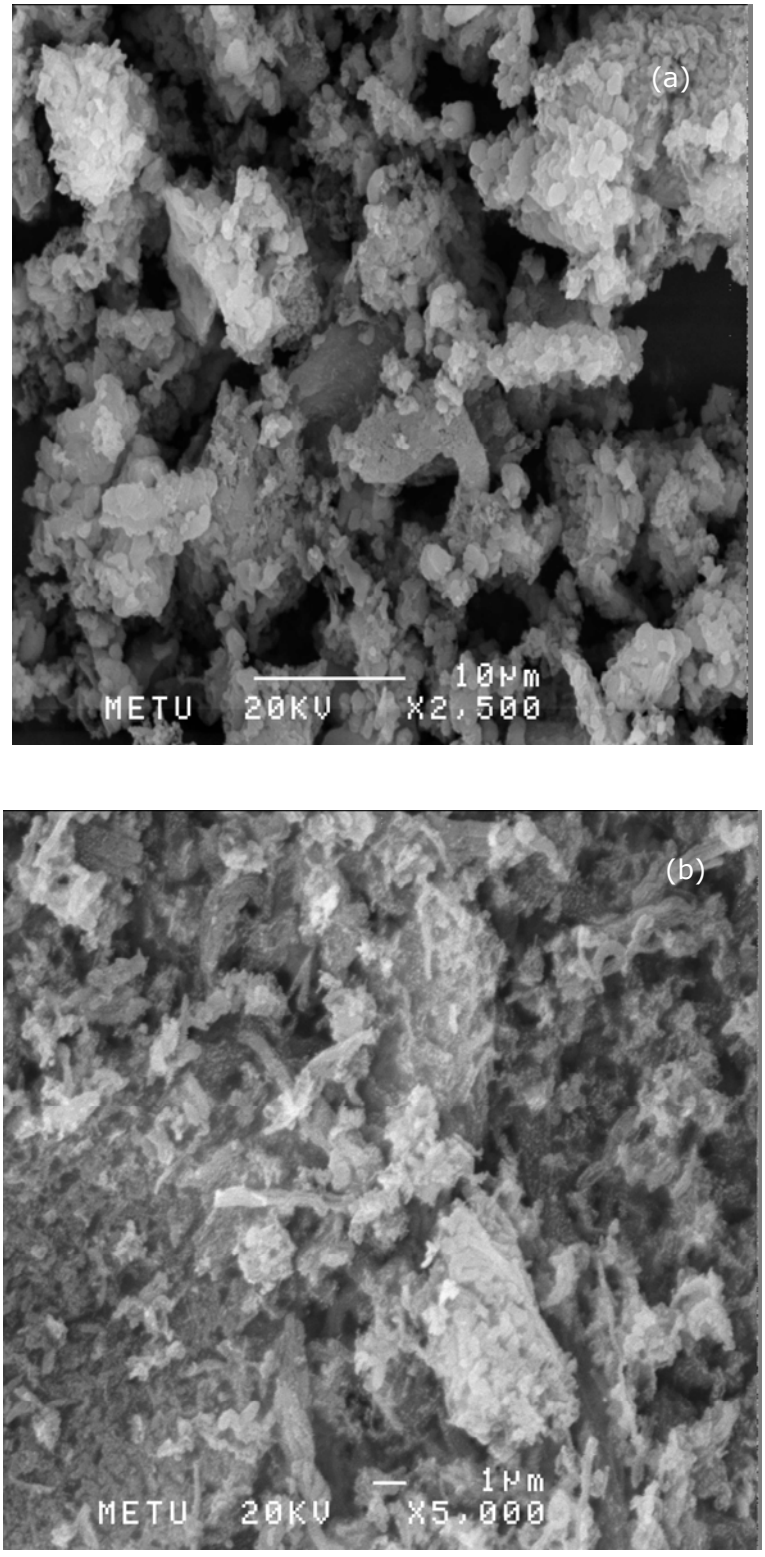

Figure 4.2.27. SEM images of (a) [Pd-MCM-41(7C)] and (b) [Pd-MCM-41(8R)]

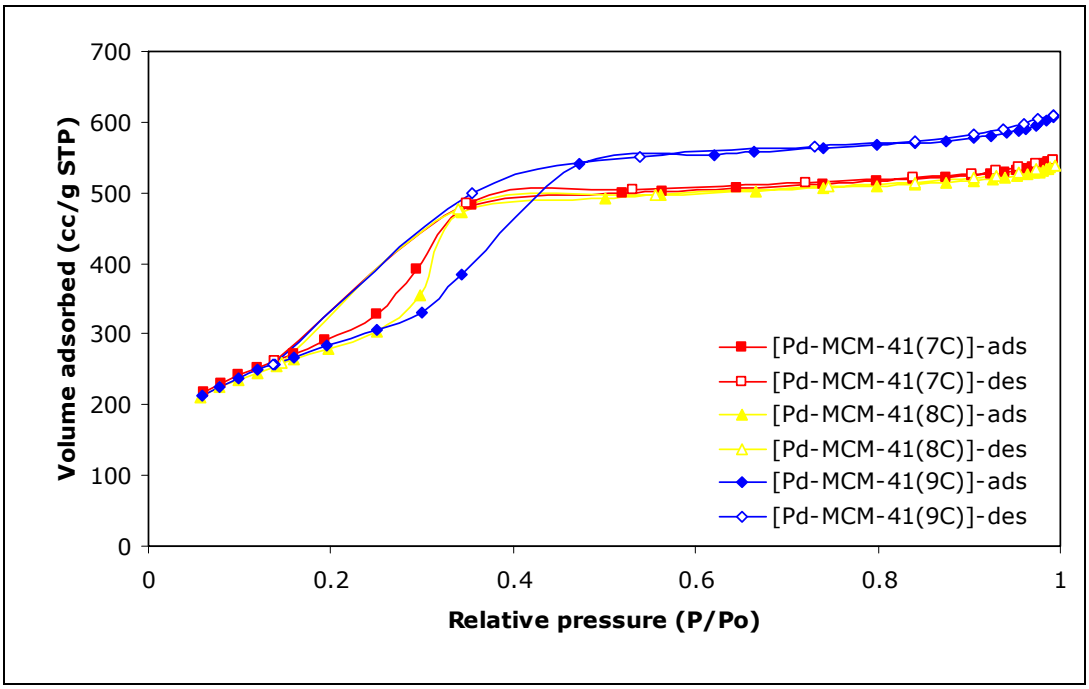

Figure 4.2.28. Comparison of nitrogen adsorption-desorption isotherms of Pd-MCM-41 samples synthesized with different Pd sources

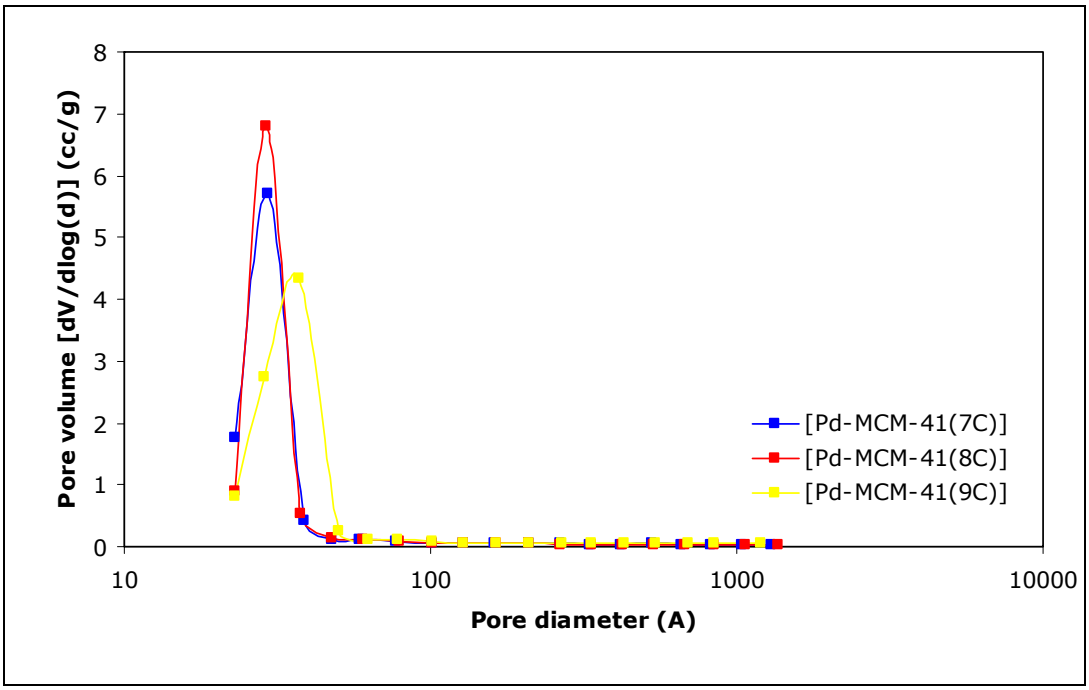

Figure 4.2.29. Comparison of pore size distributions of Pd-MCM-41 samples synthesized with different Pd sources

4.3. CHARACTERIZATION OF Pd@MCM-41 SAMPLES

The [Pd@MCM-41] nanocomposite material was obtained by the impregnation and deposition of Pd into the pores of MCM-41 following the procedure given in Chapter 3.3. [Pd@MCM-41(3)] and [Pd@MCM-41(4)] nanocomposites were synthesized with two different palladium concentrations. Table 4.3.1 summarizes the synthesis details of the materials. [MCM-41(3)] was used as the host material for [Pd@MCM-41(3)] and [MCM-41(2)] was used for synthesis of [Pd@MCM-41(4)].

Table 4.3.1. Properties of synthesized Pd@MCM-41 nanocomposites

Sample	Pd Source	Amount of Pd source added (g)	Pd %	Pd/Si Weight Ratio
[Pd@MCM-41 (3)]	$PdCl_2$	0.0496	10	0.18
[Pd@MCM-41 (4)]	$PdCl_2$	0.0330	5	0.08

Pd@MCM-41 host-guest systems were characterized by X-ray diffraction (XRD), transmission electron microscopy (TEM), scanning electron microscopy (SEM), nitrogen adsorption-desorption isotherms, energy dispersive spectroscopy (EDS).

4.3.1. X-Ray Diffraction Analysis (XRD)

XRD patterns of the samples [Pd@MCM-41(3)] and [Pd@MCM-41(4)] are given in Figure 4.3.1. For a comparison, typical XRD pattern of MCM-41 was also shown on the figure. As expected, the XRD patterns of Pd@MCM-41 and the host MCM-41 were quite similar. However, increasing the palldium loading amount affects the MCM-41 structure.

Table 4.3.2 gives Bragg peaks and corresponding d-values for the samples [Pd@MCM-41(3)] and [Pd@MCM-41(4)]. By the increase of palladium, last two reflections of XRD pattern were lost.

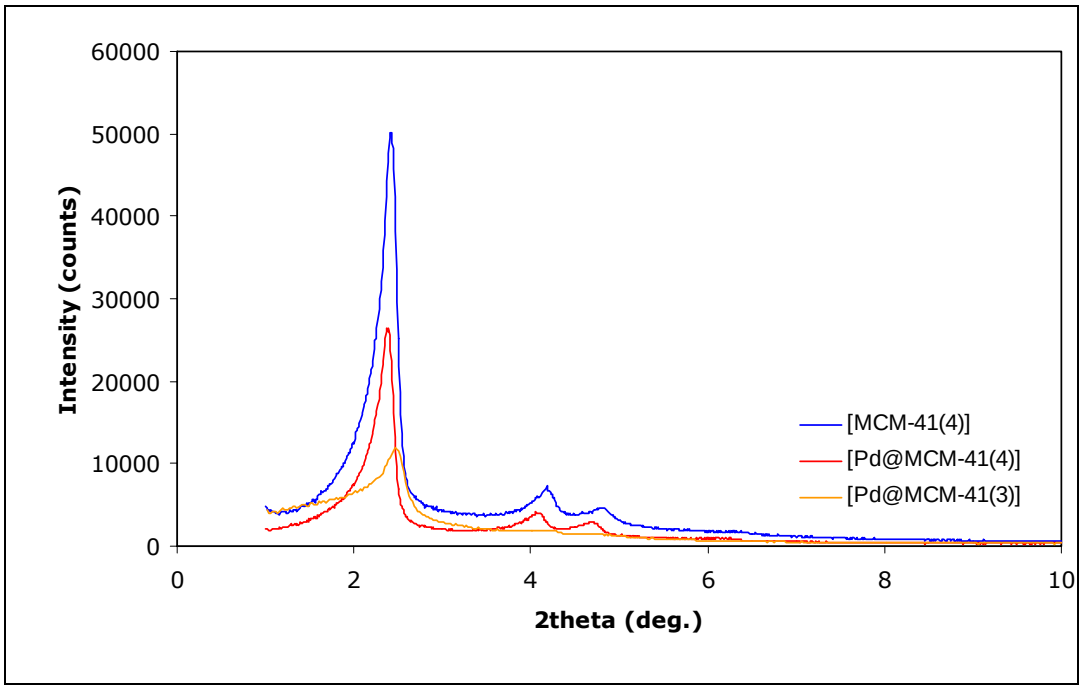

Figure 4.3.1. XRD patterns of [Pd@MCM-41] samples

Table 4.3.2. XRD results and d-spacings of Pd@MCM-41 samples

Sample	hlk	$d_{(100)}$ (nm)	Angle (2theta)
[Pd@MCM-41(3)]	100	3.59	2.460
	110	2.10	4.200
	200	-	-
	210	-	-
[Pd@MCM-41(4)]	100	3.71	2.380
	110	2.16	4.080
	200	1.88	4.700
	210	-	-

4.3.2. Energy Dispersive Spectroscopy (EDS) Analysis

The EDS results gave a Pd/Si wt ratio of the nanocomposite [Pd@MCM-41(4)] as 0.12 and that of nanocomposite [Pd@MCM-41(3)] as 0.24 (Table 4.3.3). EDS patterns of the samples [Pd@MCM-41(3)] and [Pd@MCM-41(4)] were given in Figures 4.3.2 and 4.3.3.

Table 4.3.3. EDS Analysis of Pd@MCM-41 Samples

Sample	Element	Weight Conc. (%)	Atom Conc. (%)	Pd/Si Ratio	
				Weight	Atomic
[Pd@MCM-41 (3)]	Pd	19.34	5.95	0.24	0.06
	Si	80.66	94.05		
[Pd@MCM-41 (4)]	Pd	10.41	2.98	0.12	0.03
	Si	89.59	97.02		

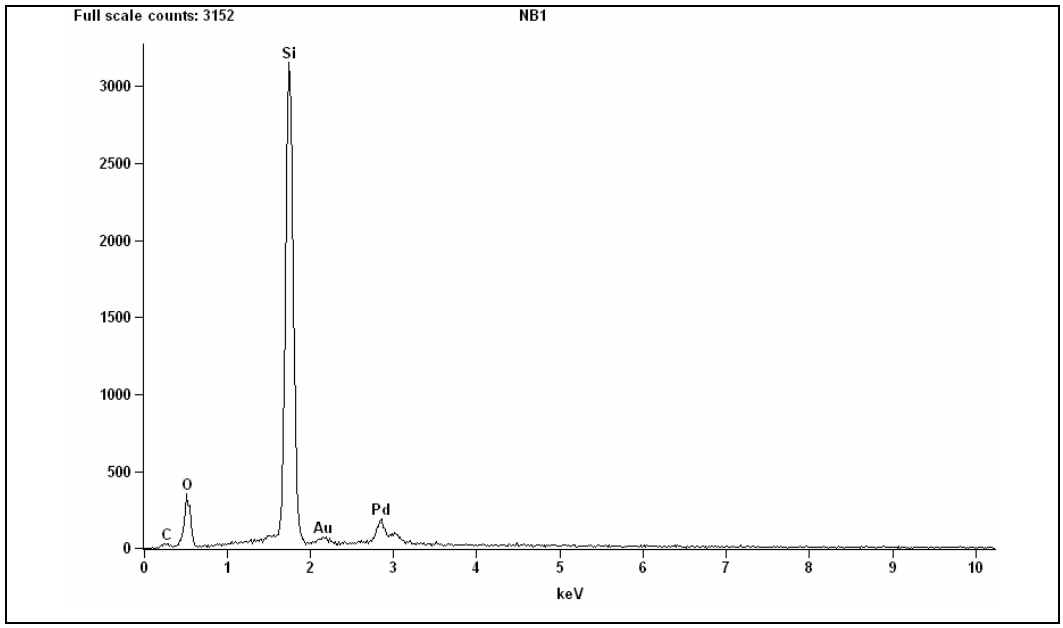

Figure 4.3.2. EDS pattern of [Pd@MCM-41(3)]

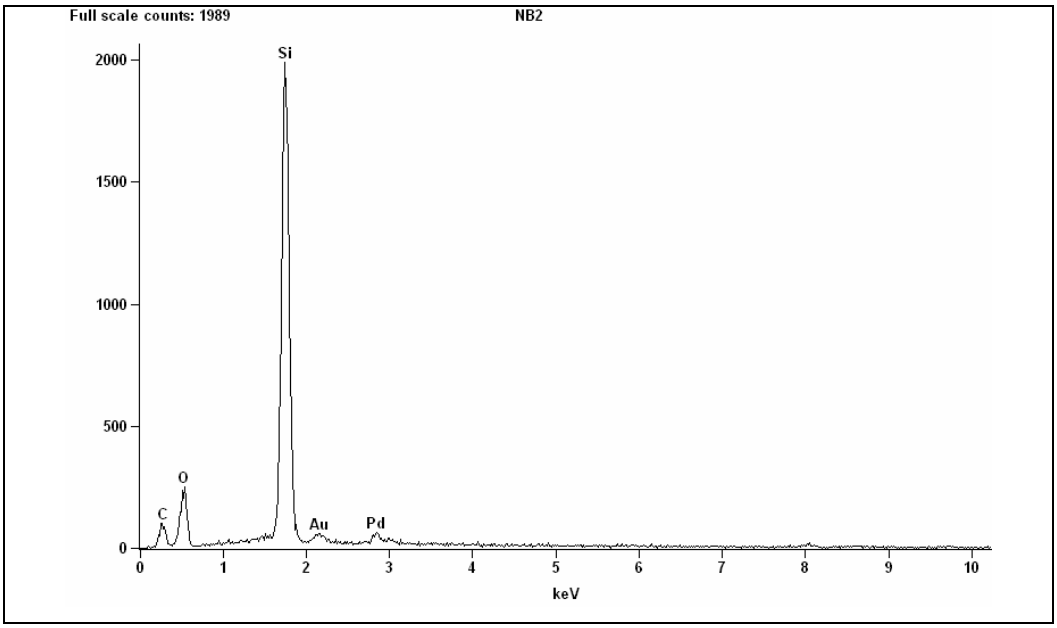

Figure 4.3.3. EDS patterns of [Pd@MCM-41(4)]

4.3.3. Nitrogen Physisorption Analysis

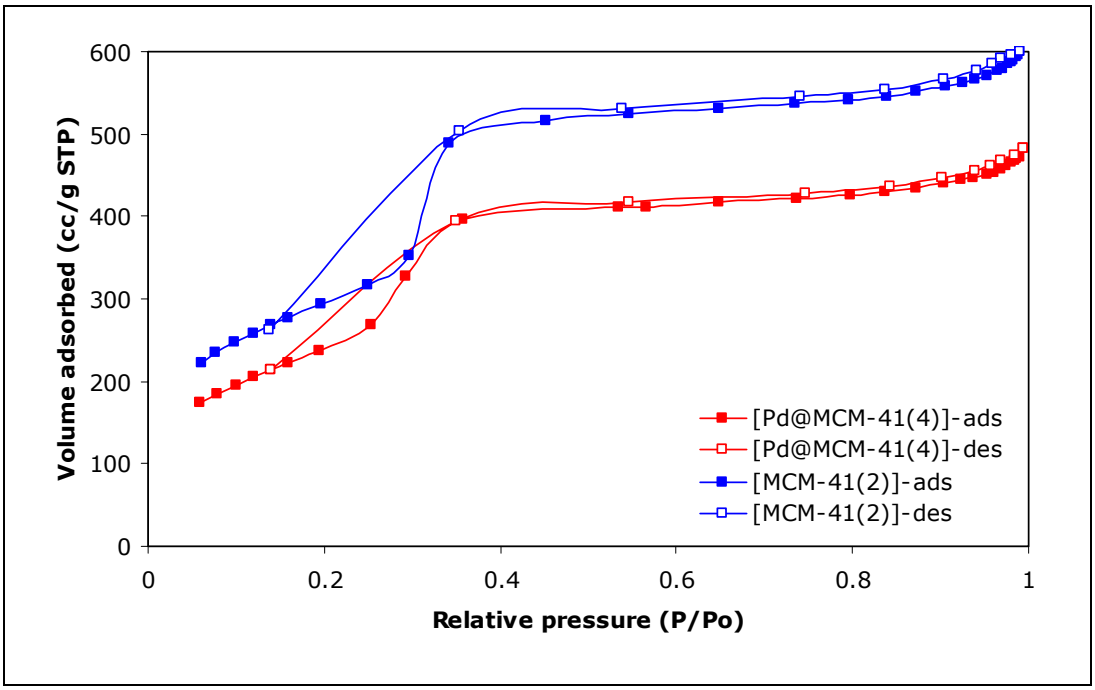

Figure 4.3.4. Nitrogen adsorption-desorption isotherm of [Pd@MCM-41(4)] material and its host [MCM-41(2)]

By the impregnation of palladium into the MCM-41, surface area and pore volume values decreased about 20 %. However, the decrease of the average pore radius was much less (about 3 %) (Table 4.3.6). The pore size distributions of Pd@MCM-41 and the host MCM-41 were quite similar, giving narrow distributions with a maximum at about the same value (Figure 4.3.5). These results indicated the plugging of some of the pores of the MCM-41 by the Pd nanoballs formed inside these pores.

Table 4.3.4. Surface area of [Pd@MCM-41(4)] and its host material

Sample	BET Surface Area (m^2/g)	BJH Adsorption Surface Area (m^2/g)	BJH Desorption Surface Area (m^2/g)	Single Point Surface Area at P/P_o 0.19 (m^2/g)
[MCM-41 (2)]	1076.3	1434.3	1944.1	1026.3
[Pd@MCM-41(4)]	883.2	1176.6	1495.0	828.6

Table 4.3.5. Pore volume of [Pd@MCM-41(4)] and its host material

Sample	Single Point Total Pore Volume at P/Po 0.98 (cc/g)	BJH Adsorption Pore Volume (cc/g)	BJH Desorption Pore Volume (cc/g)
[MCM-41 (2)]	0.91	1.03	1.02
[Pd@MCM-41(4)]	0.72	0.82	0.82

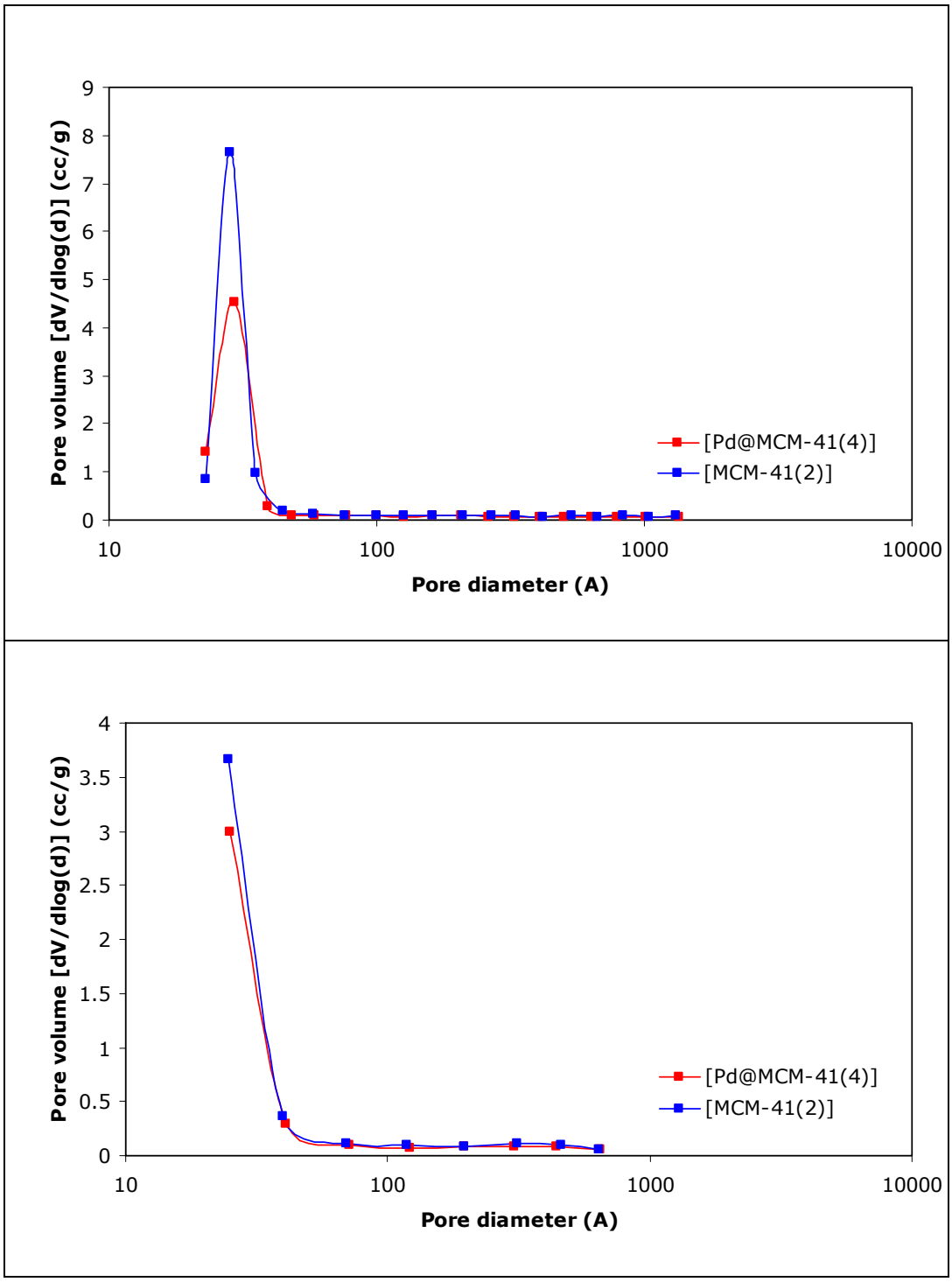

Figure 4.3.5. Pore size distribution of [Pd@MCM-41(4)] (a) BJH adsorption pore size distribution (b) BJH desorption pore size distribution

Table 4.3.6. Pore size of [Pd@MCM-41(4)] and its host material

Sample	Average Pore Diameter (nm)	BJH Adsorption Average Pore Diameter (nm)	BJH Desorption Average Pore Diameter (nm)
[MCM-41 (2)]	3.39	2.87	2.10
[Pd@MCM-41(4)]	3.27	2.79	2.19

Table 4.3.7. Pore wall characteristics of [Pd@MCM-41(4)] and its host material

Sample	$d_{(100)}$ (nm)	Lattice Parameter	BJH Pore Diameter d_p (nm)	Pore Wall Thick. δ (nm)
[MCM-41 (2)]	3.60	4.16	2.87	1.29
[Pd@MCM-41(4)]	3.79	4.38	2.79	1.59

4.3.4. Scanning Electron Microscopy Analysis (SEM) and Transmission Electron Microscopy (TEM) Analyses

In Figure 4.3.5 SEM images of [Pd@MCM-41] are shown. A different surface morphology was observed from the material synthesized by impregnation procedure.

TEM images of the sample [Pd@MCM-41] are given in Figure 4.3.6.

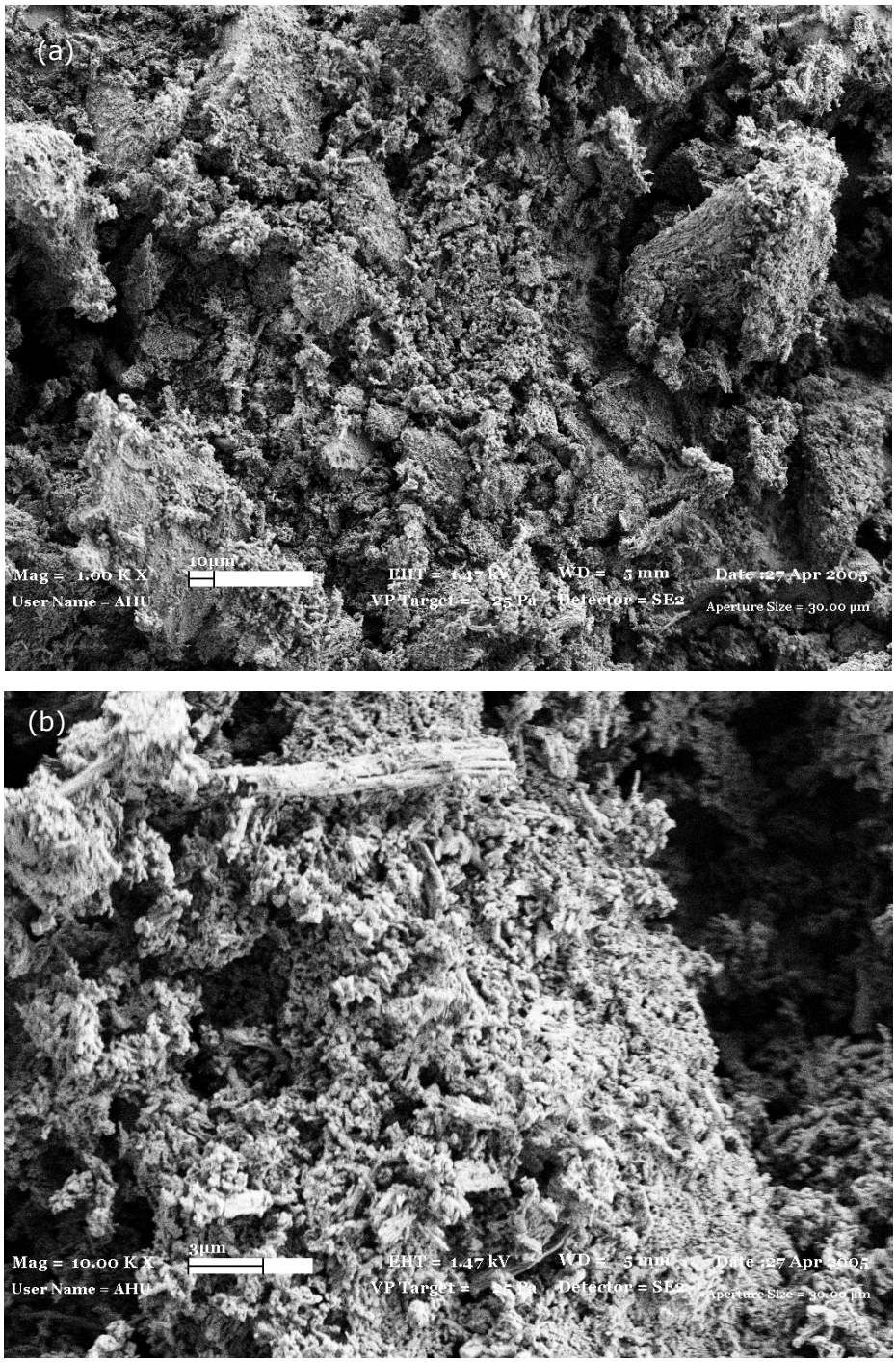

Figure 4.3.6. SEM images of [Pd@MCM-41(3)] (a) magnified 1000 times (b) magnified 1000 times

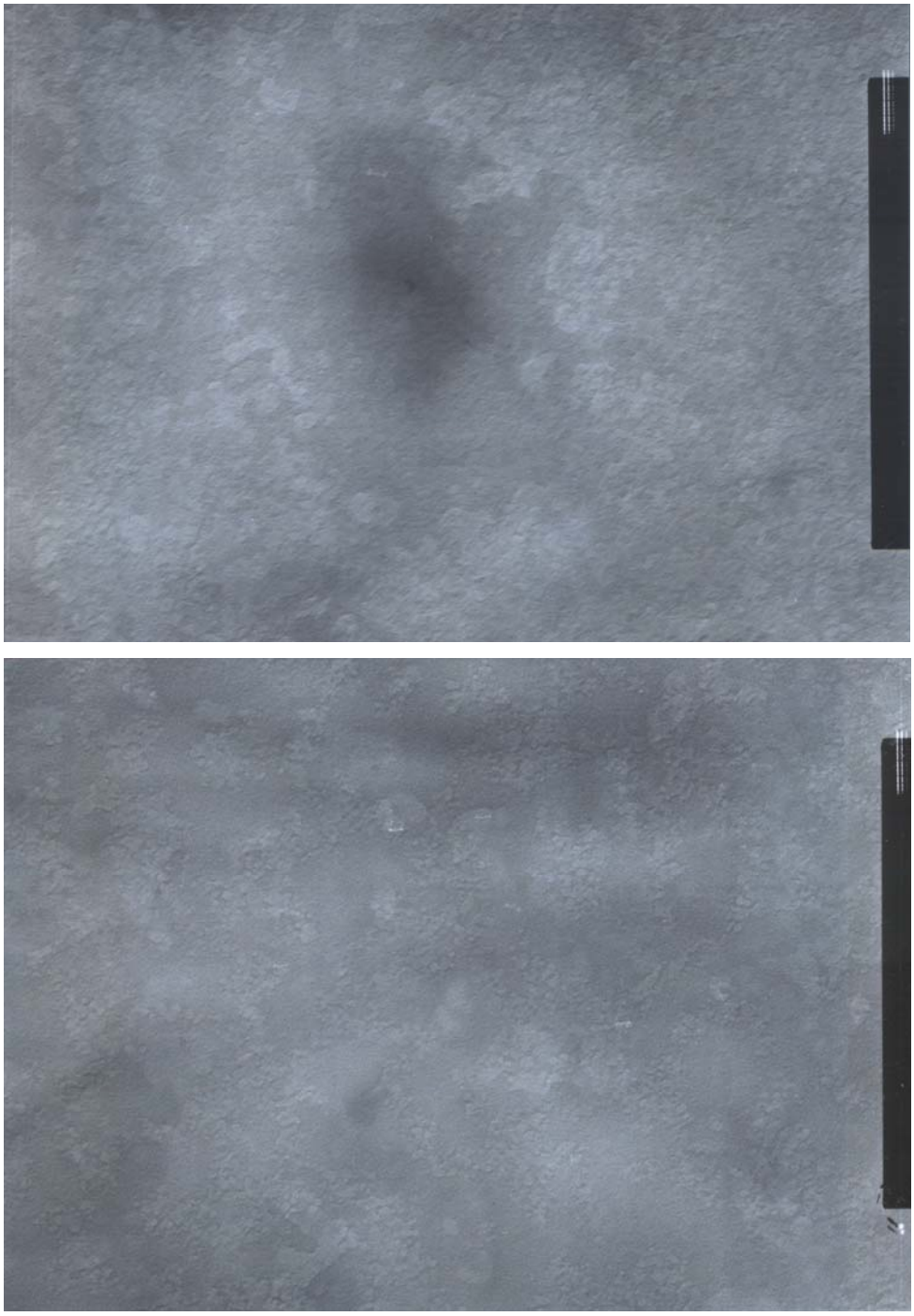

Figure 4.3.7. TEM images of [Pd@MCM-41(4)]

4.4. COMPARISON OF Pd-MCM-41 NANOCOMPOSITES SYNTHESIZED BY DIRECT HYDROTHERMAL SYNTHESIS AND IMPREGNATION TECHNIQUES

As seen in the previous sections, both direct hydrothermal synthesis and impregnation were applied successfully. In addition, comparison of these techniques would be necessary to use them for catalytic applications effectively. Calculation of Pd/Si ratio in the synthesis solution for different techniques could cause errors. It is better to select the basis as the Pd/Si weight ratio obtained from EDS analysis for the final material synthesized. For this reason, it was chosen to compare [Pd-MCM-41(8)] (Pd/Si=0.14) and [Pd@MCM-41(4)] (Pd/Si=0.12). Then, doubling the Pd/Si ratio was examined by comparing [Pd-MCM-41(7)] and [Pd@MCM-41(4)], both having the Pd/Si ratio of 0.24.

It is interesting that, same XRD patterns were obtained for direct hydrothermal synthesis and impregnation techniques for Pd/Si ratio of 0.12 (Figure 3.4.1.a). However, impregnation technique gives smaller surface areas. BET surface area of [Pd-MCM-41(8)] was found as 1054 m^2/g while that of [Pd-MCM-41(4)] was 883.2 m^2/g.

Increasing Pd/Si ratio did not affect the structure in direct hydrothermal synthesis, however MCM-41 structure slightly destroyed the structure in impregnation technique. Surface area of Pd@MCM-41(3) was measured with Monosorb-Quantachrome instrument at Gazi University. It was measured as 527.4 m^2/g. It is an expected value, because palladium nanoparticles blocks the pores and decreases surface area in this technique.

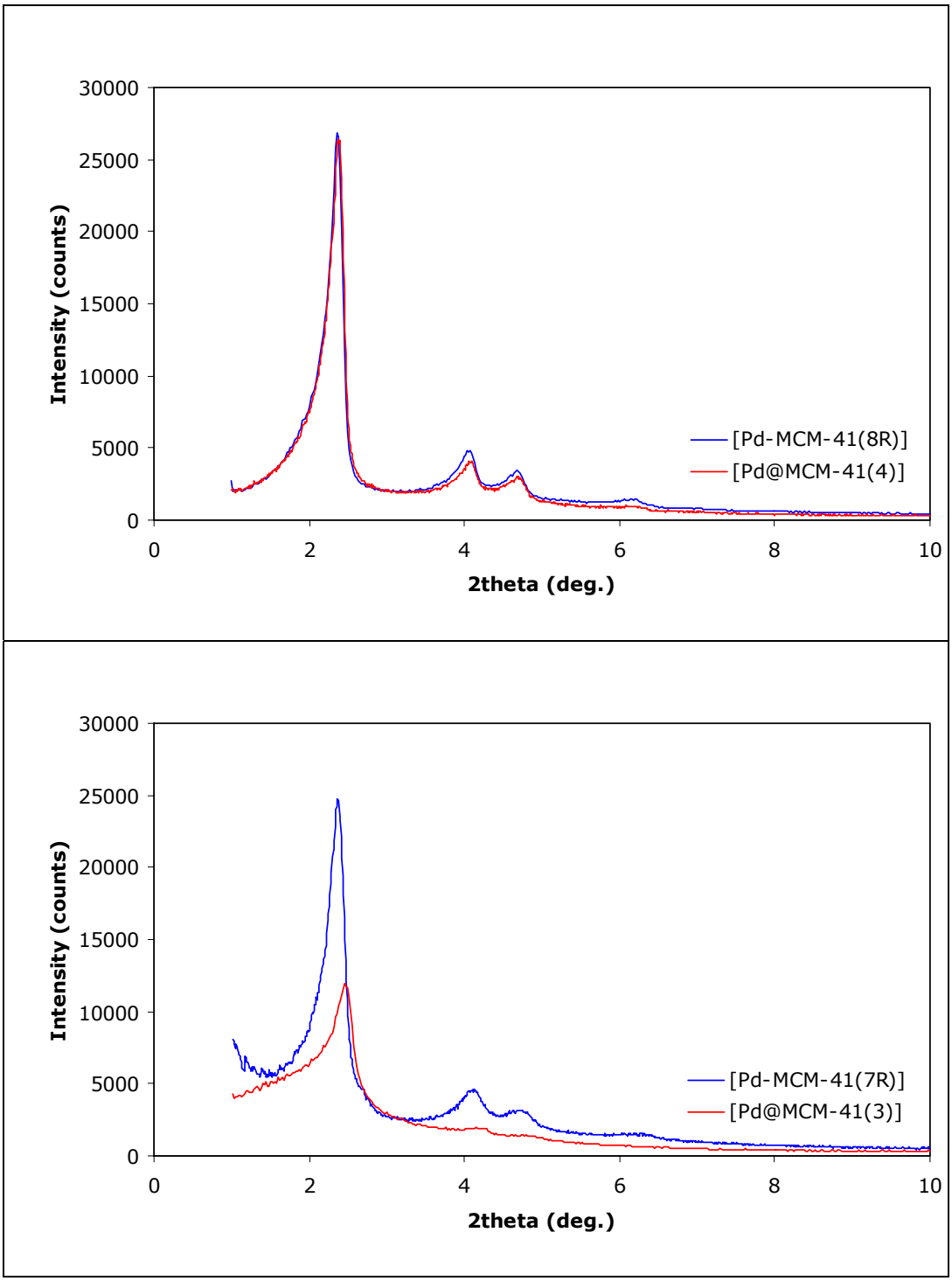

Figure 4.4.1. Comparison of XRD patterns of materials synthesized by direct hydrothermal synthesis and impregnation techniques (a) Both having Pd/Si ratio of 0.12 (b)Both having Pd/Si ratio of 0.24.

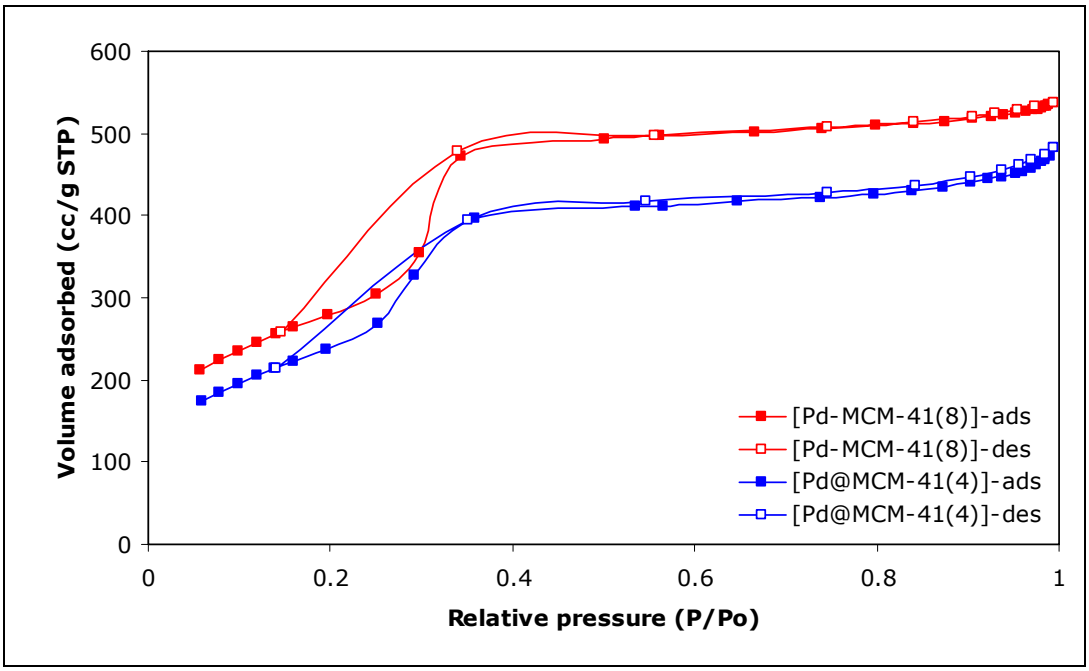

Figure 4.4.2. Comparison of nitrogen adsorption desorption isotherms of materials synthesized by direct hydrothermal synthesis and impregnation techniques both having the Pd/Si ratio of 0.12

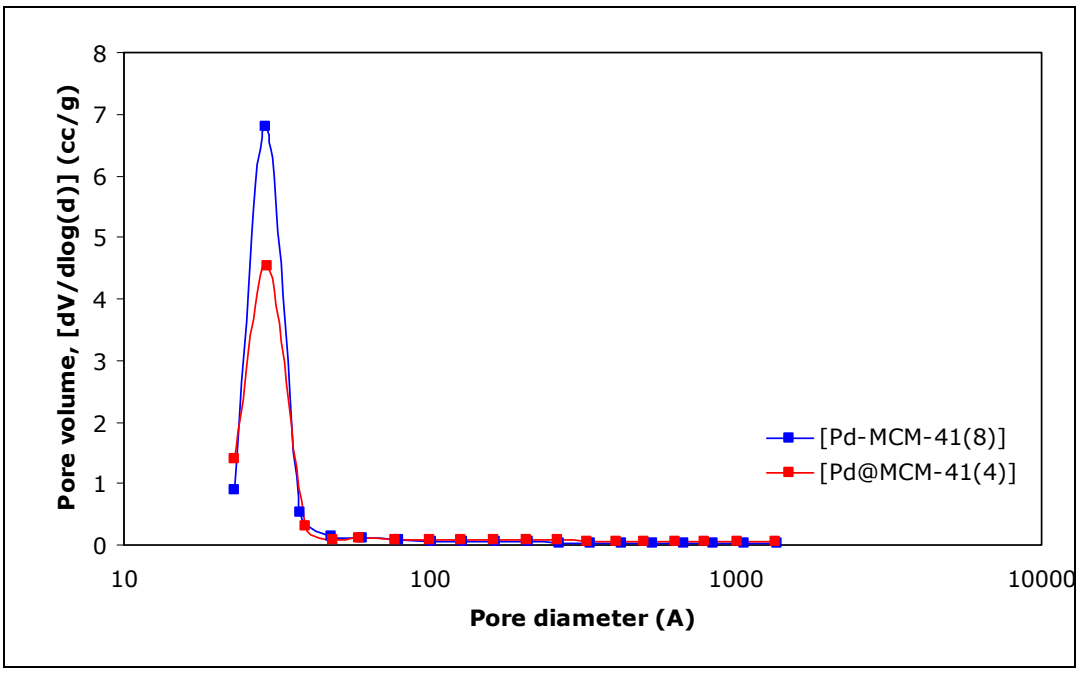

Figure 4.4.3. Comparison of pore size distributions of materials synthesized by direct hydrothermal synthesis and impregnation techniques both having the Pd/Si ratio of 0.12

By the comparison, it is clearly seen that, direct hydrothermal synthesis gives higher surface area and narrow pore size distribution at higher Pd/Si ratios that being in the impregnation method. But, it is an important fact that for some cases, having the palladium in its metallic form is much more important to have high surface area. Depending on the application, two methods have also advantages.

CHAPTER 5

CONCLUSIONS AND RECOMMENDATIONS

The goal of this thesis was to synthesize high surface area mesoporous Pd incorporated MCM-41 nanocomposite materials for both hydrogen storage and catalytic applications. Synthesized materials were characterized by using XRD, N_2 physisorption, EDS, SEM, TEM, and XPS. Interpreting all the valuable information from these analysis techniques, the following concluding remarks were obtained:

1. Using the direct hydrothermal synthesis route, high surface area (600-1500 m^2/g) Pd incorporated MCM-41 mesoporous catalytic materials were successfully synthesized under basic conditions. Moreover, the MCM-41 structure was not distorted and the BET surface area values over 1000 m^2/g were obtained for Pd-MCM-41 materials having Pd/Si wt ratios as high as 0.44.

2. In the case of acidic hydrothermal synthesis route, the XRD patterns indicated distortions of the MCM-41 structure. Furthermore, a wider distribution of pore sizes of the mesoporous Pd-MCM-41 were observed. Although Pd incorporation into the MCM-41 structure lowered the surface area of the synthesized material, the modified nanocomposite structure exhibited promising physical and chemical capabilities for many catalytic applications.

3. In order to devise the most appropriate synthesis route for Pd incorporation into the structure, three different palladium sources ($PdCl_2$, K_2PdCl_4, and $Pd(NH_3)_4(NO_3)_2$) were used. Among these

palladium sources, the best results (surface area ≈1091 m^2/g, Pd/Si ratio 0.23 wt. basis) were obtained with K_2PdCl_4 salt. Pd incorporation with other salts were also efficient and the results were close to the one synthesized with K_2PdCl_4. $Pd(NH_3)_4(NO_3)_2$ salt rather showed lower surface area and Pd/Si ratio compared to the other palladium sources used in the syntheses.

4. In the case of Pd impregnated MCM-41 material, a 20 % reduction in the pore volume and surface area of MCM-41 were observed in a sample containing a Pd/Si wt ratio of 0.12. However, the decrease of average pore radius was much less, indicating plugging of some of the pores by the Pd nanoballs formed in the mesopores of the host MCM-41.

5. To determine the reduction temperature of PdO to Pd, TPR analysis of the synthesized materials were performed in a Hiden analytical HPR20 mass spectroscopy. Results from the TPR analysis indicated that about 85 % of the PdO was reduced to Pd at temperatures around 200 ^oC. These TPR analysis also validated the accuracy of Pd/Si ratios obtained from either EDS or XPS analysis.

After all, Pd-MCM-41 nanocomposite material was synthesized in both acidic and basic media and interesting results were obtained and concluded. As a part of future work, the following recommendations could be helpful to improve the incorporation of the palladium into a silica based host:

1. A detailed analysis of the synthesized materials could be studied so as to observe the dispersion of Palladium onto the structure and to see the amount of palladium on the surface of the host structure. These observations can be detected with H_2 and CO chemisorption studies.

2. Since the synthesized materials are nanocomposite materials, a focused and detailed TEM analysis would complete the full characterization of the materials. Techniques like AFM can also be used to compare and justify the results obtained from TEM analysis of the Pd-MCM-41 materials.

3. It was a difficult task to synthesize Pd-MCM-41 in a basic medium. In order to ease the synthesis of modified MCM-41, it is suggested to incorporate aluminum into MCM-41 structure. This addition would alter the properties of the material into acidic. After having obtained an acidic structure palladium incorporation is expected to be more successful compared to the synthesis performed in this study.

4. Considering catalytic applications, it would be reasonable to increase Pd/Si ratios in the structure. For this purpose, SBA-15 is a candidate material for obtaining high Pd/Si ratios in the structure due to the acidic character of the material. However, compared to MCM-41, SBA-15 shows slightly lower surface areas. This pitfall could be overcome with the efficient dispersion of palladium into the SBA-15 structure and valuable results are expected for the modified nanocomposite material.

5. In some catalytic applications using different mesoporous materials like MCM-48 as a catalytic support might show better results due to the structure, stability, and flexible properties of the material. For comparison and effective catalyst design, it is possible to incorporate palladium into the cubic structure of MCM-48. Synthesized material could be used in specific reactions and the results can be compared with the ones obtained from this study.

6. Palladium incorporated novel materials will be tested for hydrogen storage applications as a future work. In addition, it is also planned to carry out catalytic studies with Pd-MCM-41 nanocomposite materials and yields from the reactions will be compared with the ones obtained from commercial catalysts.

REFERENCES

1. A. Taguchi and F. Schüth, *Microp. and Mesop. Mater.*, 2005, **77**, 1.

2. J. Weitkamp, *Solid State Ionics*, 2000, **131**, 175.

3. G. Øye, J. Sjöblom and M. Stöcker, *Adv. in Coll. And Inter. Sci.*, 2001, **89-90**, 439.

4. U. Ciesla, and F. Schüth, *Microp. and Mesop. Mater.*, 1999, **27**, 131.

5. A. Sayari, P. Liu, *Microporous Materials*, 1997, **12**, 149.

6. J. Xu, "Spectroscopic Studies of Synthesis, Modification and Characterization of Novel Mesoporous Molecular Sieves", PhD Thesis, University of Houston, December 1999.

7. http://web.chemistry.gatech.edu/~wilkinson/Class_notes/CHEM_3111_6170/Mesoporous%20materials.pdf

8. C.T. Kresge, M.E. Leonowicz, W.J., Roth, J.C. Vartuli, and J.S. Beck, *Nature*, 1992, **359**, 710.

9. J.S. Beck, J.C. Vartuli, W.J. Roth, M.E. Leonowicz, C.T. Kresge, K.D. Schmitt, T.T.-W. Chu, D.H. Olson, E.W. Sheppard, S.B. McCullen, J.B. Higgins, and J.L. Schlenker, *J. Am. Chem. Soc.*, 1992, **114**, 10834.

10. J.S. Beck, U.S. Patent, 5,057,296, 1991.

11. J.S. Beck, R.F. Socha, D.S. Shihabi, J.C. Vartuli, U.S. Patent, 5,143,707, 1992.

12. C.T. Kresge, M.E. Leonowicz, W.J. Roth, J.C. Vartuli, U.S. Patent, 5,098,684, 1991.

13. J.S. Beck, C.T. Kresge, S.B. McCullen, W.J. Roth, J.C. Vartuli, U.S. Patent, 5,304,363, 1994.

14. O. Collart, "Nanodesign of an Aluminasilicate Framework in Mesoporous MCM-48 Architecture", PhD Thesis, University of Antwerpen, 2003.

15. D. Zhao, J. Feng, Q. Huo, N. Melosh, G.H. Fredrickson, B.F.Chmelka, G.D. Stucky, *Science*, 1998, **279**, 548.

16. D. Zhao, P. Yang, N. Melosh, J. Feng, B.F. Chmelka, and G.D. Stucky, *Adv. Mater.*, 1998, **10**, 1380.

17. Q. Huo, R. Leon, P.M. Petroff, G.D. Stucky, *Science*, **268**, 1324.

18. Q. Huo, D.I. Margolese, U. Ciesla, P. Feng, T.E. Gler, P. Sieger, R. Leon, P.M. Petroff, F. Schüth, G.D. Stucky, *Nature*, **368**, 1994, 317.

19. J.M. Kim, G.D. Stucky, *Chem. Commun.*, 2000, 1159.

20. S. Inagaki, Y. Fukushima, K. Kuroda, J. Chem. Soc. Chem. Commun., 1993, 680.

21. T. Yanagisawa, T. Shimizu, K. Kuroda, and C. Kato, *Bull. Chem. Soc. Jpn.*, 1990, **63**, 988.

22. J.L. Blin, C. Otjacques, G. Herrier, B-L. Su, International *Journal of Inorganic Materials*, 2001, **3**, 75.

23. D. Kumar, K. Schumacher, C. du Fresne von Hohenesche, M. Grün, K.K. Unger, *Colloids and Surf. A: Physicochem. And Eng. Aspects*, 2001, **187-188**, 109.

24. V. Gusev, Molecule of the Month-MCM-41, www.chm.bris.ac.uk.

25. K.P. de Jong, A.J. Koster, *ChemPhysChem*, 2002, **3**, 776.

26. Y. Gucbilmez, "Vanadium and Molybdenum Incorporated MCM-41 Catalysts for Selective Oxidation of Ethanol", PhD Thesis, Middle East Technical University, June 2005.

27. Surface-active agent -- Encyclopedia Britannica, http://www.britannica.com/eb/article-9070437, 2006.

28. A. Monnier, F. Schüth, Q. Huo, D. Kumar, D. Margolese, R.S. Maxwell, G.D. Stucky, M. Krishnamurty, P. Petroff, A. Firouzi, M. Janicke, B.F. Chmelka, *Science*, 1993, **261**, 1299.

29. A. Firouzi, D. Kumar, L.M. Bull, T. Besier, P. Sieger, Q. Huo, S.A. Walker, J.A. Zasadzinski, C. Glinka, J. Nicol, D. Margolese, G.D. Stucky, B.F. Chmelka, *Science*, 1995, **267**, 1138.

30. Y. Gucbilmez, T. Dogu and S. Balci, *Catal. Today*, 2004, **100**, 473

31. H. Yang, G. Zhang, X. Hong and Y. Zhu, *J. Molecular Catal. A:Chemical*, 2004, **210**, 143.

32. J. Panpranot, K. Pattamakomsan, J. G. Goodwin Jr. and P. Praserthdam, *Catalysis Commun.*, 2004, **5**, 583.

33. M. L. Pena, A. Dejoz, V. Fornes, F. Rey, M. I. Vazquez and J. M. L. Nieto, *Appl. Catal A: Gen.,* 2001, **209**, 155.

34. B. Solsona, T. Blasco, J. M. L. Nieto, M. L. Pena, F. Rey and A. Vidal-Moya, *J. Catal.*, 2001, **203**, 443.

35. C. C. Liu and H. Teng, *Appl. Catal. B: Env.,* 2005, **58**, 69.

36. X. S. Zhao, G. Q. (Max) Lu and G. Millar, *Ind. Eng. Chem. Res.*, 1996, **35**, 2075.

37. B. K. Min, A. K. Santra and D. W. Goodman, *Catalysis Today*, 2003, **85**, 113.

38. B. M. Choudary, M. L. Kantam, N. M. Reddy, K. K. Rao, Y. Haritha, V. Bhaskar, F. Figueras and A. Tuel, *Appl. Catal. A: Gen.,* 1999, **181**, 139.

39. S. Albertazzi, R. Ganzerla, C. Gobbi, M. Lenarda, M. Mandreoli, E. Salatelli, P. Savini, L. Storaro and A. Vaccari, *J. Mol. Catal. A: Chem.,* 2003, **200**, 261.

40. C. A. Koh, R. Nooney and S. Tahir, *Catal. Lett.,* 1997, **47**, 199.

41. H. Kosslick, I. Mönnich, E. Paetzold, H. Fuhrmann, R. Fricke, D. Müller and G. Oehme, *Microporous Mesoporous Mater.,* 2001, **44**, 537.

42. M. Bejblova, P. Zamostny, L. Cerveny, J. Cejka, *Appl. Catal. A: Gen*., 2005, **297**, 169.

43. A. Papp, A. Molnar, A. Mastalir, *Appl. Catal. A: Gen*., 2005, **289**, 256.

44. N. Marin-Astorga, G. Pecchi, J.L.G., Fierro, P. Reyes, *Journal of Mol. Catal. A: Chemical*, 2005, **231**, 67.

45. M. W. Ryoo, S. G. Chung, J. H. Kim, Y. S. Song and G. Seo, *Catal. Today,* 2003, **83**, 131.

46. M. P. Kapoor, Y. Ichihashi, K. Kuraoka and Y. Matsumura, *J. Mol. Catal. A: Chem.,* 2003, **198,** 303.

47. O. Altinisik, M. Dogan and G. Dogu, *Catal. Today.*, 2005, **105**, 641.

48. M. Dogan and G. Dogu, *AIChE J.,* 2003, **49**, 3188.

49. Y. J. Glanville, J. V. Pearce, P. E. Sokol, B. Newalker and S. Komarneni, *Chem. Phys.*, 2003, **292**, 289.

50. A. Fukuoka, H. Araki, Y. Sakamoto, S. Inagaki, Y. Fukushima and M. Ichikawa, *Inorganica Chimica Acta*, 2003, **350**, 371.

51. I. Yuranov, P. Moeckli, E. Suvorova, P. Buffat, L. Kiwi-Minsker, A. Renken, *J. Molec. Catal. A:* 2003, **192**, 239.

52. Y. Wu, L. Zhang, G. Li, C. Liang, X. Huang, Y. Zhang, G. Song, J. Jia and C. Zhixiang, *Mater. Res. Bull.*, 2001, **36**, 253.

53. B. K. Min, A. K. Santra and D. W. Goodman, *Catal. Today,* 2003, **85**, 113.

54. H. Kang, Y. W. Jun, J. I. Park, K. B. Lee and J. Cheon, *Chem. Mater.* 2000, **12**, 3530.

55. S. Duan and S. Senkan, *Ind. Eng. Chem. Res.* 2005, **44**, 6381

56. R.A. Khan, "Metal Incorporation in MCM-41 for Hydrodesulfurization", MSc Thesis, King Fahd University of Petroleum and Minerals, January 2003.

57. V. B. Fenelonov, V. N. Romannikov and A. Yu. Derevyakin, *Microporous Mesoporouus Mater.* 1999, **28**, 57.

58. N. Yao, "Synthesis and Caharcterization of Pt/Sn-MCM-41 Petroleum Reforming Catalysts", PhD Thesis, Yale University, January 2002.

59. H. Karhu, A. Kalantar, I.J. ayrynen, T. Salmi, D.Yu. Murzin, *Appl. Catal.*, 2003, **247**, 283.

60. J.A. Dumesic, D.F. Rudd, L.M. Aparicio, J.E. Rekoske, A.A. Trevino, "The Microkinetics of Heterogeneous Catalysis", 1993, Chapter 4, American Chemical Society.

61. J.C. Wickerman, Surface Analysis The Principal Techniques, 2003, Chapter 3, John Wiley&Sons.

62. XPS International sells Spectral Data Processors, Data-Bases, VAMAS Viewers and Handbooks, http://www.xpsdata.com/, February 2002.

63. G. Karamullaoğlu, "Dynamic and Steady-State Analysis of Oxidative Dehydrogenation of Ethane", PhD Thesis, Middle East Technical University, July 2005.